



**UNIVERSITY
OF CRETE**

**DEPARTMENT OF MATERIALS SCIENCE
AND TECHNOLOGY**

**"Design of protein and peptide materials for
use in nanotechnological applications"**

PhD Thesis

Chrysoula Kokotidou

Supervisor: Prof. Anna Mitraki

December 2019

ACKNOWLEDGEMENTS

Firstly, I would like to express my gratitude to my supervisor Prof. Anna Mitraki from the Department of Materials Science and Technology, for her constant support and encouragement throughout this PhD Thesis. Her guidance, patience, motivation, and immense knowledge helped me grow up as a scientist.

Besides my supervisor, I would like to express my appreciation to all the members of my thesis committee: Asst. Prof. Phanourios Tamamis, Asst. Prof. Kelly Velonia, Dr. Androniki Kretsovali, Prof. George Chalepakis, Assoc. Prof. Maria Chatzinikolaidou and Asst. Prof. Vasiliki Iconomidou for their support all these years, their excellent collaboration, their insightful comments and encouragement.

Determinant role played also the staff of the Electron Microscopy Facility at the Biology Department. Therefore, I would like to thank Aleka Manousaki, Eva Papadogiorgaki, Alexandra Siakouli and Stefanos Papadakis for their support with the electron microscopy observations and our interesting discussions.

From the group of Dr Phanourios Tamamis at Texas A&M I wish to thank Dr Sai Vamshi Jonnalagadda and Asuka Orr for their wonderful collaboration with the computational studies and the fruitful communication we had throughout our common projects.

My sincere thanks also go to Prof. Sifis Papamatheakis, George Vrentzos, Takis Makatounakis from the Institute of Molecular Biology and Biotechnology and Dr Anthi Ranella and Dr Evi Kavatzikidou and Ritsa Babaliari from the Institute of Electronic Structure and Laser at FORTH for their hospitality in their cell culture laboratories and our fruitful discussions.

In addition, a thank you to Dr Mark van Raaij and his team for the crystallographic studies.

To the group of Prof. Athanasios Koutsolelos from the Chemistry Department for the effective collaboration and exchange of ideas.

My warmest and deepest thanks to my people, my friends and fellow lab mates for always being by my side and supporting me, for the long stimulating evening discussions, the exchange of ideas, and for all the fun we had in the past years and during this wonderful scientific journey. Thank you, Themis, Chrysa, G , Marita, Fanoula, Ariadni, Vaggelis, Petros, Graziano, Babis, Konstantina, Giorgos, Stella, Marietta, Rena F. I wish the very best to every one of you.

Finally, I would like to acknowledge the financial support of the “Maria Manassaki” scholarship for the doctoral studies 2015-2016.

This PhD Thesis is dedicated to my family for their loving support and encouragement to every crucial decision of my life. This dissertation would not have been possible without their warm love, continued patience, and endless support.

Table of Contents

ACKNOWLEDGEMENTS	2
TABLE OF CONTENTS	4
ABSTRACT	6
THESIS RATIONALE	8
Chapter 1: General Introduction	18
1 . 1. Proteins, peptides and their amyloid folding state	18
1. 2. Cell penetrating peptides as carriers.....	19
1. 3. Amyloid fibrils	19
1. 4. Amyloid peptides as biomaterials.....	22
1. 5. Adenovirus type 2 model system	23
1. 6. Amyloid Formation Inhibitors	26
Chapter 2: Adenovirus fiber as biomaterial	27
2. 1. Introduction	27
2. 2. List of chimeric proteins studied and modified	39
2. 3. Materials and methods.....	47
2. 4. Results.....	66
2. 5. Conclusions.....	101
Chapter 3: A Novel Amyloid Designable Scaffold and Potential Inhibitor Inspired by GAIIG of Amyloid Beta and the HIV-1 V3 Loop	104
3. 1. Introduction	104
3. 2. Materials and Methods	105
3 .3. Results and Discussion.....	108
3. 4. Conclusion	121
Chapter 4: Designer Amyloid Cell Penetrating Peptides for Potential Use as Gene Transfer Agents	122
4. 1. Introduction	122
4. 2. Materials and Methods	125

4. 3. Results.....	131
4. 4. Discussion	148
4. 5. Conclusions.....	153
GENERAL CONCLUSIONS.....	156
OUTLOOK.....	164
LIST OF PUBLICATIONS	166
APPENDIX.....	167
REFERENCES	169

ABSTRACT

Protein and peptide materials with a defined conformation are increasingly used in a wide area of applications. Advantages that characterize proteinaceous biomaterials are their inherent biocompatibility, biodegradability and flexibility of their design and fabrication.

The present thesis is focused on the design and study of such biomaterials using as model system a natural fibrous protein the adenovirus fiber. The Adenovirus fiber protein is a homotrimer consisting of an N-terminal tail, a long shaft, and a C-terminal knob region that is responsible for high-affinity receptor binding. The fiber adopts a trimeric nanorod conformation of 30nm length. This protein with specific modifications can be used as an efficient carrier in the area of gene transfer and therapy. In the present thesis a series of constructs were designed having as template the Ad2 fiber protein and inserting functionalities through molecular cloning techniques. These constructs were based on the fibrous shaft segment (residues 61-392) while the globular head of the fiber was replaced by the small (27 aa) trimerization domain of the bacteriophage T4 fibritin, termed "foldon". Moreover, the protein constructs were modified with metal binding sites, a His-tag tail for improving purification, a biotinylation site for streptavidin-biotin conjugation of molecules and cysteine residues at exposed positions for linkage of molecules through disulfide bonds. The chimeric proteins were rendered more stable and were targeted for potential use as delivery agents and gene therapy applications. The shaft segment consists of pseudo amino acid sequence repeats, of which the sequence GAITIG was previously identified as a minimal building block that self-assembles into amyloid-type fibrils.

Amyloid fibrils, derived from the studied adenovirus sequences and from a common sequence to Alzheimer's A β peptide and HIV-1 V3 loop, due to their intrinsic mechanical properties are excellent candidates for use as scaffolds. By applying computational methods, the peptides can be rationally designed through mutation of regions amenable to modification aiming at the fabrication of biomaterials with 'on demand' functionalities. An essential part of this PhD study was focused on the experimental study of two cell penetrating peptides that were rationally and computationally designed by the group of Asst. Prof. Phanourios Tamamis at Texas A&M University. The peptide sequences comprised natural beta-sheet cores that can self-assemble into amyloid fibrils. The peptides were designed to contain positively charged and aromatic residues exposed at key positions in order to additionally promote DNA condensation and cell internalization. The results demonstrate that these designer peptide fibrils can efficiently enter mammalian cells while carrying packaged luciferase encoding plasmid DNA and act as a protein expression enhancer. Interestingly, the peptides exhibited strong antimicrobial activity against the enterobacterium *Escherichia coli*.

In another aspect of this study instead of exploiting amyloid fibrillization advantages, we sought to inhibit or hinder the process of amyloid fibril formation. The GAIPIG sequence was inspired from the beta-sheet key determinants found in the Ad2 fiber shaft, the Alzheimer's alpha beta peptide and HIV-1 V3 loop. This peptide despite its similarity with amyloid forming sequences, contains the beta breaker residue (proline) and as a result fails to self-assemble into amyloid fibrils as verified by X-ray diffraction and electron microscopy studies. The structural and experimental information provided in this study could serve as the basis for structure-based design of potential inhibitors of amyloid formation.

ΠΕΡΙΛΗΨΗ

Τα πρωτεϊνικά και πεπτιδικά υλικά με καθορισμένη μορφολογία χρησιμοποιούνται όλο και περισσότερο σε μια ευρεία περιοχή εφαρμογών. Τα πλεονεκτήματα που χαρακτηρίζουν τα πρωτεϊνικά βιοϋλικά είναι η έμφυτη βιοσυμβατότητα τους, η βιοαποικοδομησιμότητα τους και η ευελιξία του σχεδιασμού και της κατασκευής τους. Η παρούσα διδακτορική εργασία επικεντρώνεται στο σχεδιασμό και τη μελέτη τέτοιων βιοϋλικών χρησιμοποιώντας ως πρότυπο σύστημα μια φυσική ινώδη πρωτεΐνη, την ίνα του αδενοϊού τύπου 2. Η ίνα του αδενοϊού είναι μια ομοτριμερής πρωτεΐνη που αποτελείται από ένα N-τελικό άκρο, ένα λεπτό κεντρικό μίσχο και ένα C-τελικό άκρο, το οποίο είναι υπεύθυνο για τη προσκόλλησης του ιού στους υποδοχείς των κυττάρων. Έχοντας ως εκμαγείο το μίσχο της Ad2 ίνας και εισάγοντας λειτουργικά χαρακτηριστικά μέσω τεχνικών μοριακής κλωνοποίησης, σχεδιασθηκε μια σειρά νέων υβριδικών πρωτεϊνών. Οι χιμαιρικές αυτές πρωτεΐνες καθίστανται πιο σταθερές και δυνητικά θα μπορούσαν να βρουν χρήση ως μεταφορείς φαρμάκων καθώς επίσης και σε εφαρμογές γονιδιακής θεραπείας.

Τα αμυλοειδή ινίδια που προέρχονται από τις μελετημένες αλληλουχίες του μίσχου της ίνας του αδενοϊού και από μια κοινή αλληλουχία στο Αβ πεπτίδιο του Alzheimer και στον V3 βρόχο του HIV-1, λόγω των εγγενών μηχανικών τους ιδιοτήτων είναι ιδανικά για χρήση ως ικριώματα. Με την εφαρμογή υπολογιστικών μεθόδων, τα πεπτίδια μπορούν να σχεδιαστούν ορθολογικά με την μετάλλαξη συγκεκριμένων επιδεκτικών σε τροποποιήσεις περιοχών, με απώτερο στόχο την κατασκευή βιοϋλικών με «κατ' απαίτηση» λειτουργίες. Ένα σημαντικό μέρος της διδακτορικής αυτής μελέτης επικεντρώνεται στην πειραματική μελέτη δύο ορθολογικά και

υπολογιστικά σχεδιασμένων πεπτιδίων που είναι θετικά φορτισμένα και έχουν την ικανότητα να δεσμεύουν DNA και να εισέρχονται στο κύτταρο ενώ μεταφέρουν το 'πακεταρισμένο' πλασμιδιακό DNA.

Όσον αφορά μια άλλη πτυχή αυτής της διδακτορικής μελέτης, αντί να εκμεταλλευτούμε τα πλεονεκτήματα της αμυλοείδωσης, επιδιώξαμε να αναστείλουμε ή να παρεμποδίσουμε τη διαδικασία σχηματισμού αμυλοειδών ινιδίων. Το πεπτίδιο που σχεδιάστηκε ήταν εμπνευσμένο από τις προαναφερθείσες φυσικές αλληλουχίες. Αυτό το πεπτίδιο, παρά την ομοιότητά του με τις αλληλουχίες που σχηματίζουν αμυλοειδή ινίδια, περιέχει το αμινοξύ προλίνη, το οποίο θεωρείται αναστολέας της δημιουργίας των β-φύλλων. Το σχεδιασμένο αυτό πεπτίδιο δεν αυτό-οργανώνεται σε β-φύλλα και επιπλέον καθυστερεί ή διακόπτει την αυτό-οργάνωση του Αβ πεπτιδίου σε αμυλοειδή ινίδια. Επομένως παρέχει πληροφορίες που θα μπορούσαν να χρησιμεύσουν ως βάση για -δομικά βασιζόμενο- σχεδιασμό πιθανών αναστολέων της αμυλοείδωσης.

THESIS RATIONALE

Background

Gene and cell-based therapies hold a great potential to revolutionize the clinical management of human diseases. A common limiting factor is the poor gene delivery for most of *in vivo* gene therapies. Viral vectors and especially adenoviral vectors hold much promise as platforms for targeted therapeutic delivery and are considered the most efficient gene delivery systems for a broad range of cell and tissue types and applications in clinical and preclinical studies with an emphasis in the areas of cancer treatment, regenerative medicine and vaccination.¹ Advantages of using adenovirus-based applications include well-defined biology, genetic stability, high gene transduction efficiency and ease of large-scale production. However, a significant barrier of using recombinant adenovirus systems for gene therapy is the strong immune response to virus-infected cells detected under certain circumstances. Moreover, another disadvantage is the lack of native adenovirus receptor expression in a variety of cell types, since the adenovirus fiber targets predominantly cells with CAR (Coxsackievirus Adenovirus Receptor) and/or integrin receptors.

Adenovirus (Ad) is a non-enveloped, linear double-stranded DNA virus and is comprised by structural proteins like the hexon, the penton base and the fiber proteins; the fiber proteins protrude from the twelve vertices of the viral capsid and mediate cell attachment². Alternative non-viral transfer carriers can be fabricated by using adenoviral proteins, such as the dodecahedron particles, that are comprised by the adenovirus penton (ie penton base protein + fiber protein) complex or penton base proteins alone. The penton is a complex assembled by two oligomeric proteins, the penton base protein and the fiber protein. It is involved in the cell attachment via the RGD motif present in a

loop of the penton base protein and the virus transportation into the cytosol. When these two proteins are co-expressed in cells³, they self-assemble into dodecahedron particles⁴ that are considered as a safer alternative transfer vehicle in contrast to the entire adenovirus virion that is comprised by eleven proteins. Moreover, the dodecahedron retains the gene transfer advantages of the entire virion such as: efficient cell entry, protection and release of the DNA from the endosomes and a range of cell and tissue targeting^{3, 5-6}.

The adenovirus fiber utilizes its globular head (knob domain) to trigger the trimerization of the fiber protein and initiate cell attachment through the CAR receptors. To further overcome the CAR cell target specificity of the fiber transfer vehicles in order to independently target other cell lines, the knob should be removed. In that case, the fiber could not be able to acquire its trimeric conformation which will lead to the loss of the fiber protein structural functionality. Therefore, certain approaches have been developed consisting in the engineering of virion particles that comprise modifications of the fiber protein either by incorporating cell targeting peptide sequences or by substituting the knob motif⁷. Structural inspection of the knob domain region of the fiber have pointed to two separate locations within the knob that can be exploited for genetic peptide presentation, the C-terminal end, and a region termed the HI loop. Incorporated cell targeting sequences comprise the RGD motif, polylysine, a vascular endothelial cell-targeting peptide, SY-GYLPLP or other cell targeting epitopes.⁸⁻¹¹ However, in certain cases structural conflicts have emerged as a result of the knob modifications.¹² Therefore, alternative approaches have been developed that include the deletion of the entire knob domain of the fiber protein and subsequent replacement with moieties that provide a trimerization function for the knobless fiber. The substitution motif could be a α -helix trimerization domain from MoMuLV(Moloney Murine Leukemia Virus) envelope glycoprotein¹³ or the foldon trimerization motif from the bacteriophage T4 fibrin.¹⁴⁻¹⁵

Additionally, cell-targeting motifs have to be included in the constructs that should mediate specific attachment to selected cell lines. In order to rationally insert such motifs, structural insight is absolutely necessary. Detailed structural information on the adenovirus hexon and penton proteins exists²; moreover, the structures of the entire capsid have been recently revealed at atomic scale resolution both by cryo-electron microscopy¹⁶ and X-ray¹⁷ methods. However, the fiber remains the virion protein part for which no full structural information exists to date². This is due to its asymmetric, thin and flexible nature that renders difficult the visualization by EM methods and results in no detectable electron density in X-ray studies. Previous studies conducted in our group, initiated the study of the adenovirus type 2 fiber as a model for fibrous proteins structure and assembly¹⁸. The crystal structure of the a stable domain of the fiber comprising the head and four repeats of the shaft segment was solved at 2.4 Å and revealed the “triple beta spiral” conformation of the fiber protein¹⁹. This homo-trimeric and beta-structured fiber protein is an extremely stable protein that is resistant to high temperature, pH and denaturants.¹⁸ Having as template this adenovirus type 2 fiber system, resulted in the design and fabrication of a fiber protein where the globular head was substituted with the foldon trimerization motif of bacteriophage T4 fibritin. The substitution was performed for the fiber construct comprised by 4 repeats in the shaft and yielded promising results, since the foldon chimeras could fold into trimers, with high overexpression efficacy and enhanced stability that lead to the solving of their crystal structure^{14, 20-21}. The single crystal structure confirmed that the shaft repeats were adopting their native triple spiral fold within the hybrid constructs¹⁴. Moreover, the full-length protein constructs comprising residues 61-319 of the shaft segment with the foldon domain at their C-terminus were fabricated by Dr. Papanikolopoulou in the framework of her thesis, however they have not been further studied.

It was reported that the Ad5 fiber alone mediated non-viral gene transfer in the absence of the whole virus⁶. The internalization ability seemed to proceed through the knob domain, since the fiber-mediated transduction was inhibited by a free soluble knob⁶. Moreover, other internalization mechanisms seem to participate in the fiber entry into the cells, as assessed in ref⁶ where the sequence KKTK which lies within the third pseudorepeat of the fiber shaft matches the consensus sequences for binding HS-GAGs (Heparan Sulfate Glycosaminoglycans) and subsequently could act as a HS-GAG-binding site for cell entry. This prompted us to investigate the internalization potential of the fiber protein alone, trimerized with the fibritin trimerization motif, and in the absence of the globular head.

As a result, in this PhD thesis, by combining the knowledge acquired by the aforementioned studies, we elaborated on designing and fabricating a series of stable and chimeric full-length shaft-foldon constructs with enhanced functionalities for potential use as non-viral transfer biomaterials.

In another aspect inspired by the adenovirus fiber protein self-assembly ability in the absence of the C-terminal globular head, small peptide sequences corresponding to shaft sequences were examined for their potential use as biomaterials. The reductionist approach was previously followed in our group by Dr Papanikolopoulou²² and the peptide GAITIG and the longer peptide NSGAITIG were identified as the shortest amyloid forming sequences. More specifically, a number of peptide sequences corresponding to the fold of the native adenovirus fiber structure were synthesized and examined for their eventual ability to self-assemble in the absence of a trimerization motif. They were found to form amyloid fibrils with a number of techniques, including electron microscopy, x-ray fiber diffraction and Congo Red binding. Moreover, by using implicit-solvent replica-exchange simulations conducted by Assistant Professor Phanourios Tamamis, it was further confirmed that the octapeptide NSGAITIG and its

hexapeptide counterpart, GAITIG form readily intermolecular β -sheets. Additionally, the Asn and Ser residues at the N-terminal part remain disordered in the sheets, suggesting that these amino acids are exposed at the exterior of the fibrils, accessible and therefore amenable to modifications.²³

Computational studies can identify suitable positions for rational modification of the peptide building blocks in order to fabricate novel biomaterials with specific functions. On the basis of this insight provided by molecular dynamics simulations, cysteine residues were substituted at positions 1 and 2 of the NSGAITIG sequence to promote metal binding attachment of metal nanoparticles such as: gold, platinum and silver.²⁴ Furthermore, the bioactive motif Arg-Gly-Asp (RGD) was incorporated at the amyloid forming sequence NSGAITIG, aiming for the development of a cell-attachment and biodegradable scaffold²⁵. By mimicking the cesium binding properties of proteins, amyloid scaffolds were also computationally and rationally designed in order to fabricate amyloid scaffolds with cesium binding abilities for potential application in the removal of cesium ions from nuclear waste or blood²⁶.

In this PhD thesis, the assumption that rationally designed amyloid scaffolds could also find uses in the gene transfer areas, was investigated. By having a stable fibril forming core such as the GAITIG or GAIIG core, we postulated that adding cationic and aromatic residues at flexible positions could convey DNA binding and cell penetrating propensity.

An advantage of the amyloid peptides compared to the studied protein constructs as gene transfer vehicles, could be the protein charge dependence as a function of pH. The proteins studied in this thesis under physiological pH conditions are usually negatively charged due to their pKa and therefore unable to bind the negatively charged DNA. That implies that protein solution pH should be decreased to the acidic range with potential implications in the protein structural conformation and stability. Thus, the

aforementioned engineered protein constructs could be more suitable as drug, protein or nanoparticle cargo carriers.

Thesis outline

The present PhD thesis focuses on the design, engineering, production and characterization of novel protein and peptide materials derived from the adenovirus type 2 fiber and natural fibril-forming peptides from Alzheimer's Amyloid beta and HIV-1 V3 loop sequences. This approach aims at taking advantage of their unique self-assembling properties and with the help of molecular dynamic simulations to develop functional biomaterials for use in the area of biomedicine. These biomaterials can be used as vectors or scaffolds for the insertion of additional functionalities, such as cell penetrating gene carriers, tissue-targeting motifs, enzymatic subunits, or for the fabrication of materials with potential amyloid inhibition properties. Furthermore, optimum protein and peptide self-assembling conditions were validated depending on the application of interest and the characterization of these biomaterials with electron microscopy and X-ray fiber diffraction techniques. Such self-assembling proteins and peptides offer open-ended possibilities towards multifunctional bionanomaterials of the future.

This thesis is divided into three chapters which correspond to two different but converging approaches for material fabrication. More specifically, Part 1 (Chapter 2) focuses on the production and characterization of adenovirus-based protein materials and their use as scaffolds. In this part, fiber-shaft based proteins were modified with genetic engineering: a histidine tag was inserted so as to enable efficient purification and attachment of metal nanoparticles ; a biotinylation site was inserted to enable functionalization via biotin-streptavidin chemistry; and finally, a cysteine was engineered by site-directed mutagenesis at an exposed loop, in order to enable functionalization through thiol chemistry. All these approaches were followed for

constructs that comprise almost the full-length shaft domain (residues 60-392) joined with the fibrin foldon, which is necessary for correct trimerization. Seeking to reduce the complexity of these constructs, we also created shortened versions of these proteins, that comprise residues 260-392 of the shaft segment plus the trimerization motif. All modification approaches described above were also followed for this shortened construct.

However, the ultimate thesis goal was to follow a reductionist approach, and identify minimal self-assembling building blocks that could serve as functionalization scaffolds. Part 2 (Chapter 3) focuses on the identification of the GAIIG peptide from the Alzheimer's A β peptide and the HIV gp120 V3 loop, as minimal self-assembling block and an amyloid designable scaffold YATGAIIGNII. Part 2 also comprises (Chapter 4) and epitomizes this approach with the rational design of this designable scaffold to endow it with cell-penetrating and DNA condensing properties, targeted for intracellular DNA delivery.

PART 1 (Chapter 2):

Production and Characterization of Protein Materials and their Use as Scaffolds

Stable, artificial fibrous proteins that can be functionalized open new avenues in fields such as bionanomaterial design and fiber engineering. The fibrous parts of viral proteins usually adopt trimeric β -stranded structural folds and are appended to globular-receptor binding domains. The globular domains are essential for correct folding and trimerization and can be successfully substituted by a very small 27-amino acid trimerization motif from phage T4 fibrin. The registration motif from phage T4 fibrin, a 27-amino acid C-terminal domain termed "foldon" serves as a registration motif for the segmented, triple coiled coil motif of the fibrin²⁷. This small domain in a β -propeller conformation can fold and trimerize autonomously.

Having as template the adenovirus fiber shaft sequence and by exploiting molecular cloning techniques, chimeric proteins were previously created that consist of the foldon trimerization domain, positioned at the C-terminus of the fibrous shaft (residues 61-392) with or without the use of a natural linker ²¹. Based on these proteins, we were able to create improved scaffolds using molecular cloning techniques. These include the following: a) insertion of a His-tag at the N-terminus b) a biotinylation site at the N-terminus, c) a cysteine residue at an exposed loop position at the shaft segment.

These stable chimeric adenovirus fiber proteins were further validated for their ability to trimerize into stable nanorods. Their intrinsic properties include their attachment to nanoparticles coated with Nickel-Nitrotriactic acid through their His-tag, their attachment to streptavidin coated nanoparticles, therapeutic molecules and scaffolds through their additional biotinylation site and finally, the capability of initiating polymerization and gold nanoparticle adhesion due to their exposed cysteine. They were created with the perspective of enhancing protein stability, purification effectiveness, and functionality as carriers.

One of their basic advantages is their method of heterologous production in *E.coli* cells. Heterologous production of chimeric protein constructs which bear engineered functionalities is considered a cost-effective method for producing large quantities of the protein material.

PART 2 (Chapter 3):

A Novel Amyloid Designable Scaffold and Potential Inhibitor Inspired by GAIIG of Amyloid Beta and the HIV-1 V3 Loop

In this chapter the sequence GAIIG which is common to the amyloid beta peptide (residues 29–33) and to the HIV-1 gp120 (residues 24–28 in a typical V3 loop) is detected,

along with the longer YATGAIIGNII sequence from the V3 loop, as key beta sheet determinants in the aforementioned protein/peptide sequences. These peptides can independently self-assemble into amyloid fibrils as observed under TEM, FESEM and X-ray diffraction studies. The sequence GAIIG with its homologous sequence GAITIG, also a key determinant peptide in Ad2 fiber in the absence of the trimerization motif, inspired the design and use of the GAIPIG peptide as a potential peptide with amyloid inhibitory action. Molecular dynamic simulations and experimental studies focus on the structure deciphering of the GAIPIG sequence and its binding to the Alzheimer's alpha beta and HIV-1 V3 loop corresponding sequences and its capability of slowing down the amyloid fibrillization process.

This study was published in the FEBS Letters Journal 'A novel amyloid designable scaffold and potential inhibitor inspired by GAIIG of amyloid beta and the HIV-1 V3 loop. Kokotidou et al. *Febs Letters* **2018**, 592 (11), 1777-1788. DOI: 10.1002/1873-3468.13096.' and is presented in this thesis as per se.

Part 3 (Chapter 4):

Designer Amyloid Cell Penetrating Peptides for Potential Use as Gene Transfer Vehicles

Cell-penetrating peptides (CPP) provide an efficient strategy for the intracellular delivery of bioactive molecules in various biomedical applications. They are characterized by their ability to spontaneously access the cell membrane, non-cytotoxicity and efficiently binding and protecting and releasing their cargo into the cytoplasm. The majority of CPPs are cationic which enables the interaction with the mammalian cell membrane and the conjugation with nucleic acid molecules for gene therapy purposes. In this thesis we

investigated the potential of amyloid forming materials to act as cell penetrating peptides and gene transfer agents. Amyloid materials have been used for enhancing retroviral transfer by acting as electrostatic bridges between the viral particles and the cell membrane²⁸⁻²⁹. However, there is no evidence so far that they could act as gene transfer enhancers by penetrating the cell membrane while carrying a gene encoding plasmid. Additionally some cell penetrating peptides and aggregation prone region sequences (APR) exhibit antimicrobial activity against various bacterial and fungal strains, by disturbing the microorganism's protein homeostasis.³⁰

In the current thesis we focused on the beta-sheet peptide sequences GAITIG from adenovirus type 2 fiber and the common peptide sequence GAIIG of A β peptide and HIV gp120 V3 loop, thoroughly studied in the previous chapter and in ref²², for their potential to act as cell penetrating peptides with gene transfer and antimicrobial activity. Our strategy was based on the following : we selected longer previously studied sequences which contain exposed residues, outside the β -sheet GAITIG or GAIIG core, that are accessible and available for suitable selected modifications. These sequences were used as frameworks for rational and computational designed peptides for use as cell penetrating gene transfer carriers. The designer peptides were tested for their self-assembling ability into amyloid fibrils, charge, cell penetration, cytotoxicity, DNA binding and condensing ability, gene transfer inside the nucleus and transfection efficacy. Additionally, their potential activity as antibacterial agents was investigated.

Chapter 1: General Introduction

1 . 1. Proteins, peptides and their amyloid folding state

The assembly of proteinaceous supramolecular structures is common in all living organisms. The level of molecular organization plays a pivotal role in the functionality of each protein. Proteins and peptides self-assemble into a variety of unique structures with the ability to perform a variety of essential functions for the biological world. Basic cellular components like protein enzymes adopt a quaternary structure, where the correctly folded subunits further fold into a tertiary structure retained by non-covalent interactions. Usually proteins and peptides need to reach their well-defined soluble fold in order to execute their natural processes. While in a specific conformation many proteins, when 'decorated', could be used as gene or drug delivery agents^{6, 31-33}. Protein materials are biocompatible and suitable for rational design through the fine-tuning of their biophysical and biological properties. Such configurations include the regulation of their architectural features to promote attachment of molecules of interest through bonding mechanisms (disulfide bonds, biotin-streptavidin and electrostatic interactions) and the biological interaction with the environment such as incorporation of cell receptor recognition and binding motifs, nuclear targeting domains and cell penetration sequences. For intracellular drug or gene delivery, important parameters that should be considered are the capability of the carrier for DNA condensation, intracellular trafficking, endosomal escape, nuclear transport and the carrier's stability against protease action.

1. 2. Cell penetrating peptides as carriers

Apart from proteins and protein fragments, also small peptide sequences have been explored for their potential as functionalizing and efficient delivery vectors of nanoparticles, nucleic acids, therapeutic and diagnostic molecules.³⁴⁻³⁷ Among others are the cell penetrating peptides which usually consist of 5-30 amino acids. They are typically positively charged due to their high lysine and arginine residues, a feature that allows their interaction with negatively charged nucleic acids or molecules and the interaction with the negatively charged phospholipids of the cell membrane, which they can eventually penetrate with their transporting cargo. Characteristic examples are the TAT peptide³⁸ and the polyarginine peptides³⁹⁻⁴⁰.

1. 3. Amyloid fibrils

Under various circumstances proteins or peptides fail to assemble correctly and reach their well-defined quaternary structure and consequently convert into aggregates of highly ordered fibrillar assemblies, termed amyloid fibrils. Those fibrillar assemblies can differ greatly from the native and functional folding of the protein and can self-assemble spontaneously while being thermodynamically favorable. Not only proteins or long sequence peptides can self-assemble into amyloid structures but also small peptides of less than four residues can adopt these conformations exhibiting similar properties. They are considered as supramolecular configurations in the nanometric scale that give rise to pathological disorders ranging from neurodegenerative diseases to systemic amyloidosis such as Alzheimer's,⁴¹⁻⁴² diabetes type II,^{43,44} and Parkinson's⁴⁵ disease. However, there is a variety of living organisms that take advantage of their endogenous proteins inherent tendency to form amyloid fibrils for specific functional rather than pathological purposes

-such examples as the Pmel melanosomes⁴⁶⁻⁴⁷⁻⁴⁸, A-bodies for storing protein and peptide hormones⁴⁹⁻⁵⁰ and chorion eggshell proteins.⁵¹⁻⁵²

Amyloid fibrils can self-assemble spontaneously or under environmental stimulation (alterations in temperature, pH, ionic strength). They are arranged in a crystal-like, one-dimensional way comprised of thousands of protein or peptide molecules. They are uniquely characterized by the cross- β -sheet motif, where individually inter-molecular beta strands are formed and aligned perpendicular to the fibril axis. The repetition of this motif and the lateral binding of another β -strand through hydrogen bonding, constitutes the beta sheet which proceeds throughout the fiber's entire length. The formed beta sheets are connected with a dense hydrogen bonding network and are running parallel to the fibril axis.⁵³ The first cross-beta pattern describing this architecture occurring in amyloid forming proteins was reported in 1935 for the stretched poached egg white which was studied by X-ray diffraction.⁵⁴ The protofilament consists of two β -sheets closely interacting in a sequence depending manner. The steric zipper-like interface, as viewed when looking down the axis of the amyloid fiber, is densely packed, water depleted and relies on the interaction between the side chains of β -strands that belong to opposing beta-sheets.⁵⁵⁻⁵⁶ The cross-beta pattern is the core of the protofilaments which further laterally associate to fold into mature fibrils.⁵⁷

To successfully characterize and verify the amyloid nature of an assembled moiety, a series of experimental and computational methods have been developed to analyze, verify and study the formation of amyloid fibrils. Macroscopically, the amyloid fibril structure appears as long, intertwined and unbranched fibrils that have a width that ranges in the area of 7-20nm, as imaged *in vitro* by electron microscopy observations such as Transmission Electron Microscopy (TEM), Scanning Electron Microscopy (SEM) and Atomic Force Microscopy (AFM) and depends on the self-assembly parameters and the sequence of the moiety. Fibrils are defined by a common X-ray diffraction pattern with a

4.7 Å reflection in meridian and a 10 Å reflection in equatorial, which correspond to the distances between the strands and the stacking distances between beta-sheets, respectively.⁵⁸ Moreover, they have the ability to bind specific amyloid dyes like Thioflavin T and Congo Red dye. Thioflavin T (ThT) when bound with amyloids and excited at 440-450nm, emits a strong fluorescence signal at 480nm.⁵⁹ Congo Red(CR) staining of amyloids is detected, in the amyloid's spectrum analysis, by the increase in the Congo Red absorption pattern and a red shift of the 490nm absorbance peak to 512nm as well as by the production of a new shoulder peak at around 540nm. Moreover, CR binding to the fibrils gives a yellow-green birefringence when observed under a crossed-polarizer.⁶⁰ Generally, it was considered easier to characterize a short peptide's amyloid structure rather than the structure of larger protein and peptide sequences that are not always amenable to crystallization. Recently the aforementioned problem was surpassed by utilizing cryo-transmission electron microscopy (cryo-TEM) and solid-state NMR spectroscopy. These techniques apart from revealing the basic structure of the amyloid core, they offer insight into much more structural complexity level ⁶¹⁻⁶³ (**Figure 1**).

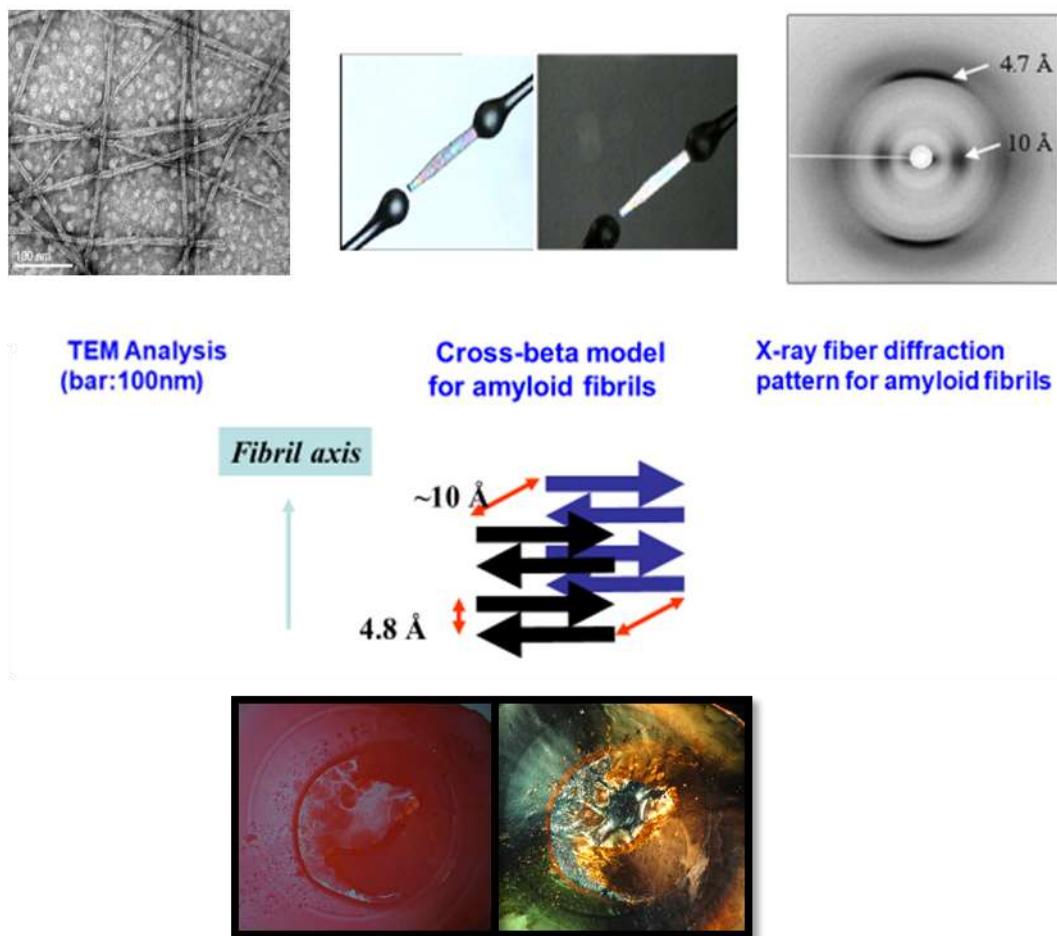


Figure 1: Characterization of the amyloid fibrils by various methods: Transmission Electron microscopy (upper left), and characteristic X-ray fiber diffraction pattern (upper right) recorded from fibrous stalks formed between two glass rods (upper center). The cross-beta model is illustrated at the middle center. Congo Red staining of amyloid fibrils as visualized under an optical microscope without (bottom left) and with (bottom right) the use of a crossed polarizer. The yellow/green birefringence is a common characteristic of amyloids.

1. 4. Amyloid peptides as biomaterials

Self-assembled beta structured peptide aggregates, either natural or synthetic have emerged as attractive candidates for the fabrication of biomaterial structures in a wide

application field. Their unique fold and structure endows them with advantageous mechanical properties such as high stability, shear modulus, bending rigidity, tensile strength and enhanced kinetic and thermodynamic stability. They are considered outstandingly strong and stable on one hand but on the other hand quite flexible. These mechanical properties in combination with their biocompatibility and the ease of introducing favorable mutations into their sequence, convey -to these assemblies- potential advantages over organic or inorganic counterparts. Areas that can find application are in tissue engineering and regenerative medicine as scaffolds for cell growth,^{64, 65} as scaffolds for cell attachment, for the delivery and controlled release of therapeutics,⁶⁶⁻⁶⁷ in nanocircuits and electronics as metal nanoparticle templates,⁶⁸⁻⁶⁹ or in biomineralization with inorganic materials (Ca²⁺ binding),⁷⁰ in environmental applications^{26, 71} (Cs or CO₂ capture) or as minimal versions of enzyme catalysts.⁷²

1. 5. Adenovirus type 2 model system

Natural or synthetic assemblies as potential biomaterials were inspired by the Adenovirus type 2 fiber due to its unique fold and characteristics that combine both a stable trimeric protein fold and an alternative fold into a beta-structured fibrillar assembly, under specific circumstances. The Ad2 fiber protrudes from the viral capsid and mediates cell attachment of the virus to the cell receptor, CAR (Coxsackie and Adenovirus Receptor⁷³⁻⁷⁴) and subsequent infection. The globular head located at the C-terminal end acts both as cell attachment organelle and as trimerization motif, which enables the trimerization and self-assembly of the fiber protein into a nanorod conformation (**Figure 2**). Similar morphologies for the fiber have been detected also in Adenoviruses Type 3 and 5. Constructs derived from the fiber sequences could be further manipulated with the addition or alteration of their sequences with extra functionalities for use in gene therapy of drug delivery areas. The fibers with the globular head can

interact with the CAR receptors in order to mediate docking with the cells. Replacing the head with another trimerization motif will seize the interaction with this receptor, however it was discovered that these trimeric proteins are still able to internalize the cell through other temperature-independent mechanisms and distribute to the cytoplasm and nucleus.¹³ A potential route could be through the heparan sulfate glycosaminoglycans (HS-GAGs) receptors found in cell lines.⁶ These alternative endocytic entry mechanisms eliminate the constraining need to use the globular trimerization motif that specifically binds to CAR cell receptors. Moreover, it was reported that the isolated fiber protein, in the absence of the penton base, can enter the cells. The globular head by itself cannot enter the cells and accumulates in the CAR receptors located in the cell surface. This report suggested for the first time a potential role of the shaft domain in cell entry.⁶

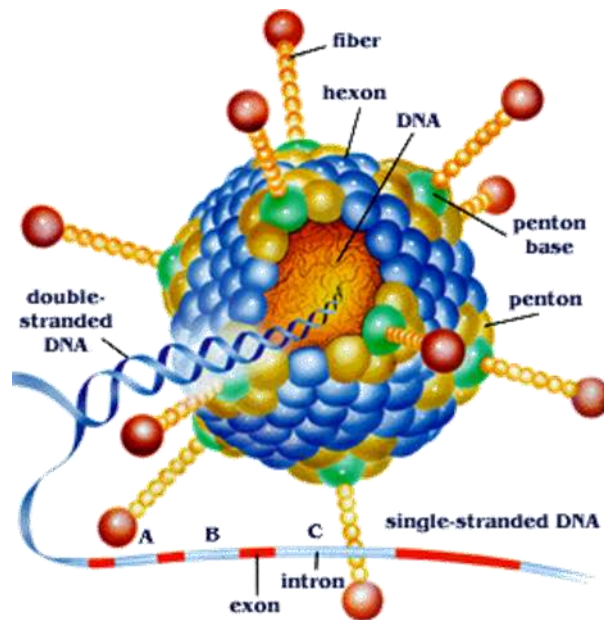


Figure 2: Adenovirus virion (https://microbewiki.kenyon.edu/index.php/adenovirus-based_gene_therapy:_a_promising_novel_cancer_therapy).

In Ad2 fiber, the loss of the globular head, and in the absence of another trimerization motif, leads to the self-assembly of the entire fiber shaft segment into amyloid fibrils and the loss of the fiber structure and conformation. In order to decipher the specific sequence that triggers this self-aggregation, a reductionist approach was followed. The initial fiber shaft sequence was dissected into smaller peptides, whose propensity for amyloid self-assembly was studied.²² It was found that the minimal self-assembling into amyloid fibrils building blocks are the octapeptide NSGAITIG and the GAITIG hexapeptide (**Figure 3**). The NSGAITIG sequence was also studied with molecular dynamic simulations and apart from confirming its beta strand configuration,²³ rational designs were also suggested and experimentally applied for the peptide use as a biomaterial for a wide range of applications.^{25, 68-69, 75}

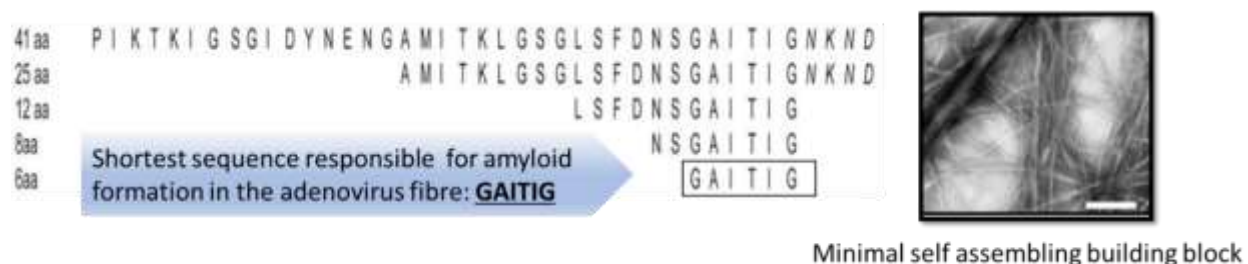


Figure 3: Studies on the detection of the minimal amyloid forming building block in the Adenovirus type 2 fiber shaft. Ref. ²²

Moreover, a homologous with the peptide GAITIG sequence, the peptide GAIIG was proven that is also a key beta sheet determinant and can spontaneously self-assemble into amyloid fibrils. The sequence GAIIG corresponds to residues 29-33 of the amyloid beta peptide associated with the Alzheimer's disease. This aggregating sequence is also common to the HIV-1 gp120 protein and is located at residues 24-28 in a typical V3 loop of gp120.⁷⁶ The longer peptide sequence YATGAIIGNII in the same V3 loop can also self-assemble into amyloid fibrils and since its terminal residues do not participate in the beta-

sheet core and are exposed, the sequence is amenable to suitable selected modifications towards its use as a functional scaffold.

1. 6. Amyloid Formation Inhibitors

By identifying the “hot regions” of amyloid self-assembly, short synthetic peptides designed as beta-sheet breakers interact with these regions in order to inhibit amyloid fibril formation and propagation. Moreover, designing beta-breaker sequences based on beta-sheet key determinant sequences through mutating of specific amino acids that are actively involved, could “trick” the amyloid fibril accumulation mechanism and eventually arrest it. Proline residues placed in key positions impair the amyloid aggregation and this inhibition is attributed to the steric hindrance created by the proline substitution, which results in disruption of the β -sheet formation process.⁷⁷

Chapter 2- Adenovirus fiber as biomaterial

2. 1. Introduction

Adenovirus system and Fiber Protein's Structure and Properties

Human Adenovirus type 2 (Ad2) is a non enveloped, icosahedral-shaped DNA virus that is associated with respiratory and gastrointestinal infections. The adenovirus capsid is comprised by 12 vertices and from each of them protrudes a trimeric protein that is responsible for the viral cell attachment and entry. Moreover, the coat protein of the adenoviral 'face' is called hexon which forms hexagonal structures and constitutes the main structural protein of the viral capsid. The trimeric fiber protein is attached to the viral capsid through a penton protein that serves as a base connector for the fiber (**Figure 4**). These fiber proteins that protrude from the vertices of the adenovirus particles are homotrimeric and contain a N-terminal end, through which they bind to the penton base of the viral capsid, a C-terminal globular head that attaches to as the Coxsackievirus and Adenovirus Receptor (CAR)⁷⁸ and a central fibrous shaft consisting of 22 pseudo-sequence repeats (

Figure 5).

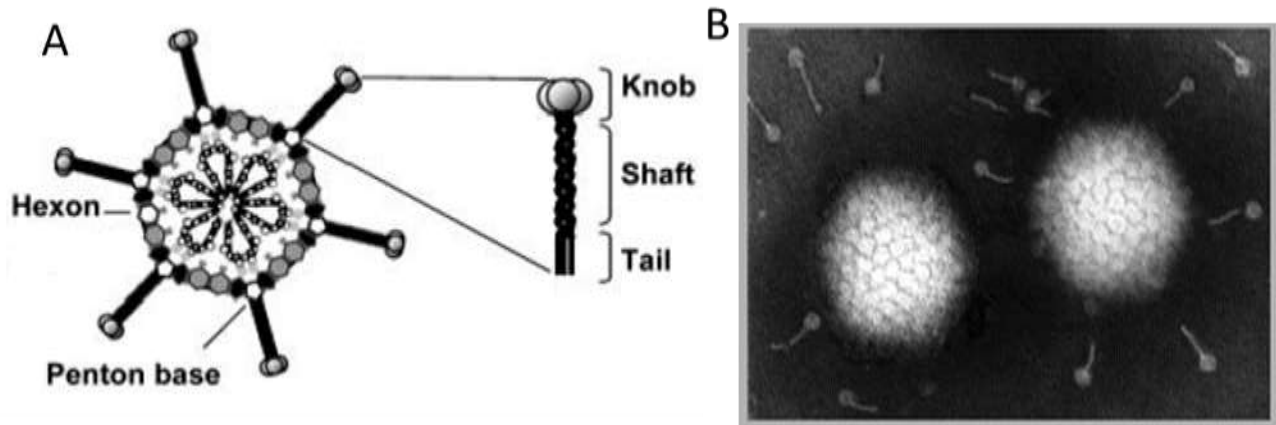


Figure 4: The Adenovirus Type 2 A) Presentation of the Adenovirus structural proteins. B) TEM picture of the adenovirus capsid and fiber protein in its trimeric and nanorod conformation.

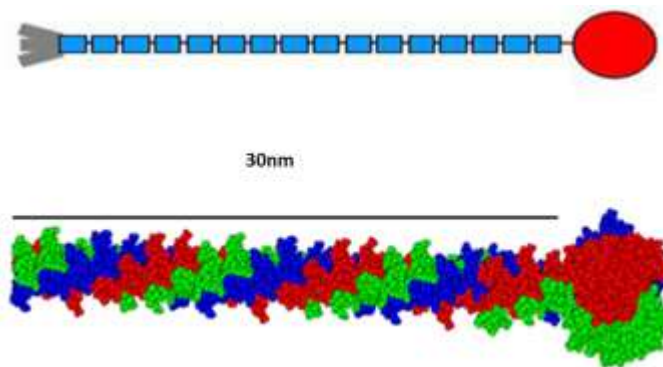


Figure 5: Model for the full-length fiber based on the single crystal structure of a stable fragment comprising four sequence repeats

Each shaft repeat is built from a repeating sequence motif with hydrophobic amino acids alternating with hydrophilic ones and glycines or prolines at conserved positions (**Figure 8**). This results into a beta structured repeat fold that consists of two beta strands, one almost parallel to the fiber axis and the other at an angle of 45°. The two strands are connected by a turn. An exposed loop follows each repeat and joins repeats together.

Additionally, the C-terminal globular part acts as a trimerization motif that initiates the self-assembly of the fiber into nanorods of specified length, depending on the number of repeats (30nm for 22 repeats of Ad2 fiber).¹⁸ The crystal structure of a stable fragment of the fiber (four shaft repeats and the head domain) was solved at 2.4 Å resolution¹⁹ (**Figure 9**). The basic framework of the fiber's structure is sustained by inter- and intra- chain hydrogen bonds and salt bridges involving side-chains.

The fiber protein is an extremely stable protein. The fiber structure is intertwined with a high proportion of buried surface. One third of the solvent accessible residues when in the monomer state of the protein are buried and become inaccessible upon trimerization. Trimerization enhances the fiber rigidity and stability of the shaft.¹⁹ Additionally, the protein is resistant to SDS, temperature, proteases and denaturants (remains a trimer in 2% SDS at ambient temperature).¹⁸ This resistance to SDS allows easy distinction of the native form of the protein from any misfolded or partially folded forms, that get denatured by SDS and migrate in the monomer position in SDS-PAGE gels. This is depicted in the cartoon that follows. Interestingly, any trimeric, partially unfolded forms migrate higher than the native trimer, since they are more expanded (the so-called "umbrella" effect) **Figure 6 and Figure 7**.

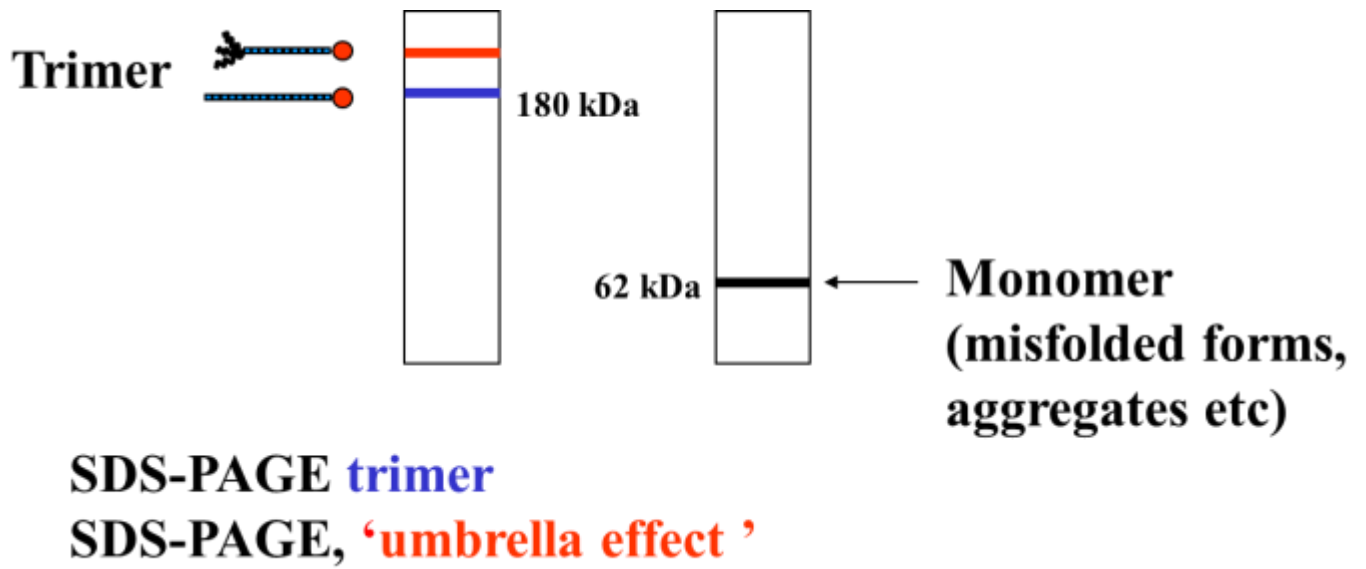


Figure 6: Representation of the protein migration on a SDS-PAGE, depending on its folding.

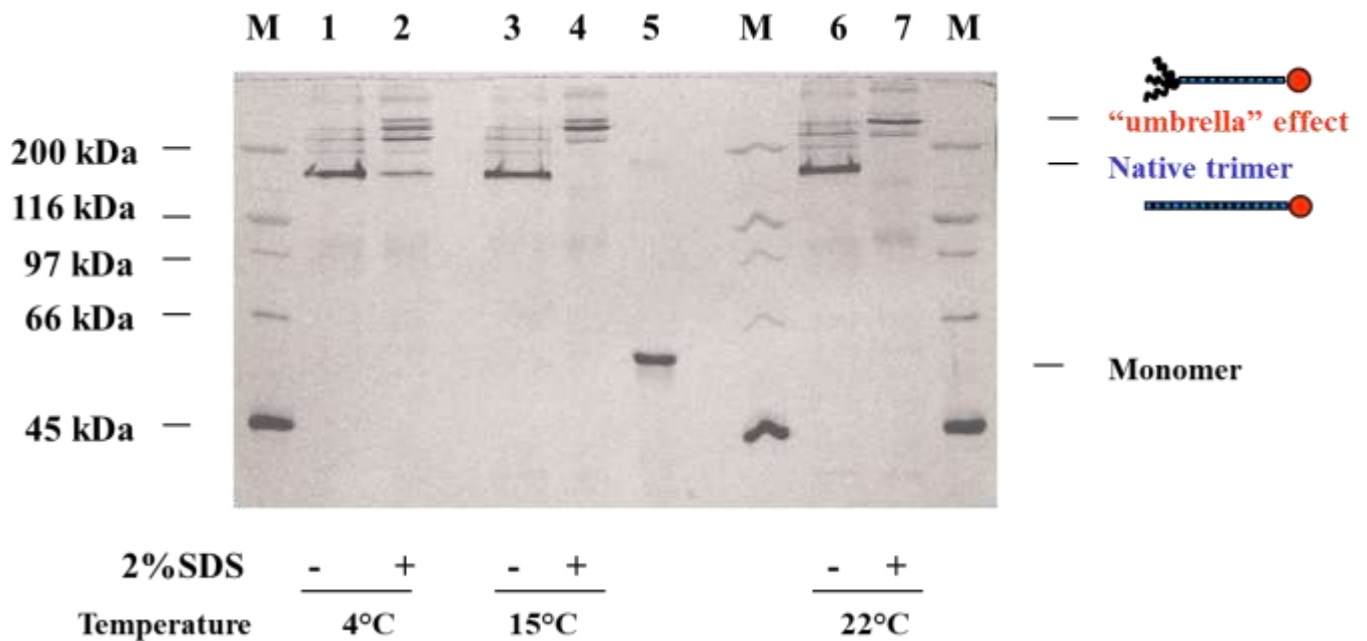


Figure 7: Effect of SDS in solution at various temperatures. Adapted from ref.¹⁸

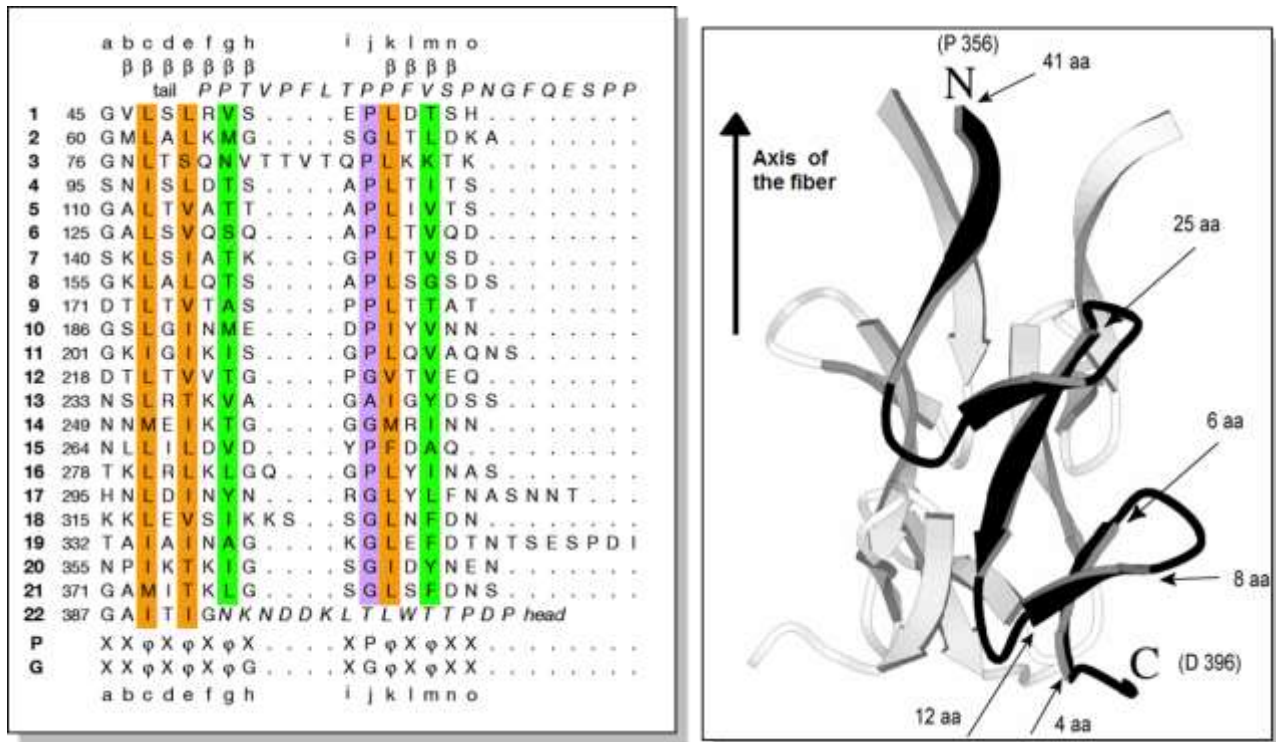


Figure 8: Each fiber monomer contains 582aa.

1.(Left) The 22 pseudo-repeats in the Ad2 shaft. The fibrous shaft is built from a repeating sequence motif with a hydrophobic amino acids (ORANGE and GREEN residues) alternating with hydrophilic ones and glycine or proline at conserved positions (PURPLE residues). At the bottom the consensus sequences are presented, φ standing for hydrophobic and X being any amino acid. Adapted from ref¹⁹.

2.(Right) The basic repeat fold contains a beta-strand almost parallel to the axis of the fiber followed by a beta turn and another beta strand which runs at an angle of 45° relative to the fiber axis. The repeats are joined by a solvent exposed loop. Adapted from ref²².

Abbreviations for amino acids are as follows : A: alanine; R: arginine; N: asparagine; D: aspartic acid; C: cysteine; Q: glutamine; E: glutamic acid; G: glycine; H: histidine; I: isoleucine; L: leucine; K: lysine; M: methionine; F: phenylalanine; P: proline; S: serine; T: threonine; W: tryptophan;
Y: tyrosine; V: valine

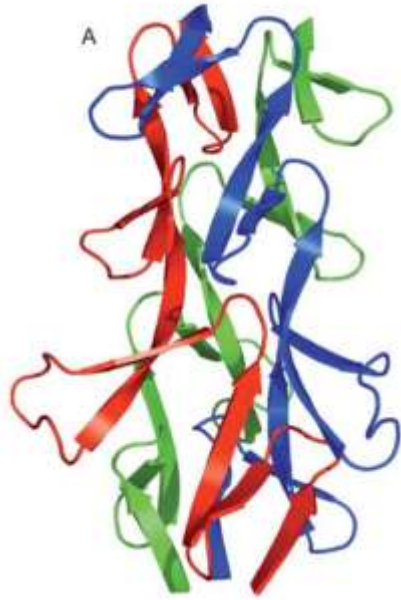


Figure 9: The triple b-spiral in the adenovirus fiber shaft. The triple b-spiral domain alone. Shown are amino acids 319–392 of each of the three chains, forming four triple beta-spiral repeats. Adapted for ref⁷⁹.

Trimerization Motifs and Fibril Formation

As mentioned above, the globular head of the fiber acts both as the trimerization but also as a receptor-binding domain. The principal conformation of the adenovirus monomer of the globular head is an antiparallel, eight stranded 'beta-sandwich'. The three monomers interact and form a three bladed propeller⁸⁰ (**Figure 10**). The C-terminal head acts as a registration motif that triggers the folding and correct alignment of the three chain monomers into stable trimers.

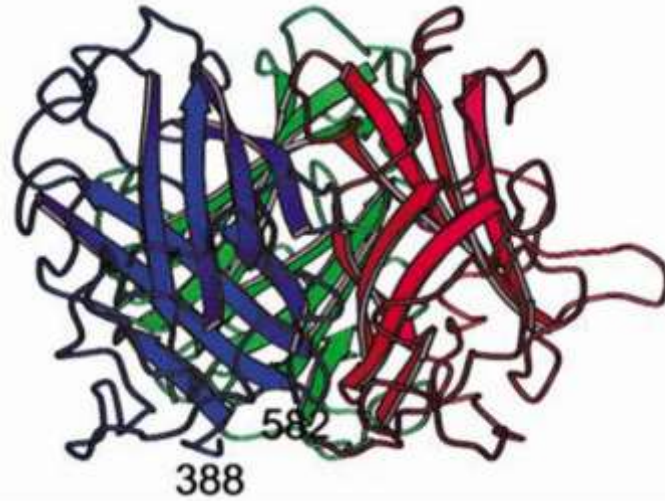


Figure 10: The C-terminal domain of Adenovirus fiber. Each monomer of the adenovirus globular head forms a 'beta-sandwich'. By further interaction of the three monomers, a distinct 'beta-propeller' is formed. Loops at the side of the moieties contain information for binding with the cell's CAR receptors.

When recombinant production of proteins that adopt the native triple beta-spiral fold is desired, the presence of a trimerization motif is necessary. When the globular head is present, the fiber fibrous sequences fold and assemble into a trimeric beta spiral conformation, whereas in its absence they adopt a completely different conformation. In the absence or by mutating the sequence parts of the C-terminal globular head in the adenovirus fiber, the correct trimerization of the fiber protein is hindered and the protein self-aggregates into an amyloid fibril formation, characterized by the cross-beta conformation (**Figure 11**). The self-assembly into amyloid fibrils is mediated by "out-of-register" or "strand-swapping" interactions between strands belonging to different peptide molecules.

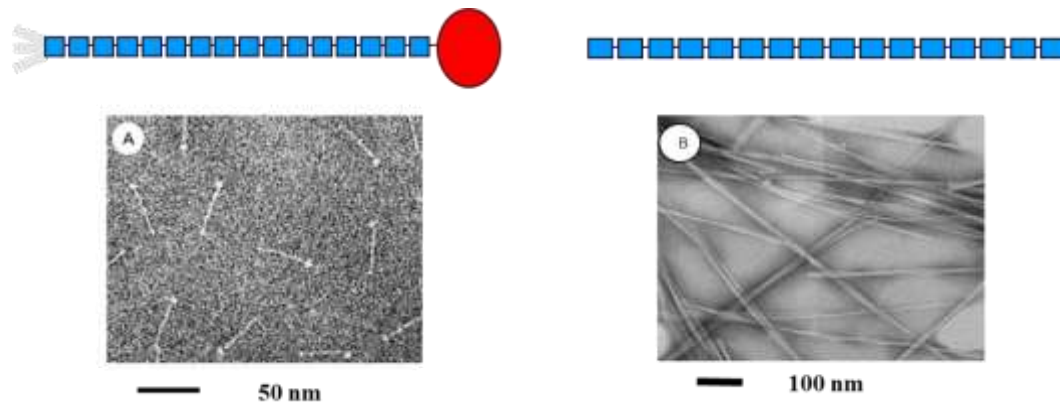


Figure 11: Schematic representation of Adenovirus Type 2 fiber. It comprises The N-terminal domain (thick grey lines), the shaft domain (rectangles joined together) and the globular head (circle) which acts as a trimerization motif for the folding into trimeric nanorods (TEM picture on the left adapted from ref ¹⁹). In the absence of the globular head, the shaft segment fails to adopt its native trimeric fold and aggregates into amyloid fibrils (TEM picture on the right, adapted from ref ¹⁸ with permission from © the American Society for Biochemistry and Molecular Biology).

An alternative registration motif that can trigger the trimerization of proteins is the ‘foldon’ motif from phage T4 fibritin that consists of 27 amino acids and can fold and trimerize spontaneously, initiating the assembly of fibritin into a triple coiled coil motif⁸¹ (**Figure 12**). When this motif substitutes the globular head at the C-terminus of the adenovirus fiber protein, new hybrid structures can be produced recombinantly²⁰ that can fold into a trimeric nanorod conformation. One such example are the shaft sequences that adopt their native triple beta-spiral conformation within the chimeric constructs as revealed by X-ray crystallography.¹⁴ They also exhibit improved stability, such as easier crystallization, enhanced overexpression levels and resistance to extreme conditions (SDS, temperature, denaturants).²⁰



Figure 12: The 'foldon' motif. The C-terminal domain of the fibrin's T4 bacteriophage is comprised by two sheets with three strands each that form a 'beta sandwich'. The foldon domain does not have a cell binding specificity and can act solely as a trimerization and registration signal.⁸²

The Fiber Protein through binding to CAR receptors mediates Adenovirus infection.

The Adenovirus infection starts with the interaction of the trimeric Ad fiber protein with a membrane glycoprotein that is exposed on the cell surface and is referred as CAR (Coxsackie Adenovirus Receptor). The binding of the CAR receptor with the elongated fiber protein is mediated by the C-terminal domain CAR binding domain also referred to as knob or globular head. Each fiber knob can support the attachment to three CAR molecules. The binding occurs through amino acid residues that are located in extended loops in the knob lateral surface.⁸³ Subsequently the fiber protein undergoes a conformational change in order to enable the optimal association of the RGD motif located in the penton base protein with the αv integrins on cell surface. Following this attachment step, adenovirus particles are internalized through clathrin mediated endocytosis⁸⁴ (**Figure 13**).

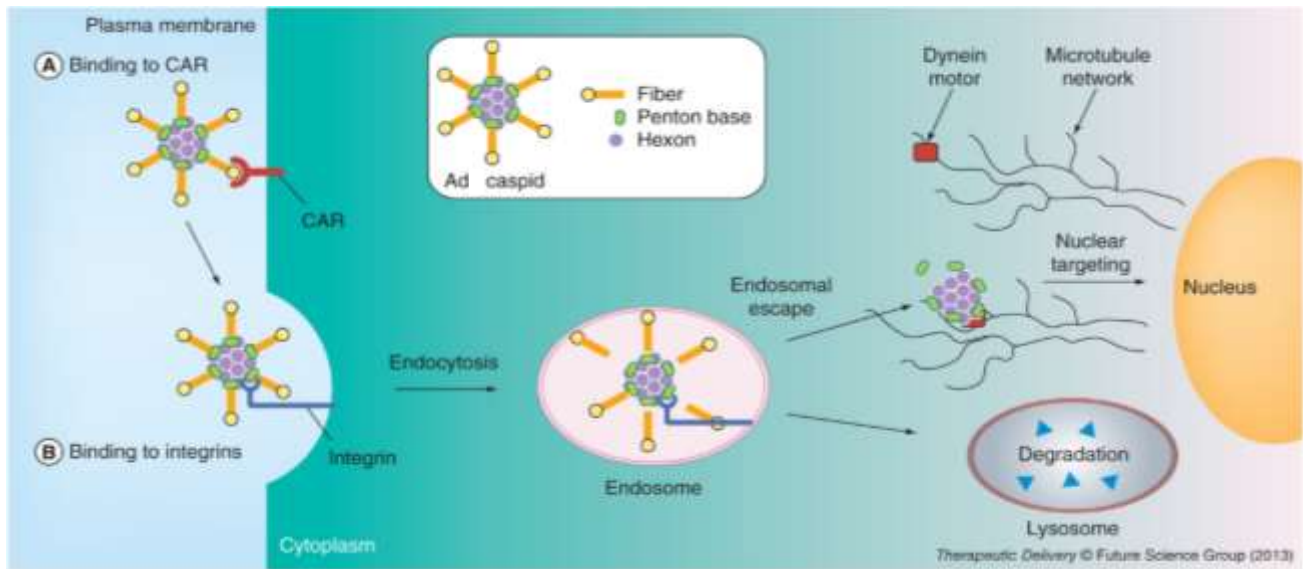


Figure 13: . Representation of adenovirus capsid (inset) and the early stages of adenovirus infection (A) Binding of the virus to the primary receptor, CAR, which initiates infection. This is immediately followed by (B) secondary binding of the virus to integrins, which triggers receptor-mediated endocytosis. CAR: Coxsackievirus adenovirus receptor.³¹

Adenovirus proteins are used for gene therapy and the targeting of specific cell types is often desirable. If the native globular head of the fiber is present, all the cells expressing the CAR receptor are going to be targeted.¹ However, if the globular head is deleted, the shaft sequences cannot adopt their native fold and they will form amyloid fibrils as mentioned above. The use of another, neutral trimerization motif such as fibrin is necessary, along with a motif that attaches specifically to the cell type targeted.^{15, 85} Therefore, the aforementioned shaft- foldon chimeric proteins can be further functionalized for applications in tissue engineering, drug delivery and gene therapy fields.

Adenovirus proteins as drug or gene carriers

Intracellular delivery of proteins or nucleic acids through a protein carrier is potentially a game-changing approach for therapeutics. However, common challenges associated with this strategy are the effective uptake of the protein-cargo carrier into the cell, the vector's stability, release of the cargo into the cytosol and the risk of the vector's cytotoxicity. To develop a protein into a delivery agent for therapeutics several important steps should be taken into account such as: an initial cell-surface binding followed by receptor mediated endocytosis, the efficient release from the endosome into the cytosol and intracellular trafficking towards the nucleus.⁸⁶

Various engineered adenovirus capsid proteins have been developed thereof for drug delivery or gene therapy purposes.^{1,7,12,31} Soluble penton base of Ad2 and Ad5 has been shown to facilitate the entry of various membrane-impenetrable molecules⁸⁷ including genes,⁸⁸ siRNA⁸⁹ and corroles.⁹⁰ Moreover, the adenoviral hexon protein when fused into a polyethylenimine-plasmid complex can enhance the nuclear delivery of DNA, due to its nuclear homing capability.⁹¹ The soluble full-length fiber (with the C-terminal knob) of Ad5 demonstrated high uptake levels into mammalian cells in the absence of the whole viral capsid, utilizing an actin-mediated and temperature independent entry pathway. The fiber protein can assemble into a complex with protamine-condensed plasmid DNA and facilitate gene transfer.⁶ To target vectors to specific cell types except from the CAR receptor, the knob CAR-binding domain should be substituted with other cell targeting motifs. However, by removing the knob, the Ad fiber loses its trimerization ability. In the study in ref ¹³ the entire knob domain of the Ad5 fiber was deleted and replaced by an α -helix trimerization motif from MoMuLV envelope glycoprotein, a Myc-epitope and a 6x-His-tag. Knobless recombinant Ad5 fibers were capable of efficient trimerization and internalization through their His-tag interaction with the anti-His single chain antibody variant displayed on the cell surface. Bifunctional adapter molecules have been

engineered that enable the targeting of the mosaic adenovirus fiber to alternative cellular receptors distinct from CAR. A metabolically biotinylated fiber mosaic Ad was fabricated through incorporation of a biotin acceptor peptide in the sequence of the fiber protein. The hybrid protein containing a luciferase expressing gene was effectively complexed with an epidermal growth factor (EGF) – streptavidin. The fiber mosaic virus was then retargeted to EGF receptor (EGFR) expressing cells and exhibited increased infectivity.⁹²

Our approach for designing Ad2 fiber proteins for therapeutic delivery.

As mentioned above, when the non-cell target specific foldon domain replaces the native globular head, the hybrid adenovirus fiber protein adopts its correct folding and trimerization into nanorods as was verified by solving the crystal structure of this chimeric protein (**Figure 14**). The hybrid protein is stable and can withstand extreme conditions. Additionally, functional specificities can be engineered into the hybrid fiber protein such as: cell- targeting motifs and metal-binding sites that will improve their properties and biomedical application use.⁹³

In this study we aimed to fabricate a series of protein fiber constructs in order to optimize the hybrid protein materials for each potential application. The work conducted in this thesis has as source of inspiration the Ad2 fiber and stems from its hybrid construct, where the globular head was substituted by the foldon trimerization motif¹⁴ (Figure 15).

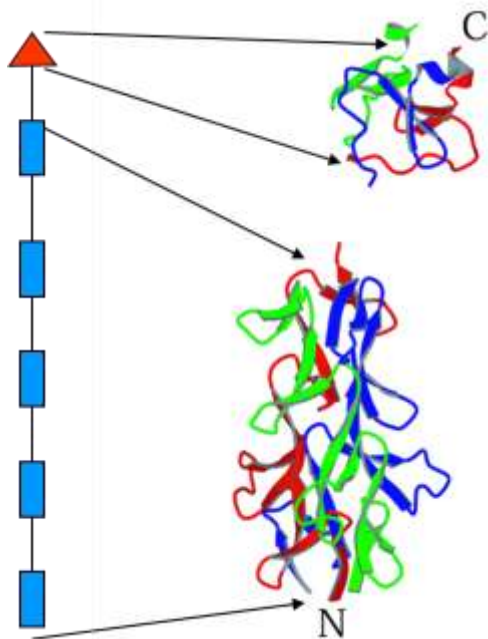


Figure 14: Crystal structure of the foldon fusion protein. Fusion construct consisting of human adenovirus type 2 fiber shaft residues 319–392 (bottom), a Gly-Ser linker, and bacteriophage T4 fibrin residues 457–483.⁹³

2. 2. List of chimeric proteins studied and modified:

Linker and NoLinker proteins [L and NoL] : Chimeric protein with shaft residues Met61-Gly392 of the natural fiber and with the foldon trimerization domain (Gly457–Leu483) substituting the globular head at the C-terminal end. The natural linker sequence (Asn-Lys-Asn-Asp-Asp-Lys residues 393-398) that connects the globular head to the shaft was used to connect the shaft sequences to the fibrin foldon domain. (**Figure 15B**). A construct without the natural hexapeptide linker was also fabricated (**Figure 15C**)

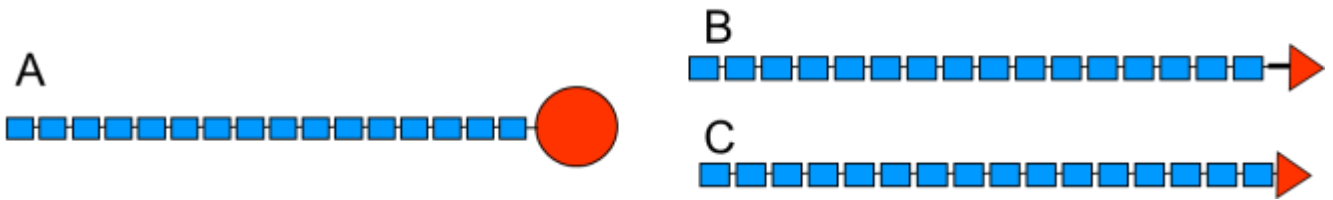


Figure 15: Schematic representation of the **A)** natural stable adenovirus fragment (residues 61-582). Residues belonging to the shaft domain (Met61-Gly392) are symbolized with blue squares and residues belonging to the globular head (Leu399-Glu582) are symbolized with a circle and residues 393–398 (Asn-Lys-Asn-Asp-Asp-Lys) form the linker that connects the two parts. **B)** Chimeric protein Linker [L] that is comprised by the fibritin foldon domain (fibritin residues Gly457–Leu483, red triangle) fused to the C terminus of the shaft domain with use of the natural linker between the two domains. **C)** Chimeric protein NoLinker [NoL] without the natural linker.

Linker-His and NoLinker-His [L-H and noL-H]: Chimeric protein with fragment residues Met61-Gly392 of the natural fiber and with the foldon trimerization domain (Gly457–Leu483) substituting the globular head at the C-terminal end. A 6xHis-tag was added to the N-terminal end of both Linker and NoLinker constructs. The His-tag was inserted in order to simplify the purification procedure by using a Ni-NTA column. From previous studies it was identified that degradation by proteases usually occurs at the N-terminal part of the protein⁹⁴ and not in the C-terminal, most presumably due to its folding (knob or foldon) that protects it from the protease action at the C-terminus. The His-tag was therefore inserted at the N-terminus with the rationale that could eventually stabilize the frail N-terminal ends. Moreover, even if degradation products should occur, only the intact protein would be collected by the nickel column. Furthermore the histidine tags can act as metal-binding sites and facilitate endosomal escape of the protein following the internalization into mammalian cells⁹⁵ (**Figure 16**).

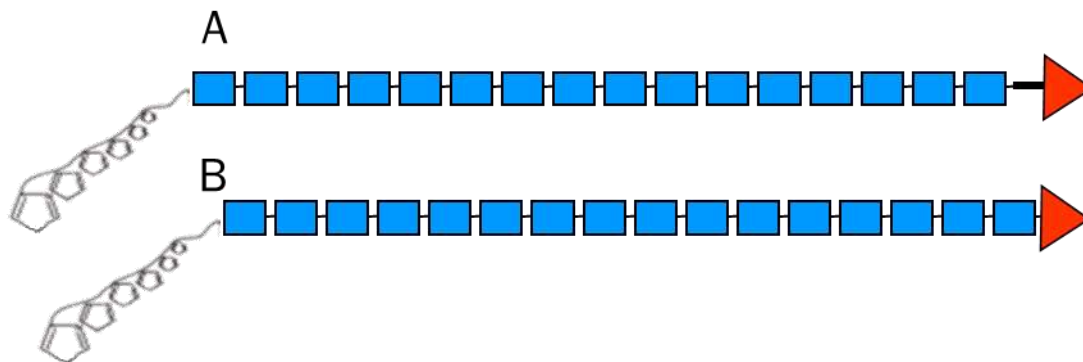


Figure 16: Schematic representation of the chimeric protein **A**) [L-His]. A His-tag was added at the N-terminal end. The same procedure was followed for the construct **B**) without the linker [NoL-His]. Residues belonging to the shaft domain (Met61-Gly392) are symbolized with blue squares and residues and the foldon domain (Gly457–Leu483) with a red triangle.

Protein Stable-Linker-His [StabL-His]: Chimeric protein with natural shaft sequence starting from Methionine 259 until Glycine 392 with the foldon trimerization motif (Gly457–Leu483). To stabilize and facilitate the purification of the construct a His-tag was added to the N-terminal end. The designed construct consists of less amino acids than the previously studied proteins starting from methionine 60, it is therefore a ‘shortened version’ of the previously described constructs. It was anticipated to be more stable, with less degradation products and could also be obtained in soluble form. These properties could increase the chances for solving its crystal structure. Also, a soluble protein construct facilitates the production and purification processes as there is no requirement to be extracted from its aggregated form within inclusion bodies through denaturation – renaturation cycles. (**Figure 17**)

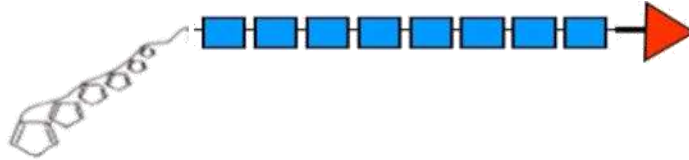


Figure 17: Schematic representation of the chimeric protein StabLH. The construct comprises the part of the natural shaft starting from Methionine 259 until glycine 392 (blue rectangles), the foldon motif (red triangle) connected with the natural linker sequence plus a His-tag in the N-terminal end.

Protein Foldon-Linker-Foldon [FLF]: Chimeric protein with fragment residues Met61-Gly392 of the natural fiber and with the foldon trimerization domain (Gly457–Leu483) incorporated at both the N- and C-terminal ends. The foldon motif was previously demonstrated that has a protective and stabilizing role.⁹⁶ The new construct has also an additional foldon and a His-tag on the N-terminal end and the natural linker sequence (Asn-Lys-Asn-Asp-Asp-Lys residues 393-398) connects the fibrin foldon domain to the shaft (**Figure 18**).

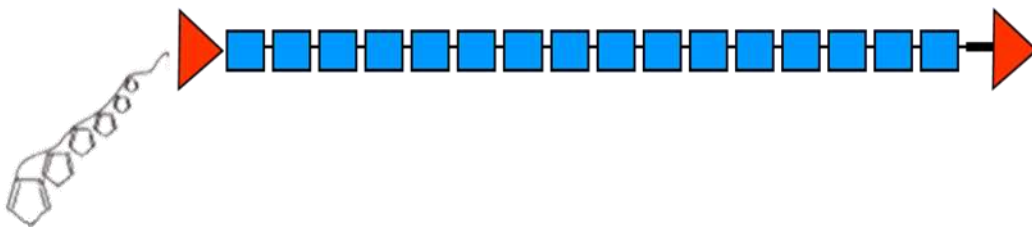


Figure 18: Schematic representation of the chimeric protein FLF (Foldon-Linker-Foldon) that is comprised by two fibrin foldon domains (fibrin residues Gly457–Leu483, red triangles) fused to the N- and C- terminus of the shaft domain. Residues belonging to the

shaft domain (Met61–Gly392) are symbolized with blue rectangles, and residues 393–398 (Asn-Lys-Asn-Asp-Asp-Lys) form the linker that connects the two parts (shaft and foldon at the C-terminal end).

Protein Linker-His-Biotin [LHB]. Chimeric protein with fragment residues Met61-Gly392 of the fiber shaft, the natural six amino acid linker and the foldon trimerization domain (Gly457–Leu483) at the C-terminal end. A His-tag was added to the N-terminal end followed by a 14-peptide biotinylation site. The biotinylation site will enable the binding of cell targeting motifs, biotinylated nucleic acids and therapeutic molecules by exploiting the strong non-covalent biotin-streptavidin bond (**Figure 19**).

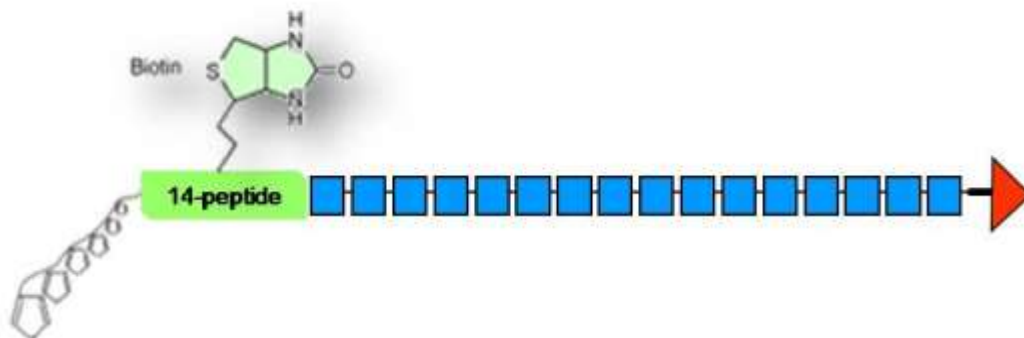


Figure 19: Schematic representation of the chimeric protein [LHB]. His-tag was added at the C-terminal end followed by a 14- peptide biotinylation site. These two sequences were connected via a sequence coding for a thrombin cutting site.

The *in vivo* biotinylation system

Due to its extremely high binding constant, the interaction between biotin and streptavidin has been exploited for a large number of biotechnological applications.

Protein biotinylation *in vivo* can be achieved by co-expressing in bacterial cells the protein of interest fused to a 14 amino acid biotinylation sequence, (G-L-N-D-I-F-E-A-Q-K-I-E-W-H) and the BirA ligase that specifically biotinylates the lysine side-chain of the protein biotinylation sequence by joining it with the carboxyl group of the biotin molecule. Advantages that are associated with the *in vivo* biotinylation in contrast to the *in vitro* biotinylation are the uniform modification of the protein that excludes the use of intervening chemistry. Additionally, there is no need to separate modified products from unreacted chains and moreover avoids the purification of the ligase enzyme from the overexpressed protein⁹⁷⁻⁹⁸(Figure 20).

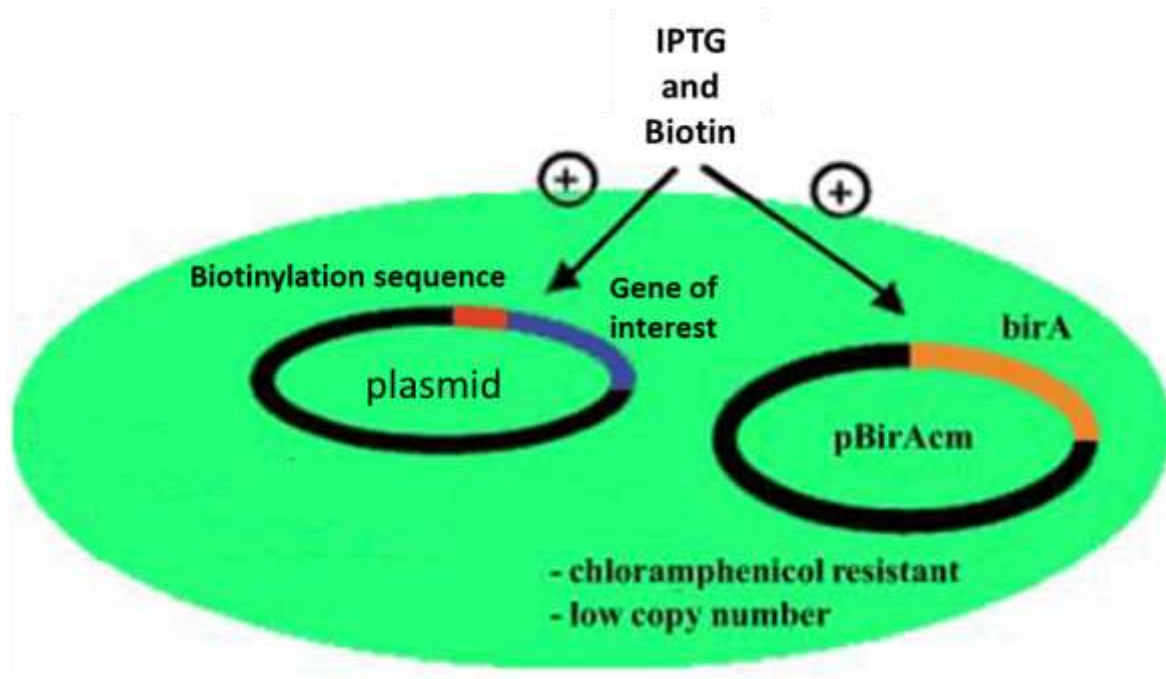


Figure 20: BL21 cells with the two IPTG inducible plasmids. The plasmid pBirAcm contain the gene of BirA biotin ligase(orange). The other plasmid contains the gene of the protein of interest to be biotinylated (blue) along with its biotinylation sequence (orange). Adapted from www.avidity.com.

Protein Linker-His-Cysteine [LHCYS]: The Linker-His [L-H] construct, as mentioned before, contains the shaft sequence (61-392), a His- tag on its N-terminal part and the natural six amino acid linker. In this construct a replacement mutation was designed where serine 350 was substituted with a cysteine. The specific position for the mutation was selected due to its location on an exposed loop (**Figure 23**). The insertion of a cysteine offers to the protein additional functionalities: formation of disulfide bonds, gold nanoparticle adhesion and interaction with maleimide initiators through the sulfydryl group of cysteine. The latter would allow the initiation of polymerization for example with polystyrene of responsive polymers (**Figure 21**). Additionally, the same replacement mutation was inserted to the LHB construct to enable also the binding of biotinylated molecules through the 14-peptide biotinylation site of the protein (**Figure 22**).

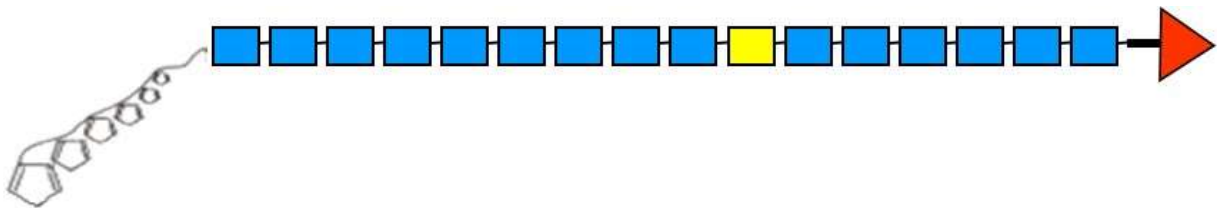


Figure 21: Schematic representation of the chimeric protein LHCYS. The new construct comprises the natural shaft starting from Methionine 60 until Glycine 392 (blue rectangles), the foldon motif (red triangle) connected with the natural linker sequence plus a His-tag in the terminal end. The exposed serine in position 350 was replaced with cysteine (yellow rectangle).

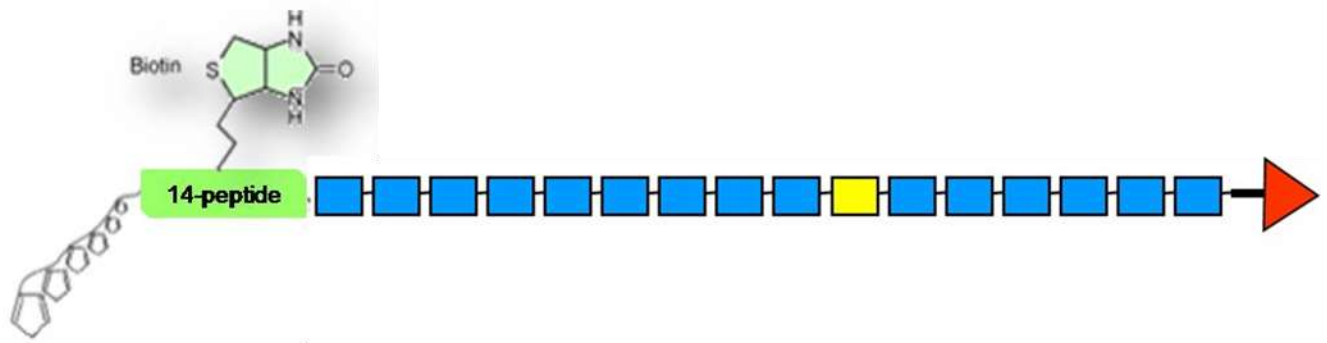


Figure 22: Schematic representation of the chimeric protein LHBCYS. The new construct comprises of the natural shaft starting from Methionine 60 until Glycine 392 (blue rectangles), the foldon motif (red triangle) connected with the natural linker sequence plus a His-tag and a 14-peptide biotinylation sequence at the N-terminal end. The exposed serine in position 350 was replaced with cysteine (yellow rectangle).

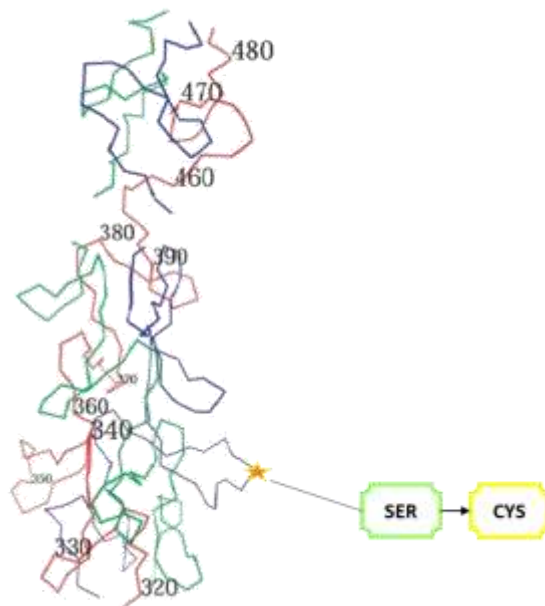


Figure 23: Representation of the Serine to Cysteine residue substitution via site directed mutagenesis. The replacement occurred in a presumably exposed loop of the adenovirus shaft sequence. The structure of the protein presented here is based on the crystallographic studies of the chimeric adenovirus fiber–fibritin foldon protein (residues 319-392).¹⁴

2. 3. MATERIALS AND METHODS

Materials

All reagents were purchased by Sigma unless otherwise stated.

Methods

Polymerase chain reaction (PCR)

PCR was conducted in order to amplify the gene of interest by simultaneously incorporating the essential restriction enzyme sites at its 5' and 3' ends, through the primers. Plasmid DNA or linear DNA containing the nucleic acid sequence of the protein of interest, is used as a template.

General Reaction for PCR :

5 μ L 10x polymerase buffer

1 μ L 100 mM MgSO₄

1 μ L 10 mM dNTP mix

1 μ L 20 μ M Forward primer

1 μ L 20 μ M Reverse primer

0.5 μ L of Deep Vent polymerase

0.5-2 μ L of DNA

H₂O up to 50 μ L

Table 1: PCR Thermocycling Conditions:

Protein Construct	Initial Denaturation	Cycles			Final Extension
L-H	95°C-5min	95°C-30s	59°C-30s	72°C-1min	72°C-5min
N-H	95°C-5min	95°C-30s	59°C-30s	72°C-1min	72°C-5min
StabL-H	95°C-5min	95°C-30s	55°C-30s	72°C-1min	72°C-5min
FLF-H	95°C-5min	95°C-30s	58°C-30s	72°C-1min	72°C-5min
LHB	95°C-5min	95°C-30s	59°C-30s	72°C-1.5min	72°C-5min
LHCYS	98°C-30s	98°C-10s	62°C-30s	72°C-30s	72°C-3.5min
LHBCYS	98°C-30s	98°C-10s	62°C-30s	72°C-30s	72°C-3.5min

Reaction for Site-directed Mutagenesis(Q5 NEB kit): Site Directed Mutagenesis is used for the insertion, deletion or substitution of up to 6 nucleotides.

1 μ L PCR product

5 μ L 2x KLD Reaction Buffer

1 μ L 10x KLD Enzyme Mix

3Ml Nuclease-free water

Double digest (cut) reaction

For a 50 μ L reaction:

10 μ L DNA

33 μ L water

The mixture was heated at 70 °C for 10 min, then cooled on ice for 1 min and spun down before the addition of the remaining reagents.

5 μ L of a 10x buffer for optimal performance (usually CutSmart® Buffer-New England Biolabs)

1 μ L of each restriction endonuclease

Dephosphorylation reaction

18 μ L vector

2.1 μ L 10x Antarctic phosphatase buffer

1 μ L Antarctic phosphatase (New England Biolabs)

Dephosphorylation was conducted at 37 °C for 15 min and the enzyme was heat-deactivated at

70 °C for 5 min. The mixture was then cooled on ice for 1 min and spun down.

Ligation reaction

50 ng dephosphorylated vector

37.5 ng insert gene

1 μ L T4 ligase (New England Biolabs)

2 μ L T4 ligase buffer

water was added to a final volume of 20 μ L

The reaction was conducted overnight at 16 °C

Plasmid isolation with mini-preps

The DH5a *E.coli* cells were transformed with 10 μ L of the ligation products. The produced colonies were inoculated O/N at 37°C in 5ml LB. Plasmid isolation followed with mini-preps. Successful cloning of the gene into the plasmid was verified by the digestion of the plasmid with the corresponding restriction enzymes and the existence of a band at the specific kb in an agarose gel.

Table 2: Protein constructs fabricated in this study

Protein Construct	Vector	Modification	Primers	Restriction Enzymes
L-H	pet28a	Addition of a 6xHis-tag at the N-terminus	FW:TATACCCGGGAATGCTTGCCTTAAAATG RV:CCGCATCGATCTATAAAAAGGTAGAAAGGAATACC CA	SmaI/ClaI
N-H	pet28a	Addition of a 6xHis-tag at the N-terminus	FW:TATACCCGGGAATGCTTGCCTTAAAATG RV:CCGCATCGATCTATAAAAAGGTAGAAAGGAATACC CA	SmaI/ClaI
StabL-H	pet28a	Construct start at Methionine-259	FW: GCGGCATATGCGTATAAATAACAACCTGTTAATTC RV: CGGGCTCGAGTCTATAAAAAGGTAGAAAGGAA	XhoI/NdeI
FLF-H	pet28a	Addition of a foldon motif at the N-terminus	FW:GCGCCATATGGGTTATATTCTGAAGCT RV: CGGGCTCGAGTCTATAAAAAGGTAGAAAGGAA	SmaI/ClaI
LHB	pet28a -biotin	Addition of a biotinylation site	FW:GGCCGAATTCATGCTTGCCTT RV: CGGGCTCGAGTCTATAAAAAGGTAGAAAGGAA	XhoI/eCoRI
LHCYS	pet28a	Substitution of a Serine with Cysteine	FW: TACAAACACATGTGAGTCTCCAG RV: TCAAACCTCCAGACCTTTC	-
LHBCYS	pet28a -biotin	Substitution of a Serine with Cysteine	FW: TACAAACACATGTGAGTCTCCAG RV: TCAAACCTCCAGACCTTTC	-

Agarose gel electrophoresis

Agarose gel electrophoresis is a method used for the separation of DNA fragments according to their size⁹⁹ and is used in order to evaluate and isolate the desired products

from PCR and cut reactions. A 1% w/v or 4% agarose in TAE buffer mixture was prepared. The mixture was heated in a microwave until agarose was dissolved. Gel red stain (GelRed™ Nucleic Acid Gel Stain, 10000x in water – BIOTIUM) was also diluted 10000-fold. The agarose gel was deposited in a horizontal electrophoresis apparatus and the apparatus was filled with 1x TAE buffer. A DNA sample was mixed with Gel Loading Dye (New England Biolabs) and loaded into the wells of the gel. A 2-log DNA ladder (New England Biolabs) was also mixed with the loading dye and loaded in the gel. An electric field of 90 V was applied until the samples entered the gel and then the voltage was increased to 120 V. Agarose gels were viewed using a UV-lamp. UV light excites the gel red stain which is bound to DNA, rendering the samples visible.

Tris-Acetate-EDTA (TAE) Buffer (50x stock): 242 g/L Tris, 18.61 g/L EDTA, pH is adjusted to 8 using Acetic Acid

Competent cell preparation (for E. coli DH5 α and BL21(DE3) and BL21(PG-KJE8))

E. coli cells were prepared in order to yield transformed colonies. A variation of the protocol described by Sambrook¹⁰⁰ was followed. For the preparation of competent cells, 5 ml of LB medium were inoculated with the desired strain and the cells were incubated overnight at 37 °C. Then 50-100 ml LB medium were inoculated with 0.5-1 mL of the overnight cultures. The cells are incubated at 37 °C with shaking at 250 rpm until the optical density at $\lambda=600$ nm (O.D.₆₀₀) was 0.4-0.6. The cultures were then centrifuged in falcon tubes at 2500 rpm for 10 min at 4 °C. Cells were gently resuspended in 15-30 ml TfbI buffer and incubated on ice for 30 min. The suspension was centrifuged again at 3500 rpm for 10 min at 4 °C and the cells were resuspended gently in 2-4 ml TfbII buffer. Aliquots of 100 μ L were transferred in pre-cooled eppendorf tubes tubes, frozen in liquid N₂ or dry ice and stored at -80 °C.

TfbI buffer: 30mM CH₃COOK, 50mM MnCl₂, 100mM KCl, 10mM CaCl₂, 15% glycerol. water was added to reach the final volume (usually a 100 mL stock solution was prepared)

TfbII buffer: MOPS pH:7 10 mM, 75mM CaCl₂, 10mM KCl, 15% glycerol

water was added to reach the final volume (usually a 100 mL stock solution was prepared)

Transformation of competent *E. coli* cells with plasmid DNA

The competent cells prepared were transfected with the plasmid DNA. A variation of the protocol described by Sambrook¹⁰⁰ was followed. An aliquot of competent cells (~100 µL) was thawed on ice and mixed with 1-10 ng of plasmid DNA. For the biotinylation of the LHB protein, an equal quantity of the pBirAcm plasmid, coding for biotin ligase, was also added. The mixture was left on ice for 30 min. A heat-shock was induced by incubation at 42 °C for 90 sec and then on ice for 2 min. After the heat-shock, 900 µL of LB medium were added and the cells were incubated for 1 h at 37°C with shaking at 250 rpm. Subsequently, the suspension was centrifuged at 2000 rpm for 2 min and most of the supernatant was removed. The pelleted cells were resuspended in the remaining supernatant (ca. 100 µL) and plated onto LB/agar plates containing the selection antibiotic(s). The plates were incubated at 37°C overnight.

Recombinant Protein Overexpression

E. coli BL21(DE3) and *E. coli* BL21 PG-KJE8 (strain with the chaperones dnaK, dnaJ, grpE, groES, groEL - for enhancement of protein folding) cells were used for recombinant protein overexpression. Precultures were prepared by resuspending a single colony from the LB/agar plates in liquid LB medium with antibiotic(s). Precultures were incubated overnight at 37 °C with shaking at 250 rpm. LB medium with antibiotic(s), ca. 25 times

the preculture volume, was then inoculated with the preculture and incubated at 37°C with shaking at 250 rpm until the optical density at $\lambda=600$ nm (O.D.₆₀₀) was 0.5-0.8 . For the biotinylation of the LHB protein, a solution containing 1.2mg biotin in 10ml of 10mM Bicine buffer pH:8 is added in the culture to reach a final biotin concentration of 12 $\mu\text{g}/\text{mL}$. Protein expression was induced with IPTG at a final concentration of 1 mM and cells were incubated at 37 °C for 4 h or 16 °C, 30 °C overnight, aerated by shaking at 250 rpm. Cells were harvested by centrifugation of the culture at 7000 rpm for 15 min. For a long-term storage of the bacterial strains, bacterial stab cultures were prepared by mixing 500 μL of a grown preculture with an equal volume of 80% glycerol. The stab cultures were stored at -80 °C.

Antibiotics used, depending on E.coli strain and plasmid vector used

Ampicillin (Sigma-Aldrich) in water (100 mg/mL)

Kanamycin (Sigma-Aldrich) in water (50 mg/mL)

Chloramphenicol (Sigma-Aldrich) in ethanol (34 mg/mL)

were diluted 1000-fold in Luria Bertani (LB) medium or LB-agar for negative selection.

Cell Lysis

After harvesting, the cell pellet was resuspended in four volumes of lysis buffer (buffer depending on the construct-**Table 3**). The lysis method includes three freeze-thaw cycles at -80 °C and 37 °C respectively, the addition of 2 mg/mL lysozyme with 1h incubation at 37°C and the addition of 1x protease inhibitor cocktail. Three more freeze-thaw cycles followed and the cell suspension was incubated for 30 min at room temperature while shaking with DNase I (Roche) at a final concentration of 100 $\mu\text{g}/\text{mL}$ as well as MgSO_4 at a concentration of 100 mM. The cell lysate is compressed in French press at 1000 psi followed by 10 x sonication cycles on ice each of 30 s sonication pulse followed by cooling intervals of 30 s. French press could only be used for culture volumes above 1L. After

lysis, the lysate is centrifuged at 7000 rpm for 30 min and the supernatant was separated from the pellet. The pellet (this step should be applied only if the protein aggregates into inclusion bodies) is 'washed' under shaking for 10min and a following centrifugation, with Urea 1M then Triton 1% and Tris-HCl pH: 9, to remove unspecific bound impurities. The resultant pellet is resuspended in the initial volume in resuspension buffer. For cultures where the protein aggregates into inclusion bodies (IB) the resuspension buffer for the pellet contains 6 M of urea to unfold the IB and is mixed overnight at 4 °C. After mixing, the remaining insoluble products were separated by centrifugation at 7000 rpm for 30 min.

Table 3: Table of Buffers

Lysis buffer	Resuspension buffer - Native -for purification into a Ni-NTA column	Resuspension buffer for inclusion bodies unfolding	Dialysis buffer
50mM Tris-HCl pH 9	20mM Tris-HCl pH 9	20mM Tris-HCl pH 9	20mM Tris-HCl pH 9 or Phosphate buffer pH:9
2mM EDTA	Imidazole 10mM	6M Urea	NaCl 0.2M
Triton 4%	NaCl 0.5M	NaCl 0.5M	
Glycerol 5%	*For purification in a non Ni-NTA column, NaCl 0.2M, and no Imidazole is used.	Imidazole 10mM	
NaCl 30mM		*	

Protein purification (Ni-NTA column, streptavidin column, Q-Sepharose column)

Cytosoluble proteins were purified from the supernatant obtained after the lysis, whereas insoluble proteins were purified from the supernatant obtained after resuspension of the pellet in 6M urea. The proteins that contained a C-terminal 6x His-tag were purified using

a Ni-NTA affinity purification column. 2 ml of bulk Ni-NTA beads was used. The beads were deposited in a gravity-flow column and the supernatant was passed three times. Then, the beads were washed with 8 volumes of two washing buffers with increasing imidazole concentration (10 and 30 mM). The protein was eluted with increasing imidazole concentration (50, 75, 100, 150, 250 and 500 mM).

Elutions and washing buffers should also contain 0.5M of NaCl to reduce binding of unspecific proteins.

Biotinylated proteins could also be purified using a streptavidin column (Streptavidin-Sepharose™ High Performance affinity column-Amersham Biosciences AB). The column was equilibrated with 10 volumes of binding buffer and the protein solution was passed three times. Subsequently, the column was washed with 10 volumes of binding buffer and with 20 volumes of elution buffer. Every 2 mL of the eluate were gathered in 2 mL-ependorf tubes and were neutralized with 200 µL 1M Tris-HCl pH 9.

Elution buffer: 8 M guanidine-HCl (GdnCl), pH 1.5

Binding Buffer: 20 mM sodium phosphate, 0.15 M NaCl, pH 7.5

Proteins that do not contain any functional group were purified by a Q-Sepharose column. This column is comprised by positively charged beads, so only the negatively charged proteins are being bound to the column. The proteins to be purified should be resuspended in a buffer with a $pH > pI$ in order to render them negatively charged. The bound proteins are eluted with increasing concentrations of NaCl (50, 75, 100, 250, 500mM). This method is not protein specific and usually another purification method is needed in combination, to get rid of impurities unspecifically bound to the column.

Dialysis

A buffer exchange was achieved using dialysis. After the purification, the elution fractions were pooled and sealed in a dialysis tubing cellulose membrane (14 kDa molecular weight cut-off). The membrane was transferred in 2 L of the desired buffer (50 mM sodium phosphate pH 9 or 50 mM Tris-HCl pH 9 and NaCl 0.2M) and dialyzed for 1h, for an exhaustive dialysis the membrane was immersed into a fresh dialysis buffer and left to additionally dialyze overnight at 4 °C. The dialyzed samples were concentrated using an Amicon centrifugal filter (10 or 30 kDa molecular weight cut-off) in order to achieve increase to protein's concentration.

Sodium Dodecyl Sulfate - Polyacrylamide Gel Electrophoresis(SDS-PAGE)

SDS-PAGE is a method used for the separation of proteins according to their molecular weight.¹⁰¹ In this study, it was used to monitor the expression of the proteins as well as their condition after each processing step (e.g. possible impurities, degradation products). SDS, boiling, and β -mercaptoethanol are used in order to denature the protein. SDS binds to the linear protein molecule and confers a uniform negative charge. Then, the proteins are loaded on the SDS polyacrylamide gel and migrate across the gel in the presence of an electric field. The migration is size-dependent; larger proteins migrate less than smaller proteins, since they cannot fit easily into the pores of the gel. In this study, the separating and stacking polyacrylamide gels were used with an acrylamide content of 7.5% or 12% and 4.5% respectively. The separating gels were prepared by mixing acrylamide with water and separating buffer. Polymerization was induced when APS and TEMED were added and the mixture was deposited between glass plates for electrophoresis. Isopropanol was added on top and the mixture was left to harden for approximately 1h. After gel polymerization, isopropanol was removed and the stacking

gel mixture was deposited on top of the separating gel. Gel combs were placed on top of the stacking gel mixture for the formation of wells. The stacking gel was also left to polymerize for 30 min and the gel was transferred in the electrophoresis apparatus, which was filled with running buffer (1x). The samples studied were mixed with loading buffer for SDS-PAGE, boiled for 5 min at 100 °C and loaded in the wells. Protein molecular weight marker (Precision Plus Protein™ Dual Color Standards – BIORAD) was also loaded in a well and electrophoresis was performed at 200 V for ca. 1h. For samples containing GdnCl, a precipitation protocol was followed before loading in the gel. An aliquot of 25 µL from each sample was transferred in 225 µL cold 100% ethanol, vortex-mixed, and left at -20 °C for 10 min. The mixture was centrifuged at 15000 g for 5 min and the supernatant was removed. The pellet was vortex-mixed in 90% cold ethanol and centrifuged at 15000 g for 5min. The supernatant was removed and the pellet was mixed in 25µL 1x loading buffer, boiled at 100 °C for 5 min, and loaded in the gel. The gels were stained with Coomassie Blue stain, which binds to protein molecules. After destaining the gels, only the protein bands remained colored.

Lower Separating buffer: 187 g/L Tris-HCl pH 8.8, 0.4% w/v Sodium Dodecyl Sulfate

Upper Stacking buffer: 60.5 g/L Tris-HCl pH 6.8, 0.4% w/v Sodium Dodecyl Sulfate

Running buffer 10x: 30.3 g/L Tris, 144.1 g/L glycine, 10 g/L SDS

Loading buffer for SDS-PAGE (For 100 mL stock 3x solution): 18.8 mL 1 M Tris-HCl pH 6.8, 6 g SDS, 15 mL β-mercaptoethanol, 30 mL glycerol, a pinch of Bromophenol blue

Western Blot

Western blot is a technique that involves the immunological recognition of a protein using monoclonal antibodies. In the present study, monoclonal anti-His and anti-biotin antibodies were used. A PVDF membrane (Westran S - Whatman) was activated by submerging in methanol. An electrophoresed polyacrylamide gel and the membrane

were sandwiched between paper and sponges soaked in Transfer buffer 1x. All these were tightly packed and submerged in the transferring apparatus, which was filled with Transfer buffer 1x. An electrical field of 35 V was applied for ca. 2.5 h for the protein transfer onto the PVDF membrane. The membrane was blocked by mild shaking in 5% w/v skimmed milk in 1x phosphate-buffered saline (PBS) for 1 h at room temperature. After blocking, the PBS-milk was removed and the membrane was soaked in a solution of PBS-milk containing the primary antibody, mouse anti-His (Qiagen) or streptavidin alkaline phosphatase from *Streptomyces avidinii* diluted 2000-fold. The membrane remained in this solution overnight at 4 °C under mild shaking. The next day, the membrane was washed three times by shaking for 15 min in a solution of 1x PBS with 0.04% Tween 20. Then, the membrane was washed again with PBS-milk and soaked in a solution of PBS-milk containing the secondary antibody (anti-mouse IgG-alkaline phosphatase) diluted 20000-fold. The membrane remains in the solution of the secondary antibody for 2 h at room temperature under mild shaking. After the addition of the secondary antibody, the membrane was washed three times by shaking for 15 min in PBS-Tween 20 and then quickly washed with 1x alkaline phosphatase buffer. The protein bands detected by the antibodies were colored when 176 μ l/10ml NBT-BCIP in 1x alkaline phosphatase buffer was added. Alkaline phosphatase dephosphorylates BCIP which in turn reacts with NBT to form an indigo-blue precipitate. For biotin identification the antibody streptavidin alkaline phosphatase needs only one hour incubation in room temperature and subsequent wash with PBS-Tween 20 and 1x alkaline phosphatase buffer, followed by the NBT-BCIP color detection.

Transfer buffer 1x (18.8g/L glycine, 3g Tris).

Dot Blot

In a strip of a PVDF membrane, are blotted 10 μ l of different concentrations of recombinant protein or 10 μ l of 100 μ g/ml of primary antibody onto membrane. The membrane is incubated 1 hour at room temperature. The membrane and the spots should be dry before proceeding to the next step. The membrane is blocked with 5% dry milk in TTBS (50 mM Tris, 0.5 M NaCl, 0.05% Tween-20, pH 7.4) for 1 hour at room temperature. Block buffer is removed after this period but the membrane should be kept wet at all times for the remainder of the procedure. Incubation of the membrane with primary antibody for 1hr at RT in TTBS (anti-His or streptavidin alkaline phosphatase). The membrane is washed 3 times (10 minutes each) in TTBS on rocker. Incubation of the membrane with secondary antibody(anti-goat-alkaline phosphatase) for 1 hour at room temperature in TTBS.(for streptavidin-AP this step and the following are skipped). 3 times washes (10 minutes each) of the membrane in TTBS on rocker. Chemiluminescent detection with the 176 μ l/10ml of BCIP-NBT.

Cell internalization of the proteins and protein conjugates

All cell lines were cultured at 37°C, 5% CO₂ in DMEM (Gibco) supplemented with 10% fetal bovine serum (Gibco) and 50 μ g/ml gentamycin. 5x10⁴ HeLa, HEK293T or fibroblast NIH3T3 cells were seeded for 24h in a 24 well plate after addition of a 13mm TC Coverslip at the bottom of the well. The culture medium (DMEM) was replaced and 50-100 μ g of the protein or protein-conjugate, diluted in 0.5ml DMEM, was added for overnight incubation. Culture media was aspirated and the cells were carefully washed two times with PBS 1x. The cells were fixed with 4% formaldehyde for 15min, washed with PBS 1x and permeabilized for 5 min with 0.1% Triton X-100. After washing twice with PBS 1x and incubating for 30min with BSA2%-PBS 1x, the cells were treated with the staining

solution containing the AlexaFluor 680 Phalloidin dye. Two additional washing steps with PBS 1x followed before the coverslip was mounted on a microscope coverslip containing a drop of the DAPI nuclear staining dye. The internalization and subcellular localization of the stained pDNA was assessed in a Leica SP8 inverted confocal microscope at ex/em 679/702 nm for the AlexaFluor 680 Phalloidin dye, ex/em 488/520nm Fluorescein-protein conjugate and ex/em 360/460nm for DAPI nucleus stain.

MTT cell proliferation assay

Cell viability in the presence of the peptides was studied by monitoring the conversion of Thiazolyl Blue Tetrazolium Bromide reagent (MTT) into formazan by the mitochondrial dehydrogenases of the living cells. Fibroblast cells with concentrations of 7×10^3 cells/well were cultured in a 96-plate for 24h. Removal of the medium was followed by treatment of the cells with increasing concentrations (10-800 μ g) of the protein, suspended in a total volume of 200 μ l of culture medium. Cells which were not treated with the peptide, served as control. After 48h incubation, the medium was carefully removed and replaced with 100 μ l of fresh medium and 10 μ l of MTT (5mg/ml) was dissolved in PBS 1x. The cells were incubated for 4 h to allow the development of the purple formazan products and the MTT-culture medium was substituted with 100 μ l of isopropanol-DMSO 1:1 solution. The formazan crystals were allowed to dissolve for 15min at 37°C. The absorbance was measured at 570nm in a Synergy HTX BioTEK Plate Reader.

TEM

Transmission Electron Microscopy was used to observe protein molecules after purification as well as protein nanostructures. A sample solution of 8 μ L was deposited

onto a copper grid covered with formvar or carbon/formvar. The sample solution was left onto the grid for 2 min and the excess solution was removed using a filter paper. Subsequently, 8 μL of 1% Uranyl acetate (for sample $\text{pH} \leq 7$) or Phosphotungstic acid (for sample $\text{pH} > 7$) negative stain was applied, left for 2 min and the excess solution was removed using a filter paper.

Protein labeling with NHS-fluorescein

N-Hydroxysuccinimide (NHS)-ester Fluorescein is a simple and common labeling reagent for labeling proteins. It reacts efficiently with primary amino groups ($-\text{NH}_2$) in pH 7-9 buffers and forms stable amide bonds. Proteins generally have several primary amines in the side chain of lysine (K) residues that are available as targets for NHS-ester reagents. Buffers that contain primary amines (e.g., Tris or glycine) are not compatible with NHS-Fluorescein because they react with the NHS-ester moiety and compete with the intended reaction. When conjugating antibody with NHS-Fluorescein, a 15- to 20-fold molar excess of the fluorescent dye is optimal.

Labeling Reaction:

1. Dissolve 1mg of NHS-Fluorescein with 100 μL of DMF or DMSO.
2. Calculation of the appropriate amount of Fluorescein and protein.

Calculate millimoles of NHS-Fluorescein labeling reagent to add to the reaction:

$$\text{mL protein} \times \frac{\text{mg protein}}{\text{mL protein}} \times \frac{\text{mmol protein}}{\text{mg protein}} \times \frac{15 \text{ mmol NHS - Fluorescein}}{\text{mmol protein}} = \text{mmol NHS - Fluorescein}$$

Calculate microliters of NHS-Fluorescein solution to add to the reaction:

$$\text{mmol NHS - Fluorescein} \times \frac{473.4\text{mg}}{\text{mmol NHS - Fluorescein}} \times \frac{100 \mu\text{L}}{1\text{mg}} = \mu\text{L NHS - Fluorescein}$$

- 15 = Molar excess of NHS-Fluorescein to protein
- 473.4 = Molecular weight of NHS-Fluorescein
- 100 = Microliters of solvent in which the 1mg of NHS-Fluorescein is dissolved

3. Mixing and incubation at room temperature for 1 hour or on ice for 2 hours.
4. Removal of the non-reacted NHS-Fluorescein by dialysis and storage of the labelled protein at 4°C.

Protein conjugation with Nanoparticles NPs

Protein conjugation with Ni-NTA NPs through the His-tag

The 5 nm Ni-NTA NPs (Nanogold) are designed for the detection or localization of Histidine (His)-tagged recombinant proteins in multisubunit protein complexes, tissue or cell samples using transmission electron microscopy (TEM). The labelling can occur under both non-denaturing and denaturing conditions.

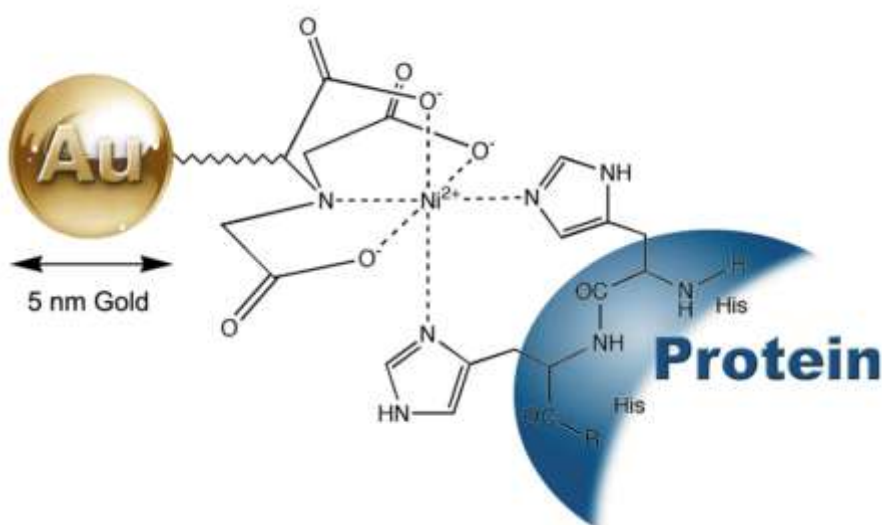


Figure 24: Interaction between a His-tagged protein and 5 nm Ni-NTA-Nanogold®

Labelling Reaction:

1. The protein should be prepared ideally at pH:7-9 (20 mM Tris at pH 7.6 with 150 mM NaCl).
2. Incubation of the protein with 10 molar excess of 5 nm Ni-NTA-Nanogold® for 30 minutes at room temperature or 4°C.
3. Remove the unbound gold nanoparticles from labeled protein conjugates centrifugation or dialysis.
4. Load gold labeled protein complex on a carbon coated EM grid and observe under TEM

Protein Labelling with Alexa Fluor® 594 Fluoronanogold-Streptavidin NPs

AlexaFluor594 FluoroNanogold-Streptavidin consists of a streptavidin protein conjugated to AlexaFluor 594 dye (red) and the 1.4 nm Nanogold® particle. The combination of the fluorescent and the gold nanoparticle, allows imaging of the same exact structure in both TEM and confocal microscopes.

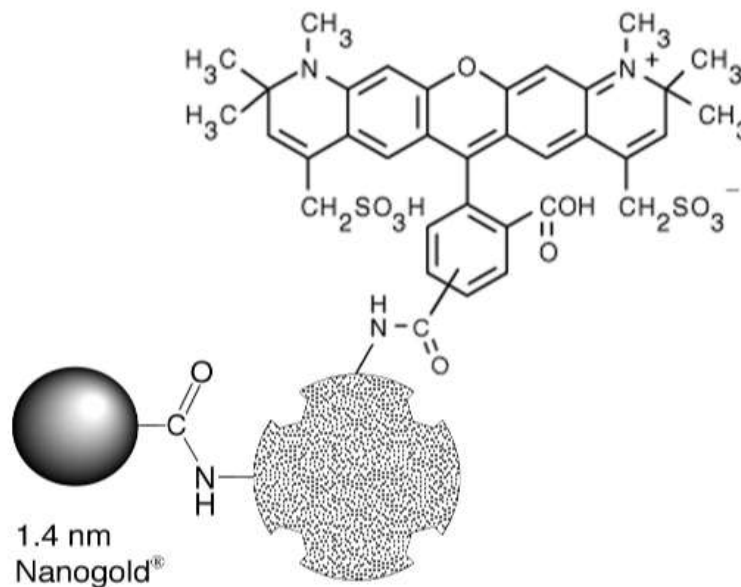


Figure 25: Streptavidin covalently conjugated to AlexaFluor®594 and Nanogold® to give Alexa Fluor® FluoroNanogold™ - Streptavidin.

Labelling process:

Incubation with the appropriate concentration of biotinylated protein for 1 hour at room temperature. The biotinylated protein can also be stained with NHS-fluorescein(green). Removal of NPs excess with dialysis in Amicon concentration tubes. Incubation with the cell line of interest for 24h hours and a final stain of the cells with nuclear dye Hoechst 33342, fixation with paraformaldehyde and observation of the protein-NP conjugate with confocal microscopy.

2. 4. RESULTS

All protein constructs were designed with molecular cloning techniques and produced with bacterial overexpression. The purification was performed for the majority of the proteins under denaturing conditions that were followed by refolding through dialysis. Each protein construct was modified to improve specific protein properties like stability, reduced degradation products or high protein production, or serve a specific purpose and application. Results will be recited according to each protein construct.

Proteins Linker [L] and NoLinker [NoL] 

The chimeric proteins with fragment residues Met61-Gly392 of the natural fiber and with the foldon trimerization domain (Gly457–Leu483) substituted at the C-terminal end instead of the native globular head were designed and cloned by Dr. Papanikolopoulou (ref²⁰) The proteins were overexpressed and purified in order to verify their ability to self-assemble into the stable trimeric form and adopt a nanorod conformation.

Overexpression of the chimeric proteins

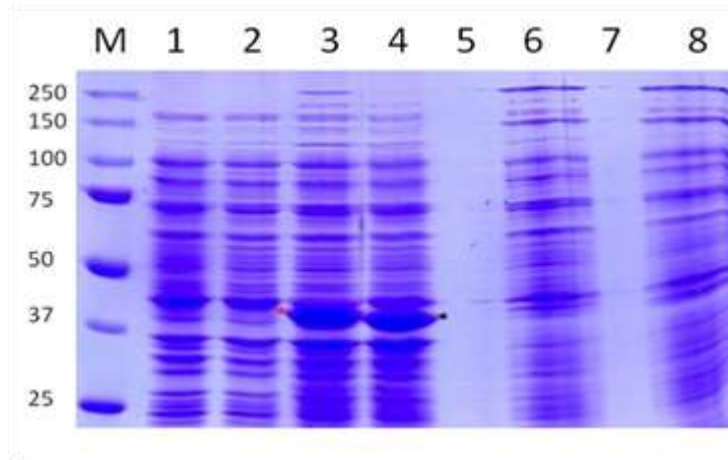


Figure 26: Overexpression of chimeric proteins [L] and [NoL] before and after induction with IPTG. Lanes: M: protein markers, 1+2: proteins[L] and [NoL] accordingly before induction with IPTG, 3+4: proteins [L] and [NoL] after 4 hours of the induction. The samples are boiled at 100°C for 5min before loading. At ~40kD a discrete band is observed for both proteins which confirms that the proteins are overexpressed. The red asterisk indicates the band of L which is slightly higher than the band of NoL (black asterisk). The mobility difference of the two bands which is due to the presence of the linker, is clearly observed. 6+8: Protein [L] and [NoL] after 4h of induction without boiling the sample. The monomeric bands disappear and two new bands appear at around 150 and 250kD. In the presence of SDS and upon boiling at 100°C, the full length protein starts to unfold from its N-terminus end.¹⁸ This result suggests that the two proteins [L] and [NoL] must adopt a trimeric form and unfold to the monomer form only upon boiling. Therefore, the foldon functions successfully as a trimerization motif for these constructs.

Inclusion bodies lysis and purification under denaturing conditions.

After cell lysis the proteins are located in the remaining pellet, indicating that they were folded, aggregated and stored into inclusion bodies.

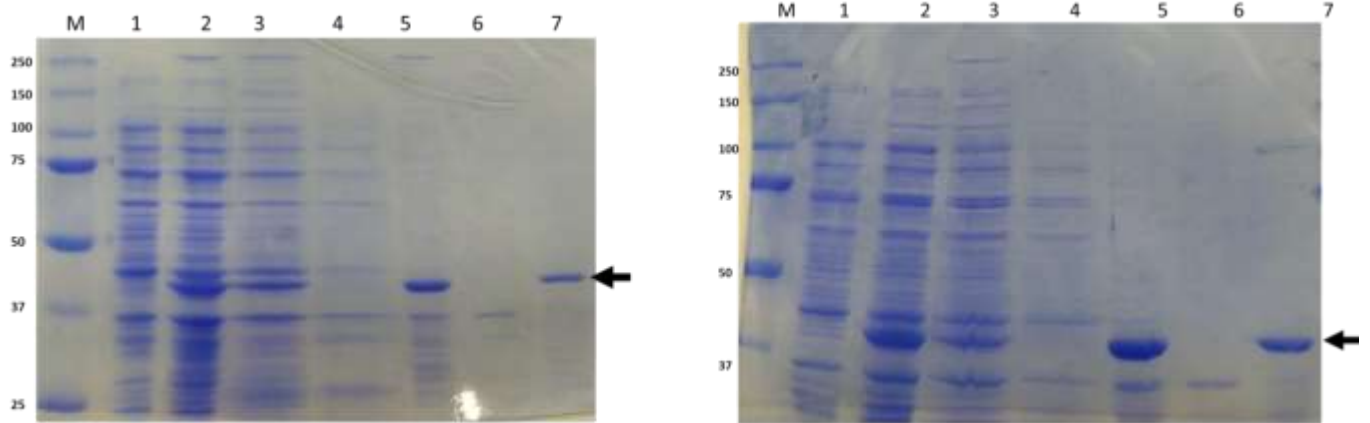


Figure 27: Cell lysis and Inclusion bodies' washes. Left Gel for the Linker protein and Right Gel for NoL protein.

Lanes

M: protein markers

1: 0h before IPTG induction

2: overexpressed 4h after IPTG induction

3: protein lysate

4: supernatant after centrifugation of the lysate

5: pellet after centrifugation of the lysate

6: supernatant after pellet washes

7: pellet after washes

Cell lysis is complete and protein is clearly located into the inclusion bodies pellet. To retrieve the proteins in their trimeric form, the inclusion bodies aggregates comprised by the protein should be denatured by Urea, purified and refolded after dialysis to remove the denaturing agent.

Striking observation: although in the pellet, the proteins remain in their trimeric form which means that partial unfolding and aggregation probably drives the partially trimeric chains to aggregate and form a pellet. This hypothesis is further corroborated from the observation of lower molecular mass bands than the monomer, indicating that,

to some extent, the partially unfolded chains get digested by proteases during the expression and / or post lysis steps (see below).

Purification of the protein with a Q-Sepharose column

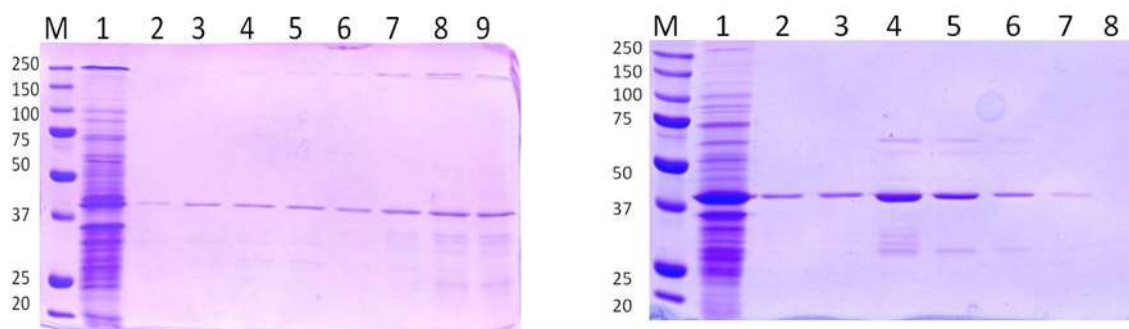


Figure 28: (Left) Purification of protein [L] with Q-sepharose column. Elution of the protein with increasing concentrations of NaCl. The protein was eluted at 50-100mM NaCl. **Lanes:** M: protein markers, 1: Supernatant of the protein after cell lysis with Urea 6M. 2-5: elution fractions of the protein at 50mM NaCl. 6-9: elution fractions of the protein at 100mM NaCl.

(Right) Purification of protein [NoL] with Q-sepharose column. Elution of the protein with increasing concentrations of NaCl. The protein was eluted at 50-100mM NaCl. **Lanes:** M: protein markers, 1: Supernatant of the protein after cell lysis with Urea 6M. 2-8: elution fractions of the protein at 100mM NaCl.

Dialysis and protein refolding into its trimeric state

Exhaustive dialysis followed the purification for both proteins in order to remove urea and to change the buffer to 20mM phosphate pH:7. Excess of protease inhibitors was used in order to inhibit protein degradation due to possible recovery of the protease activities during the removal of urea-which keeps them unfolded and inactive.

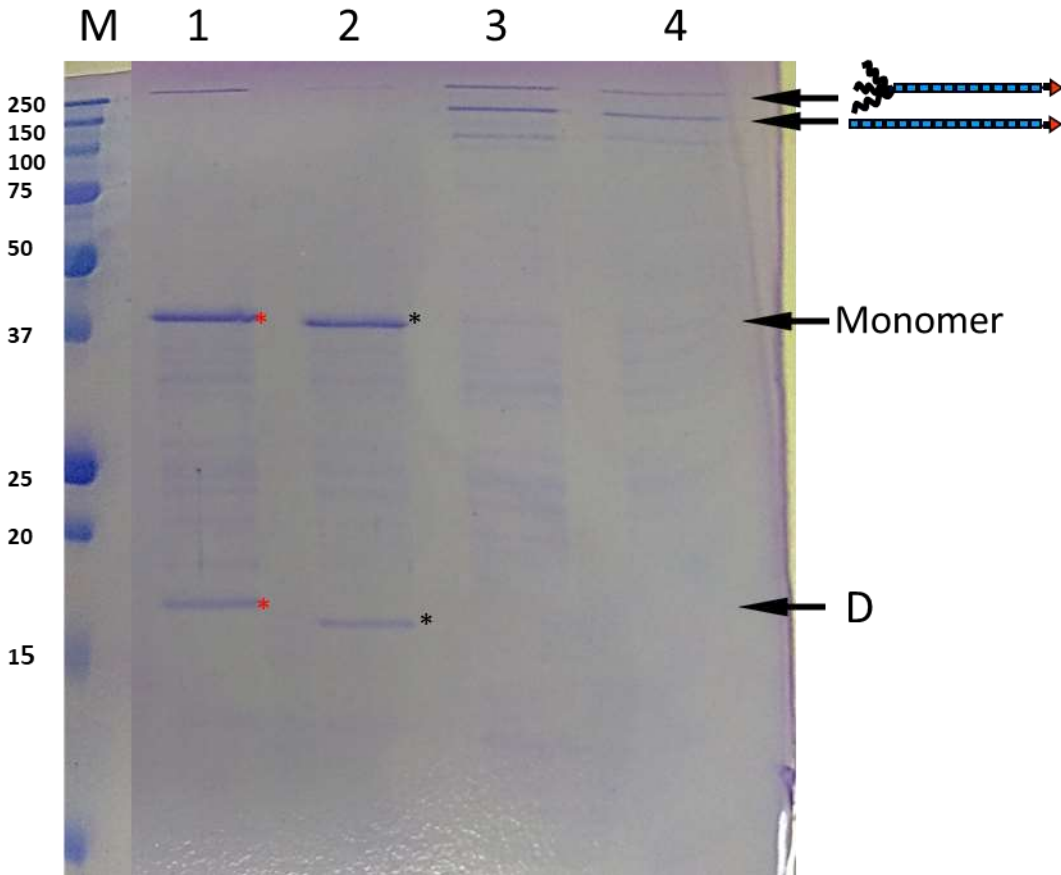


Figure 29: Refolding of the proteins after Dialysis. Protein [L](red asterisk) is detected higher than [NoL](black asterisk), at 38.3kDa and 37.5kDa accordingly. The partially unfolded trimer migrates higher in the SDS-PAGE gel than the correctly trimerized protein. Below the monomer protein bands are detected the degradation products of the same proteins which must be a result of the protease activity during protein overexpression and cell lysis.

Lanes:

- 1: protein markers
- 2: protein[L] dialysed, boiled
- 3: protein[L] dialysed, unboiled .
- 4: protein[NoL] dialysed, boiled
- 5: protein[NoL] dialysed, unboiled

The difference in molecular mass between the two constructs is attributed to the presence or absence of the six amino acid natural linker that connect the shaft segment with the trimerization motif. At lower molecular weights between 15-20kDa one extra band is detected that corresponds to a shorter version of the protein, whose amino acid sequences were most probably truncated by proteases (degradation products). Furthermore, at lanes 3 and 4 two bands are detected at 250 and 150kDa that represent the folded and trimeric version of the proteins (arrows). The presence of the highest band at 250kDa is attributed to a partially unfolded and expanded conformation of the folded protein due to SDS (termed “umbrella effect”).

Proteins L and NoL are adopting a nanorod conformation.

Both proteins seem to form rods as was observed with TEM observation (**Figure 30** and **Figure 31**).

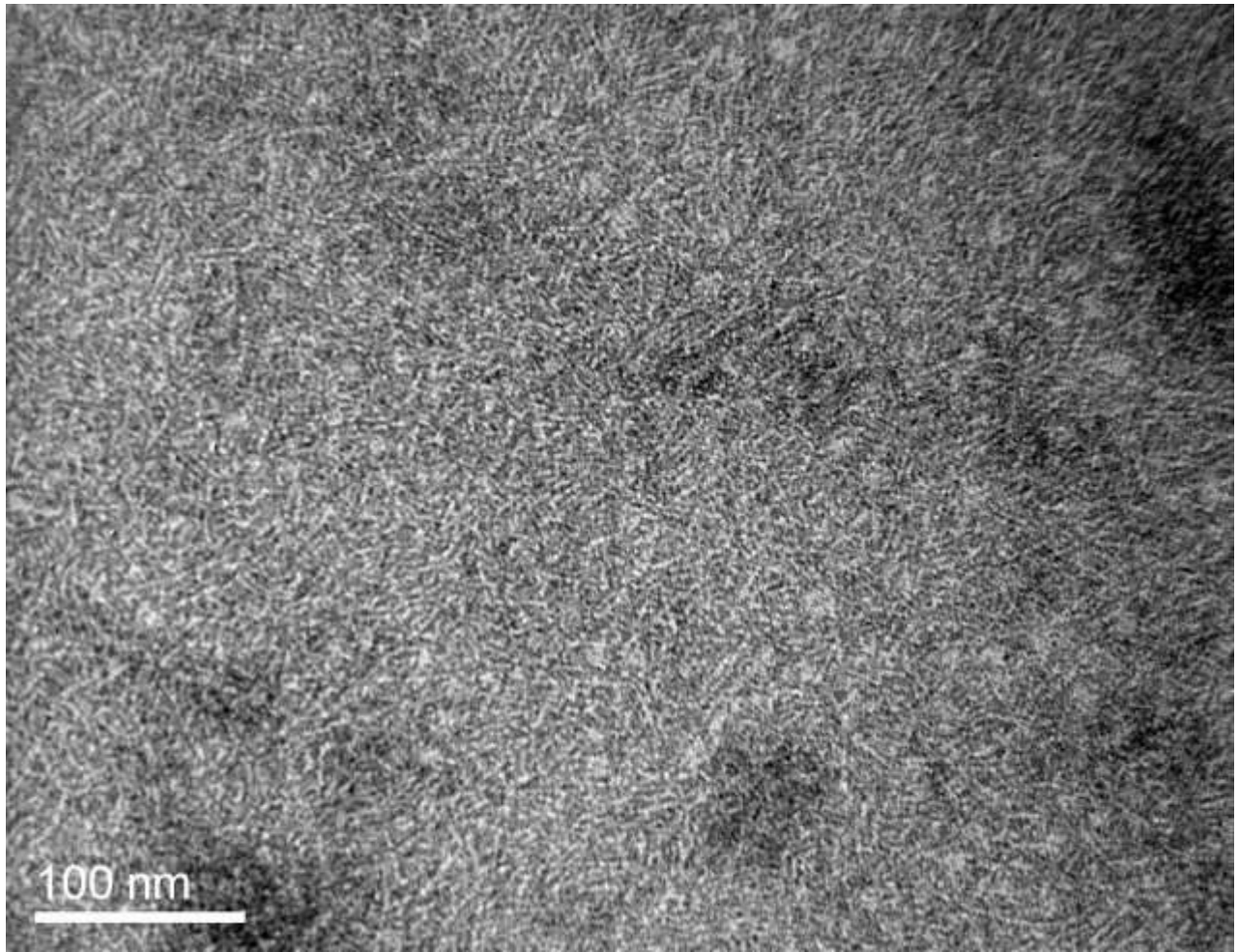


Figure 30: TEM picture of concentrated, purified and folded protein [L]. Nanorods are distinguished indicating that the protein must adopt a trimeric conformation.

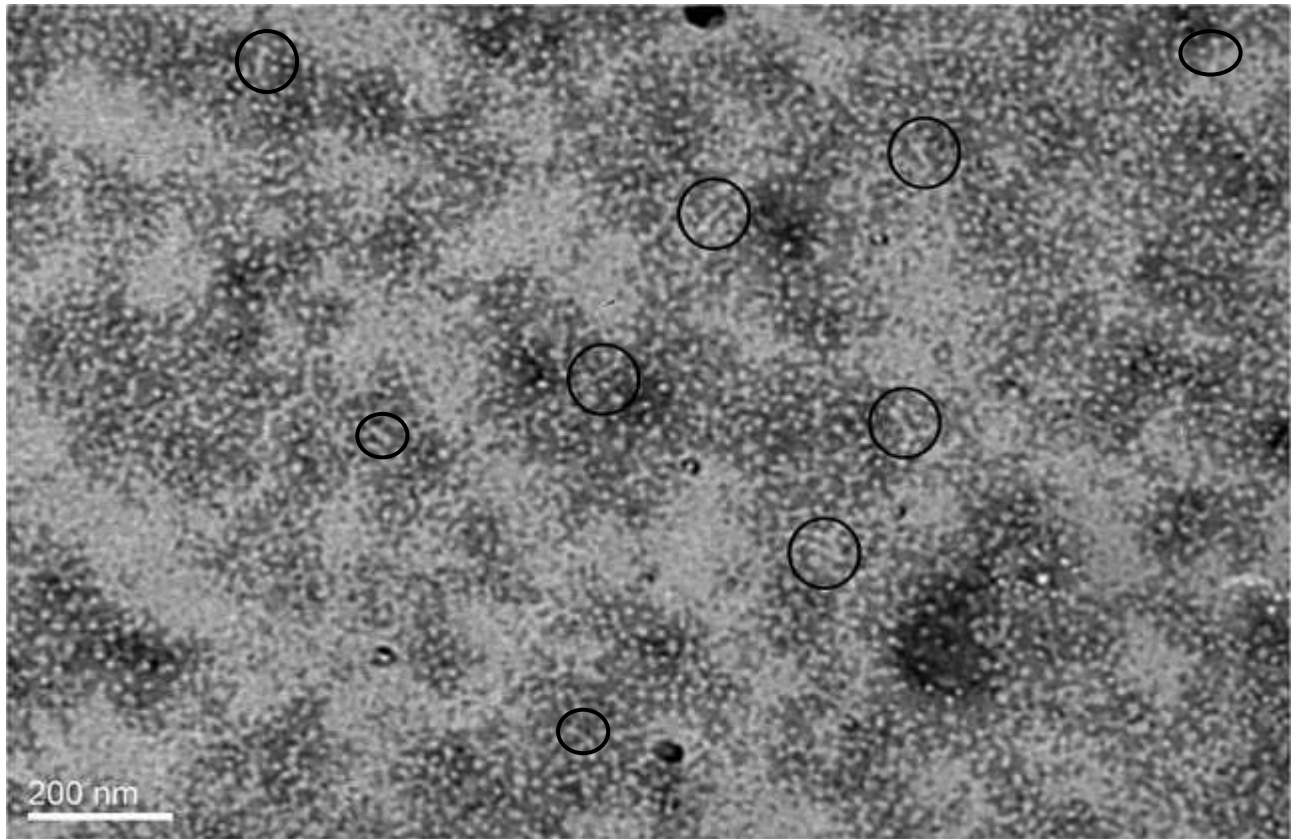


Figure 31: TEM picture of purified protein [NoL] diluted in water at 1:10. There are many visible nanorods (some of them are marked with black circles) indicating that the protein must adopt a trimeric conformation. Further observations should be made with more diluted protein samples for optimal pictures.

The above TEM images suggest that the shaft sequences retain their capacity to fold into their native beta-spiral fibrous fold when fused to the fibrin C-terminal trimerization motif.

Through the foldon addition at the C-terminus, we achieved increased overexpression of the protein compared to the native fiber protein with the globular head, although the production of degradation products could not be avoided even if protease inhibitors were used throughout the protein manipulation. It was deduced that the protein may be affected by proteases and being truncated at the very beginning or during the protein

overexpression. The same problem was noted with the shaft segment alone which contained no trimerization motif (Met61-Leu392)- in Ariadni Prigipaki's PhD Thesis¹⁰². The extra bands migrating below the monomer molecular mass were confirmed with amino acid sequencing to be a shorter version of the protein processed in its N-terminus. Taking this into account, we hypothesized that inserting a Histidine – tag at the N-terminus might convey decreased sensitivity to proteases, therefore proceeded to fabricate these constructs.

Linker-His [L-H] and NoLinker-His [NoL-H]



Overexpression of the chimeric proteins L-His and NoL-His

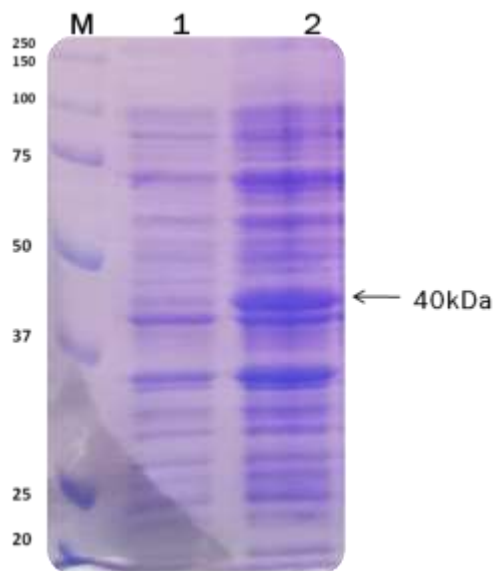
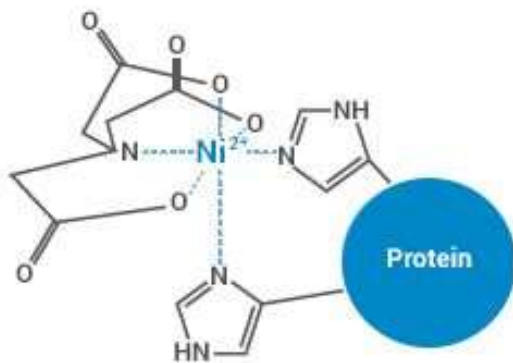


Figure 32: Overexpression of the chimeric proteins [L-His] before and after induction with IPTG (boiled). Lanes: M: protein markers, 1: protein[L-His] before induction with IPTG, 2: protein after 4 hours of the induction (boiled sample at 100°C for 5min. Same results also apply for NoL-H. At ~40kD a discrete band is observed for both proteins [L-H & NoL-H] which confirms that the proteins are overexpressed.

Purification, refolding and trimerization control of the constructs Linker-His and NoLinker-His

The stages that followed the protein overexpression were the following:

- Purification with the use of Urea in a Nickel-NTA column.
- Dialysis for the removal of Urea, Imidazole and salts.



The results of the above procedures are summed up in the following polyacrylamide gel.

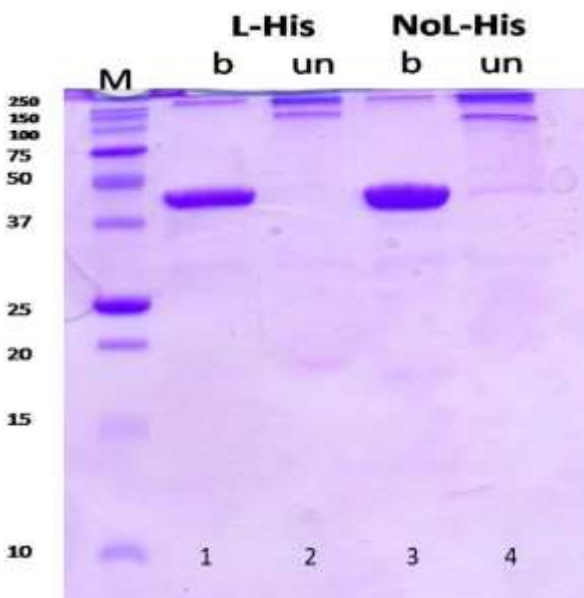


Figure 33: Linker-His and NoLinker-His refolding into their trimeric conformation after dialysis.

In Lane 1 and 3 is distinguished the purified protein at 40kDa after boiling at 100°C. (A procedure which in combination with SDS unfolds the protein to its monomers). No other proteins were detected which confirms the successful purification of the protein.

In Lanes 2 and 4 the band at 40kDa disappears with concomitant appearance of two thinner but higher molecular weight bands between 250 and 150 kDa. The same protein samples were loaded but without boiling. Therefore the successful trimerization of the proteins was confirmed. Moreover, no lower molecular mass bands are observed underneath the boiled samples, (in comparison to Figure 29). From these results it is evident that the chimeric proteins Linker-His and NoLinker-His are able to adopt their trimeric conformation with no proteolytic degradation products. Therefore, the addition of a His-tag at the N-terminus ends indeed stabilizes against “frailing” of this end and proteolytic degradation.

Foldon-Linker-Foldon with 6xHis-tag (FLF-His)



This construct was amplified with an additional “foldon” motif for potentially increasing its stability against unfolding and/or against proteases.

Overexpression of the chimeric protein FLF-H (Foldon Linker Foldon with His-tag) and cell lysis.

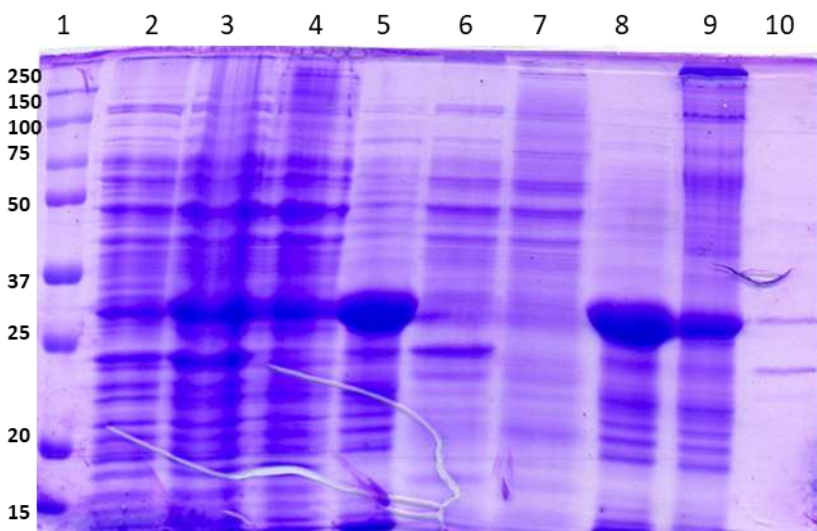


Figure 34: Overexpression of the chimeric protein FLF-H before and after induction with IPTG (boiled and unboiled). Cell lysis of the FLF-H. Lanes: 1: protein markers, 2: protein [FLF-H] before induction with IPTG, 3: protein [FLF-H] after 4 hours of the induction (boiled sample at 100°C for 5min.4: protein [FLF-H] after 4 hours of the induction (unboiled sample). 5: pellet after cell lysis, boiled, 6: supernatant after cell lysis, boiled.7: supernatant after cell lysis, unboiled sample) 8: washed pellet, boiled. 9: washed pellet, unboiled. 10: supernatant,boiled.

At ~40kD an intense discrete band is observed which confirms that the protein is indeed overexpressed.

Purification of FLF-H protein with Ni-NTA column

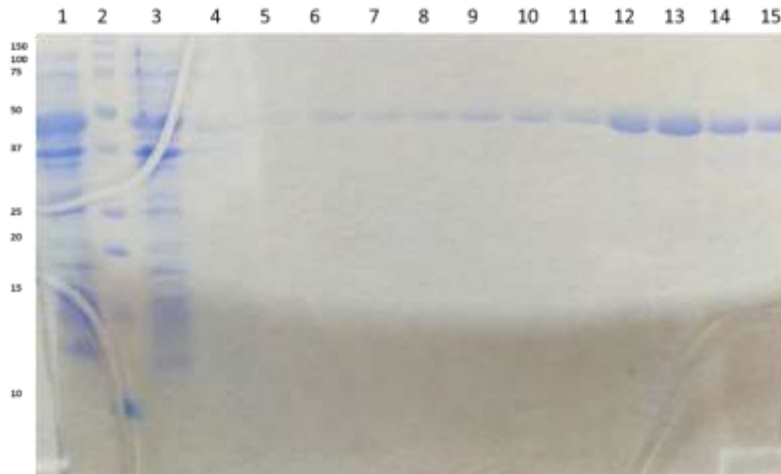


Figure 35: Affinity Purification of the protein through the interaction of its His-tag with the Ni-NTA beads

Lane 1: Supernatant after cell lysis

Lane 2: Protein markers

Lane 3: Flow-through

Lane 4&5: Wash

Lane 6-15: Elution with increasing concentrations 50-250mM of Imidazole.

Proper Refolding of FLF-H

Chimeric protein FLF, (one foldon on each end) was tested whether it was able to trimerize properly following in vitro refolding. The protein FLF previously unfolded and in the monomeric state, was able to fold successfully in its trimeric state.

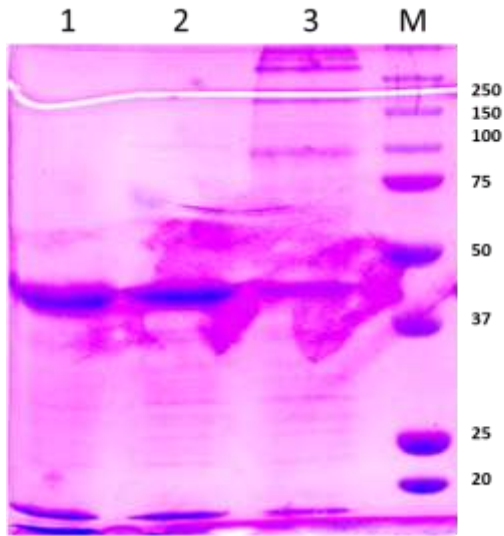


Figure 36: Refolding studies of FLF-H. SDS electrophoresis were performed in the cold room with sample buffer containing 0.1% SDS. **1:** Protein after purification and before dialysis **2:** refolded protein after dialysis, boiled **3:** refolded protein after dialysis, unboiled, **M:** protein markers

The addition of an extra fibrin foldon at the N-terminal end seems therefore to have a protective and stabilizing role.

Protein construct StabL-H



The designed clone consists of less amino acids starting from Met259 than the previously studied proteins starting from methionine 60. It was anticipated to be more stable and offers the following advantages that were confirmed after repetitive experiments: It can be obtained in soluble form as it is located partly in the supernatant after lysis. That increases the chances for solving the crystal structure of a construct. We obtain predominantly one band at approximately 100kDa for the trimer in the gel

electrophoresis and that may indicate that this construct may be more stable than the longer ones. Also, the fact that it is more soluble allows to remove some steps in the production and purification procedure as we no longer need to extract the protein from inclusion bodies through denaturation – renaturation cycles. Moreover, no harsh conditions are used for the manipulation of the protein such as denaturing agents (urea, guanidine hydrochloride).

Overexpression of the chimeric protein StabLH and localization in the cell lysate

The protein was coexpressed with the chaperones dnaK-dnaJ-grpE-groES-groEL that are encoding in the plasmids incorporated in BL21 strain PG-KJE8. These chaperones enhance the chances of a proper folding of the protein right after its synthesis in the cell. It was overexpressed at 30°C for 20h and induced with 1mM IPTG. Overexpression at lower temperatures in combination with the help of chaperones increases the solubility ratio of the protein in the bacterial cell.

Western Blot is performed for the protein in order to define its ability to retain its trimeric conformation and examine its solubility.

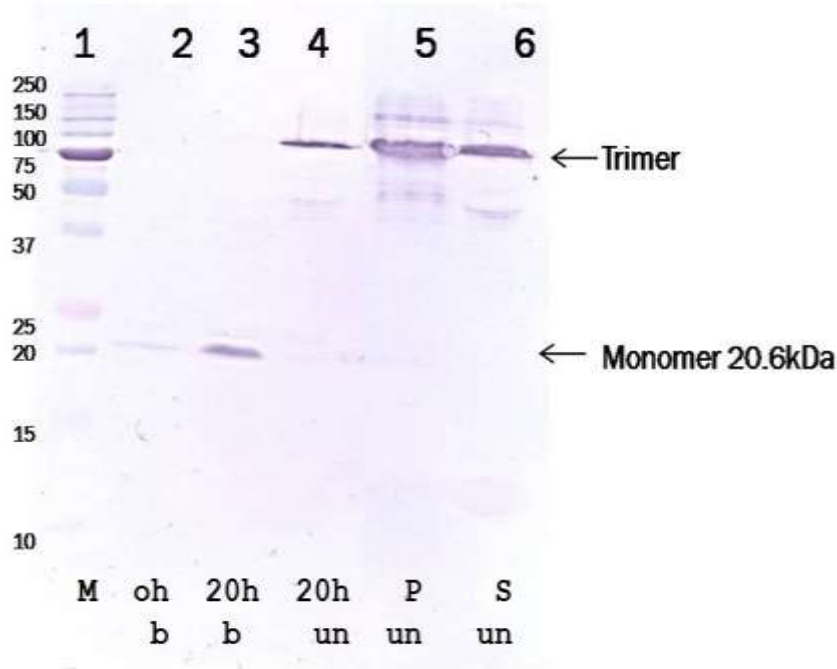


Figure 37: Western blot. Overexpression and lysis of the chimeric protein [StabLH] before and after induction with IPTG (boiled and unboiled). Protein is distributed in pellet and supernatant after lysis with French press and lysozyme.

Lanes:

- 1) protein markers
- 2) protein[StabLH] before induction with IPTG
- 3) protein after 4 hours of the induction (boiled sample at 100°C for 5min. At ~20kD a discrete band is observed which confirms that the protein is overexpressed.
- 4) protein after 4 hours of the induction (unboiled sample)
- 5) pellet after lysis, unboiled
- 6) supernatant after lysis , unboiled

The protein is overexpressed at ~20kDa (lane 3). It adopts its trimeric formation as observed by the absence of the band in lane 4. Also, the protein with seems to exist both in soluble and insoluble form after cell lysis (lane 5 and 6). Moreover, the His-tag could have a protective role since no degradation products are observed in lower molecular masses

Purification, dialysis and trimerization of the construct StabLH

The stages that followed the protein overexpression were the following:

- a. Purification with the use of Tris-HCl 50mM pH :9, NaCl 0.5M and increasing concentrations of imidazole in a Nickel-NTA column.
- b. Dialysis for the removal of Imidazole and NaCl.

The results of the above procedures are summed up in the adjacent polyacrylamide gel.

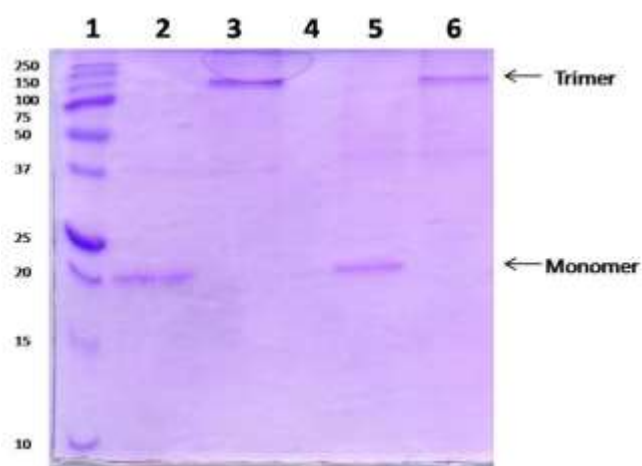


Figure 38: Refolding of StabLH

Lane 1 :markers

In Lane 2 and 5 is distinct the purified protein at 20kDa after boiling at 100°C, procedure which in combination with SDS unfolds the protein to its monomers. No other proteins were detected which confirms the successful purification of the protein. The difference in those two lanes is that the stabLH protein is expressed in different *E.coli* strains, in the first case the protein is coexpressed with chaperones while in the second in their absence. Nonetheless the results after purification and dialysis are the same.

In Lane 3 and 6 the band at 20kDa is shifted in one higher molecular weight band at around 100kDa. The protein sample loaded is the same but without boiling. Therefore, the trimerization of the protein was confirmed.

From these results it is evident that the chimeric protein seems to keep its natural trimeric conformation and would form stable nanorods which ideally can be crystallized. This would subsequently lead to their structure analysis.

Attachment of the stabLH with gold nanoparticles coated with Nickel-Nitrotriacetic acid through its His-tag tail.

The purified protein was incubated with the nanoparticles for 1 hour in the cold room (4°C) under smooth shaking. The sample was centrifuged in a concentration falcon with cut off of 30kDa for 30 min. In this way all the unattached nanoparticles (5nm) will be removed as well as all the protein molecules that are in their unfolded state (20kDa).

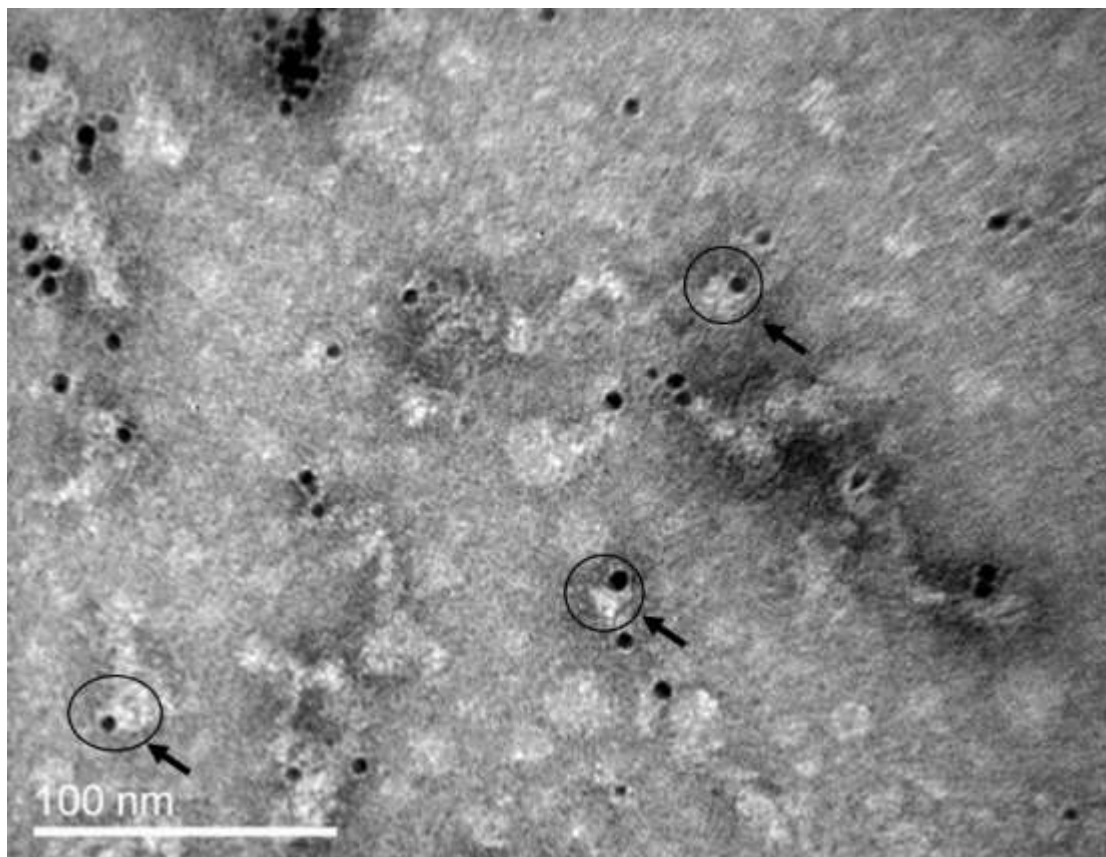


Figure 39: Transmission electron microscopy picture of the protein StabLH in conjugation with Ni-NTA nanoparticles. The black spots are the nanoparticles and the white parts are protein molecules attached to the nanoparticles.

The binding of the protein with the metal coated gold nanoparticles further suggests that the protein contains a functional metal binding site through its His-tag.

Protein construct Linker-Histag-Biotinylation site (LHB)



In this protein construct were engineered a combination of functional groups such as: a foldon domain at the C-terminus for enabling correct trimerization, a His-tag for stabilization of the N-terminus and a 14-peptide that enables binding with biotinylated molecules.

Overexpression of the chimeric protein LHB

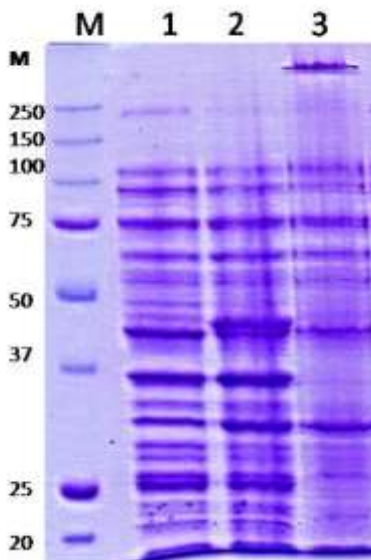


Figure 40: Overexpression of LHB

Lane M: Markers

Lane 1: LHB before induction with IPTG/ boiled

Lane 2: LHB after induction with IPTG/ boiled

Lane 3: LHB after induction with IPTG/ unboiled

At approximately 43kDa in lane 2, a distinct band after induction is observed, confirming the overexpression of the construct. In lane 3 the band is absent which indicates that in the unboiled sample the protein is in its trimeric form and is located in higher molecular weight or unable to internalize the gel.

Purification with Ni-NTA

The cells were lysed with the French press method and since the protein is located in the pellet, a further solubilization procedure with urea was followed. The supernatant after the denaturation step of inclusion bodies was incubated with Ni-NTA beads or, alternatively, streptavidin coated beads for purification.

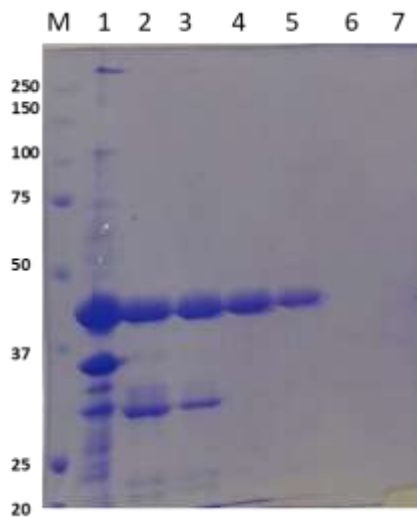


Figure 41: Purification with a Ni-NTA column. His-tag

Lane M: Protein markers

Lane 1: supernatant of LHB after urea treatment

Lane 2: Flow-through

Lane 3-7: elutions with Imidazole 50-250mM

The “cleaner” elutions at Lanes 4 & 5 were kept for dialysis. Flow through and elution sample (Lanes 2 &3) were collected for an extra step of purification with the streptavidin column.

Purification of LHB using a streptavidin column

Previously collected samples were incubated with the streptavidin beads. The aim is to take advantage of the very strong non-covalent bond that forms between biotin and streptavidin.

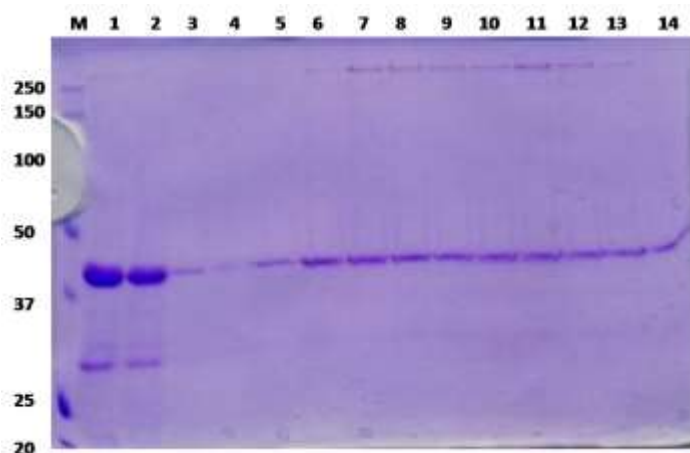


Figure 42: Purification of LHB with a streptavidin column

Lane M: protein markers

Lane 1: LHB sample for purification

Lane 2: LHB sample for purification

Lane 3: Flow-through

Lane 4: Wash

Lane 5 & 6: Elutions with GuHCl pH: 1.5

The protein is clearly purified after strongly binding with the streptavidin coated beads through the biotin molecule. The resulting elutions contain no degradation products.

Dot Blot

Dot Blot was used as an extra confirmation step for the effective biotinylation during protein overexpression and the ability of efficient conjugation with a streptavidin molecule.

A drop of the protein was deposited onto a PVDF film (with 2 extra dilutions) and incubated with an alkaline phosphatase conjugated with streptavidin antibody. The successful binding with the LHB was confirmed by the chemiluminescence signal detection due to the addition of BCIP-NBT.



Figure 43: Dot Blot for verifying successful biotinylation. From left to right: LHB protein drops at 1mg/ml, 0.5mg/ml, 0.2mg/ml. Alkaline Phosphatase-Streptavidin was used as control.

LHB protein construct exhibits no cytotoxicity against the mammalian cell lines tested

In order to ensure that the potential protein carrier does not affect the viability of eukaryotic cells, we conducted cytotoxicity experiments with the use of the MTT assay. No significant decrease of the viability of the cells was observed in lower protein concentrations. Thus, the protein constructs are non-cytotoxic and could be employed for delivery into mammalian cells.

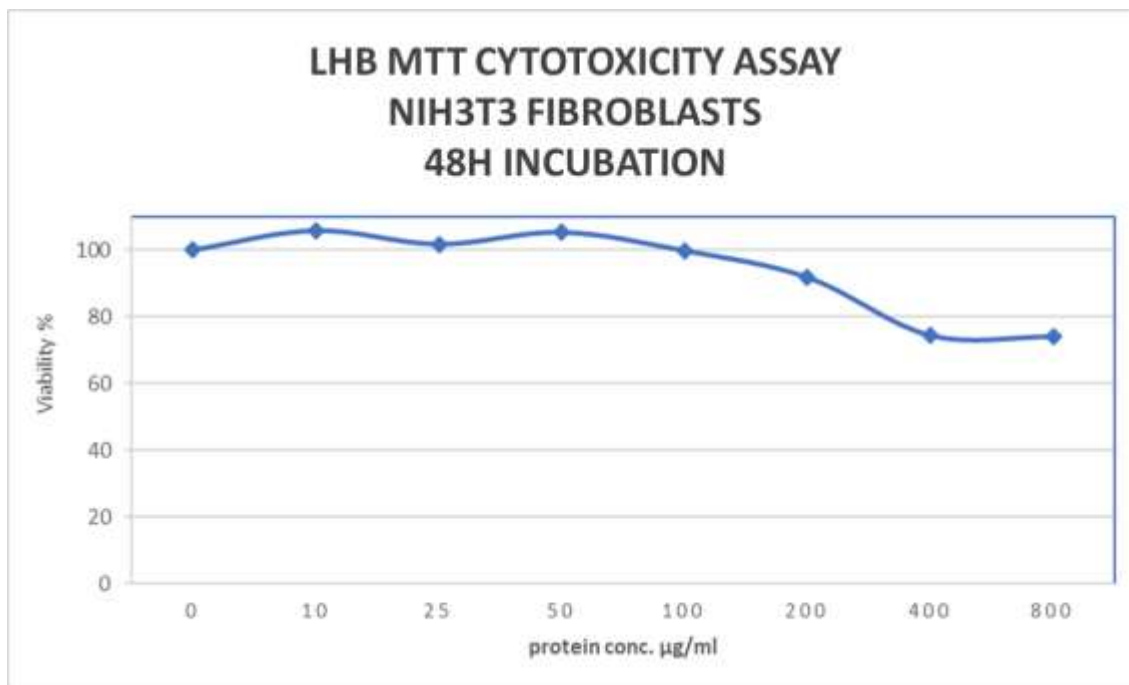


Figure 44: LHB in phosphate buffer pH:9 . Incubation of fibroblasts with increasing protein concentrations for 48h.

Intracellular localization

We utilized immunostaining with DAPI (nucleus) and Phalloidin dye (actin) in confocal microscopy to visualize NIH3T3 fibroblasts, HEK293T and HeLa cells after treatment with the LHB-fluorescein protein. The stained proteins are able to effectively and spontaneously access the cells and are detected in the cytoplasm and the perinuclear area.

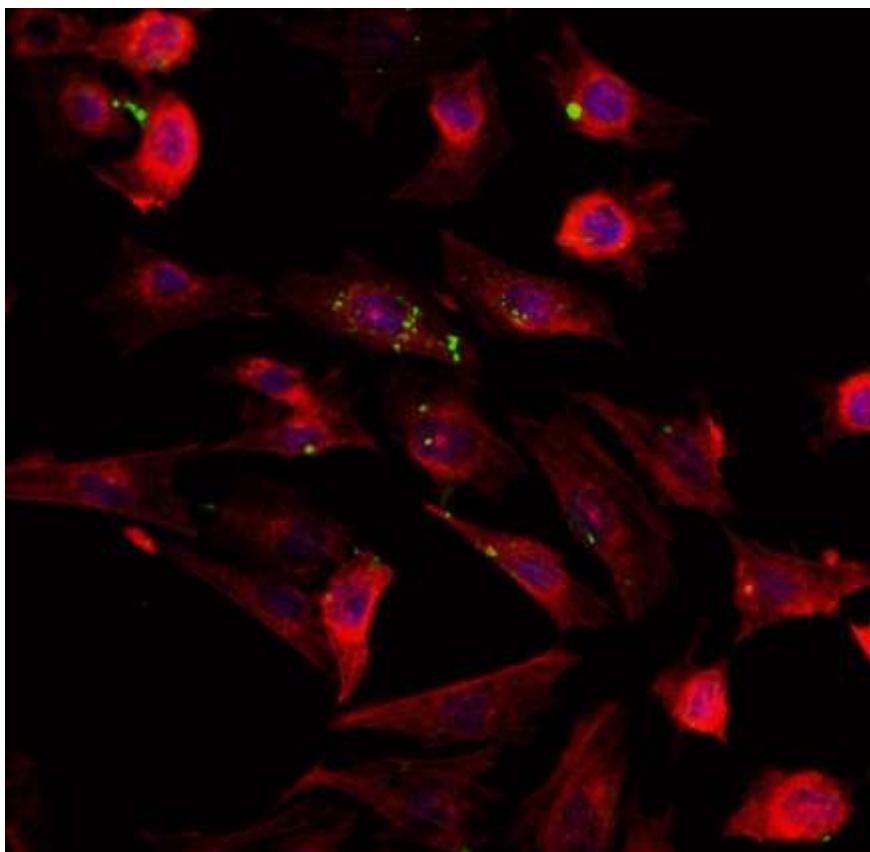


Figure 45: Intracellular delivery of LHB-Fluorescein protein into NIH3T3 cells at 37C with c: 100 $\mu\text{g}/\text{ml}$. Protein is depicted with green since is bound to fluorescein. Actin is red. The nuclei are stained with DAPI (blue).

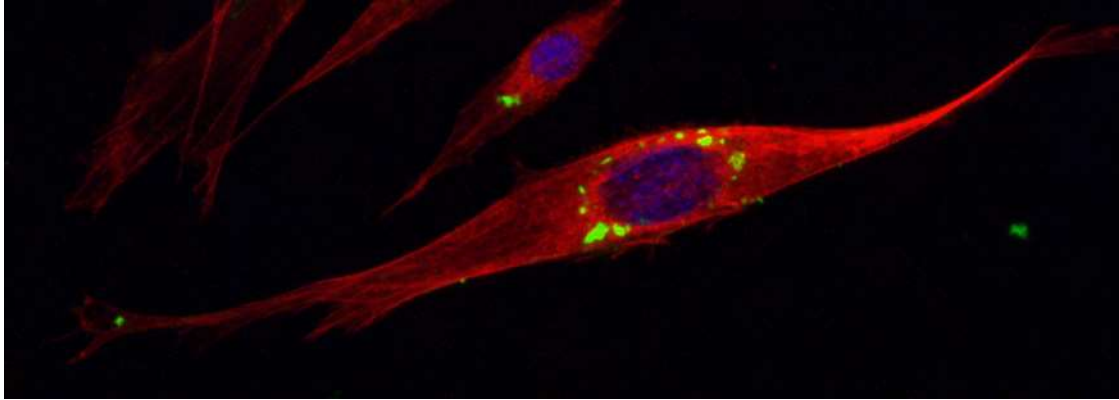


Figure 46: Intracellular delivery of LHB-Fluorescein protein into NIH3T3 cells at 37C with c: 100 $\mu\text{g/ml}$. Protein is depicted with green since is bound to fluorescein. Actin is red. The nuclei are stained with DAPI (blue).

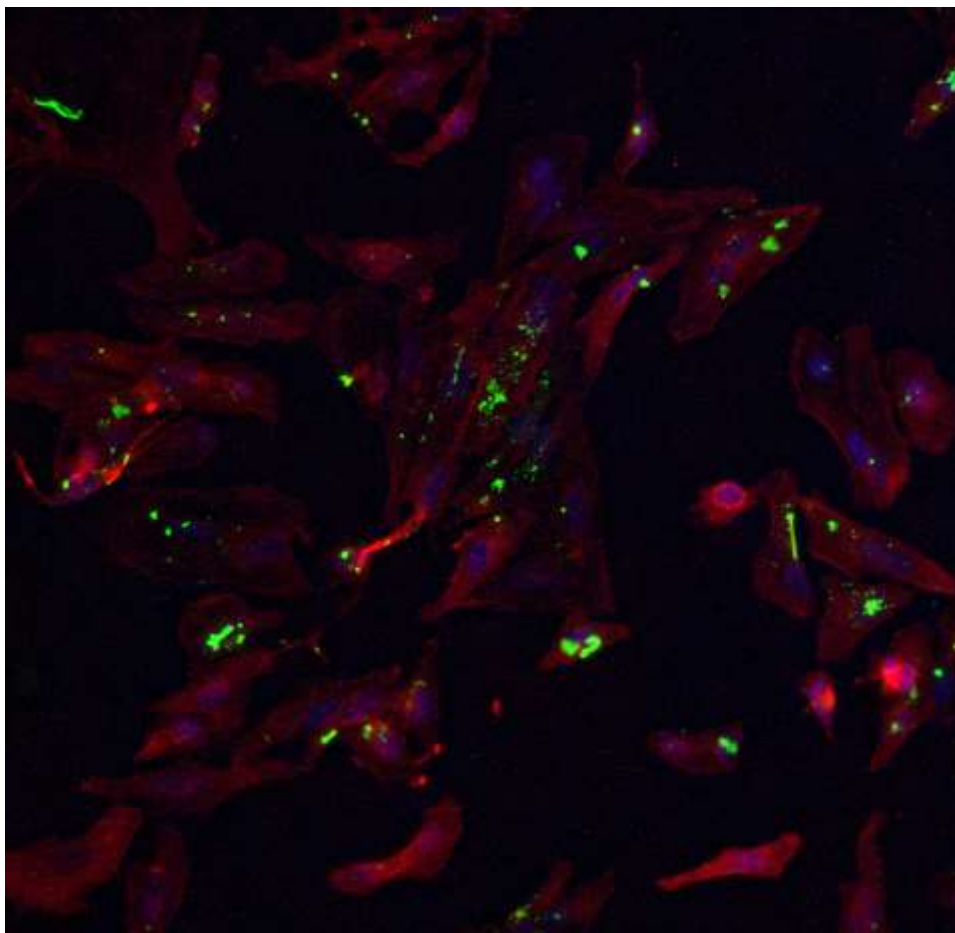


Figure 47: Intracellular delivery of LHB-Fluorescein protein into HeLa cells at 37°C with c: 100µg/ml. Protein is depicted with green since is bound to fluorescein. Actin is red. The nuclei are stained with DAPI (blue)

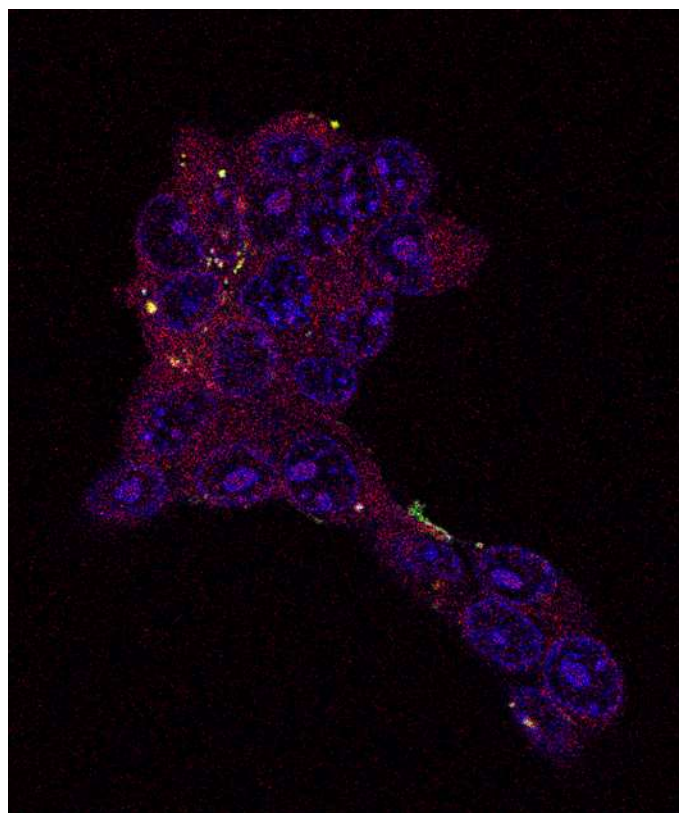


Figure 48: Intracellular delivery of LHB-Fluorescein protein into HEK293T cells at 37C with c: 100ug/ml. Protein is depicted with green since is bound to fluorescein. Actin is red. The nuclei are stained with DAPI (blue)

Efficient transfer of the streptavidin-gold-Nanoparticle into the cells by the LHB protein carrier and through the biotin-streptavidin bond.

LHB protein molecules are incubated with the AlexaFluor®594 FluoroNanogold™-Streptavidin (Nanoprobes) which consists of a streptavidin protein conjugated to

AlexaFluor® 594 dye (red) and the 1.4 nm Nanogold® particle (**Figure 25**). The conjugation is achieved by the attachment of the biotinylated proteins to streptavidin coated nanoparticles which are also conjugated with Alexa Fluor® 594 FluoroNanogold allowing the localization of the protein e.g. in a human cell line.

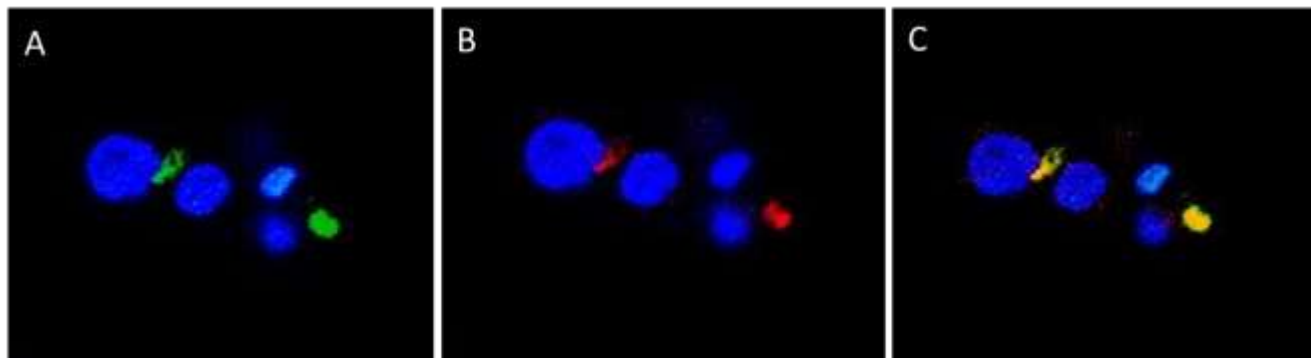
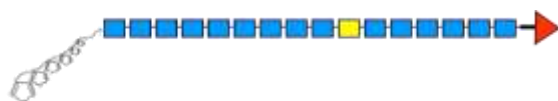


Figure 49: Cell internalization studies of the LHB protein-streptavidin gold NP in HEK293T cells. A) The protein construct is stained with fluorescein (green) and further conjugated with the streptavidin -gold NP which contains an exposed Alexa595 dye (red). Cell nuclei are stained with DAPI (blue). Z-stack measurements of the cells were also obtained to ensure that the protein conjugates localize inside the cells at the same level. A) only the nuclei (blue) and the fluorescein (green) filters are active in the confocal microscope B) only the nuclei (blue) and the AlexaFluor594 (red) filters are applied. C) All filters are applied and the green and red signals are co-localized, indicated the effective transport of the intact conjugate.

The merged image (yellow) indicates that the fluorescein (green) and AlexaFluor594 (red) signal are co-localized, therefore the LHB protein acted as an effective carrier for the transportation of the streptavidin-NP into the cell and has the potential to act as a protein vector for cell internalization.

Protein constructs L-H and LHB with a serine to cysteine substitution (LHCYS and LHBCYS)



Polymerization of styrene from the protein initiator (in collaboration with Prof. K. Velonia)^{6,7}

These protein constructs were fabricated in order to combine all the aforementioned advantages with an extra functionality for the interaction through disulfide bonds, binding with gold nanoparticles and the ability to trigger styrene or responsive molecule polymerization through a maleimide initiator. This could enable the fabrication of responsive protein polymers for use as a drug delivery carrier.

Overexpression and Purification of the LHCYS protein construct

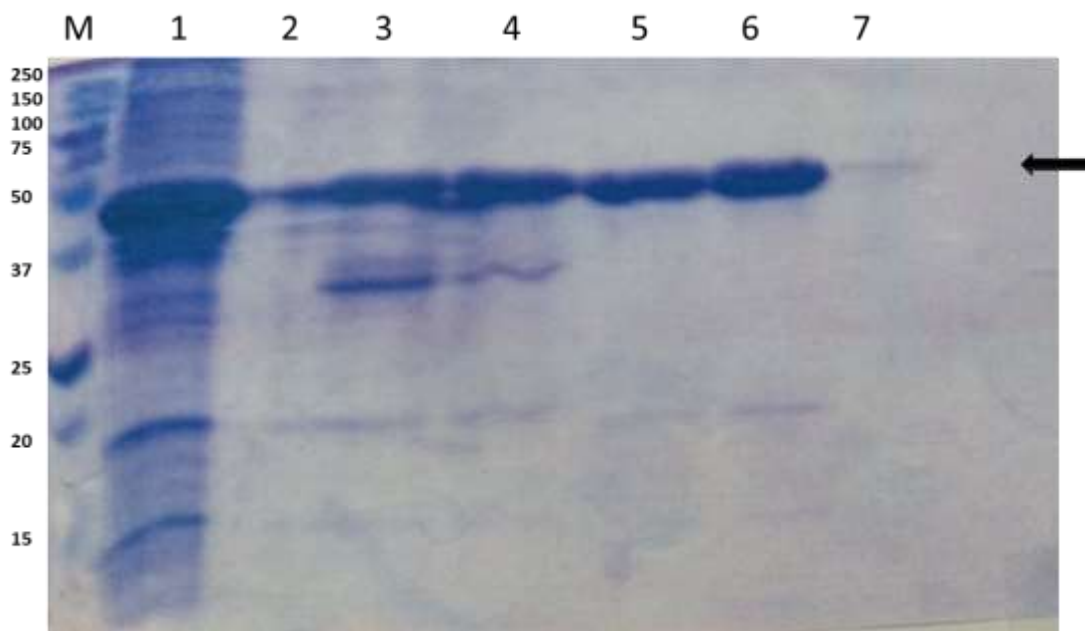


Figure 50: Purification with Ni-NTA column of the bacterial lysate containing the overexpressed protein. The protein is purified at imidazole concentration 50-250mM. The purest samples (Lanes 5 & 6) are collected for dialysis and refolding.

Lane M: Protein markers

Lane 1: Bacterial lysate after treatment with Urea to denature the inclusion bodies

Lane 2: Flow through

Lane 3: Wash

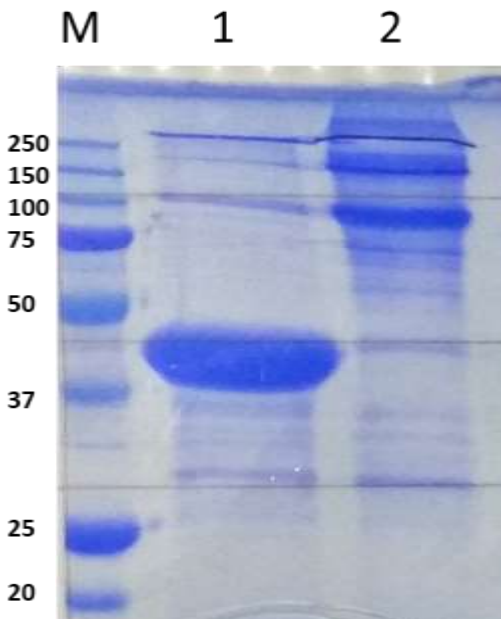
Lane 4: Elution at 50mM Imidazole

Lane 5: Elution at 75mM Imidazole

Lane 6: Elution at 100mM Imidazole

Lane 7: Elution at 250mM Imidazole

Trimerization of the LHCYS protein



Lane M: protein markers

Lane 1: LHCYS after dialysis, boiled

Lane 2: LHCYS after dialysis, unboiled

Figure 51: Trimerization of the LHCYS protein construct. The protein is overexpressed abundantly and after dialysis the protein is able to correctly fold into its trimeric conformation as depicted in the polyacrylamide gel (Lane 2).

Synthesis of the Bio-Initiator (Binding of the maleimide initiator)⁸

The purified concentrated protein was incubated overnight in the cold room with excess of the maleimide initiator (20 times excess in DMSO, total DMSO content below 10%) under constant mild shaking. After the incubation, the sample was dialysed against Tris pH:9 buffer in order to remove the unbound initiator.

Reactions

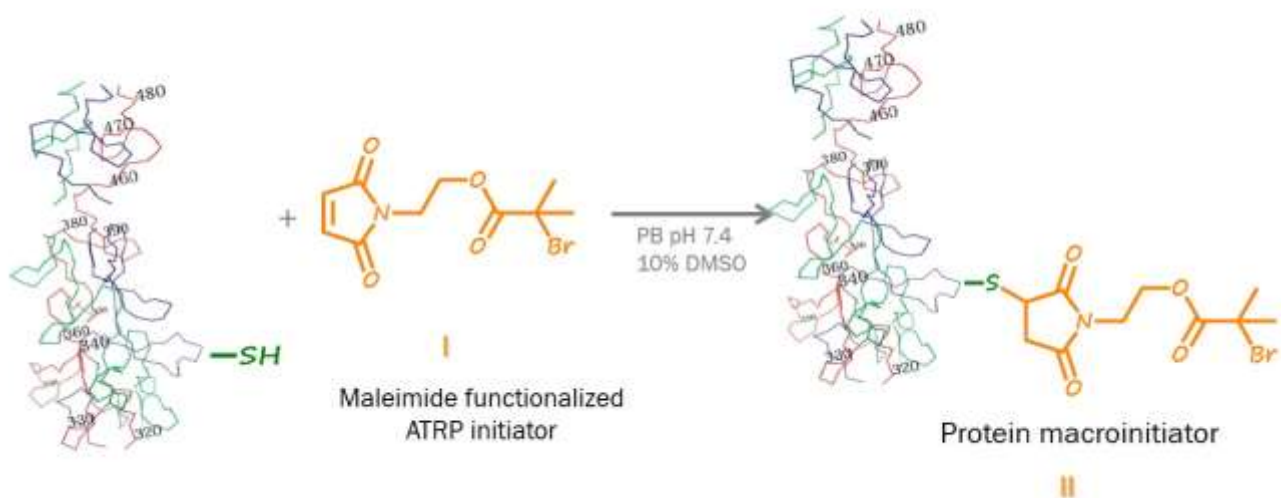


Figure 52: Reaction of the protein LHCYS with the exposed sulfhydryl group from the cysteine with the maleimide functionalized initiator, forming the protein macroinitiator. (The reaction representation is courtesy of Prof. Velonia)

The protein macroinitiator creation was furthermore confirmed by the MALDI (Matrix-Assisted Laser Desorption/Ionization) technique (**Figure 53**).

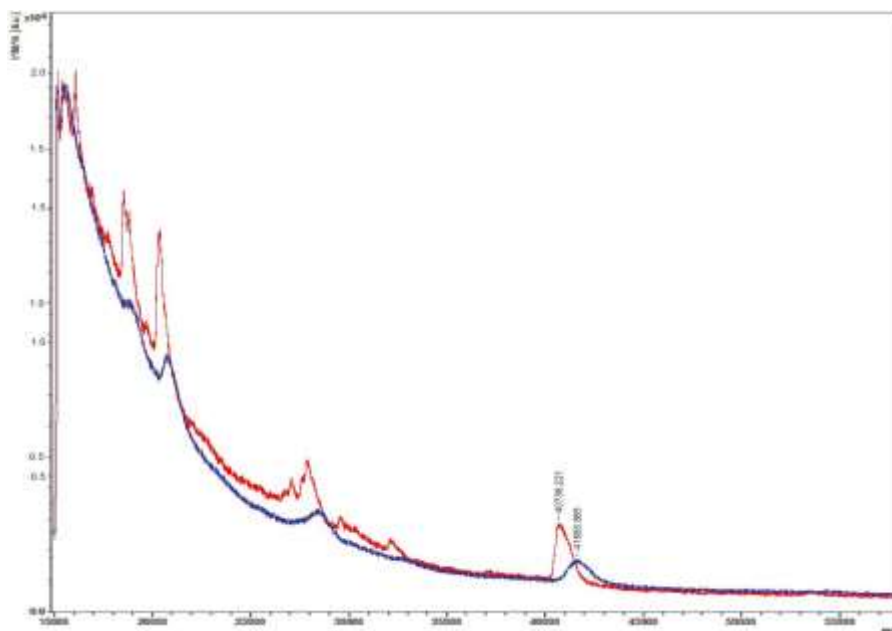


Figure 53: MALDI results from the protein-maleimide initiator. The red trace indicated was the trace of the native protein (~ 40kDa) (i.e. without the attachment of the maleimide initiator) whereas the blue trace (~41kDa) confirms that there is attachment of the initiator.

Polymerization of styrene from the protein macroinitiator

Reaction

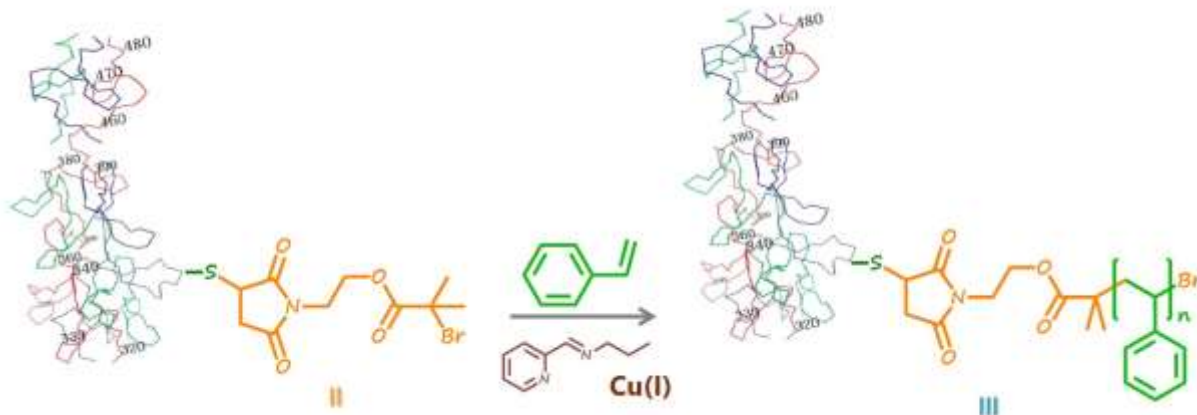


Figure 54: Reaction of the protein macroinitiator (II) with the styrene monomers resulting in a hybrid protein-polymer (III)

The reaction was performed under classical ATRP conditions, using copper (I) and a ligand in the absence of oxygen. A preliminary confirmation for the creation of this hybrid was obtained from the results of gel electrophoresis where the hybrid was unable to enter the pores of the 7.5% polyacrylamide gel indicating that both that the hybrid's size increased drastically due to the polymerization and the amphiphilic character of the products.

Addition of the maleimide macroinitiator and TCEP keeps the cysteines from creating disulfide bonds between protein molecules. TCEP (tris(2-carboxyethyl)phosphine) is a reducing agent and is particularly useful when labeling cysteine residues with maleimides. TCEP can keep the cysteines from forming di-sulfide bonds and unlike dithiothreitol and β -mercaptoethanol, it will not react as readily with the maleimide.

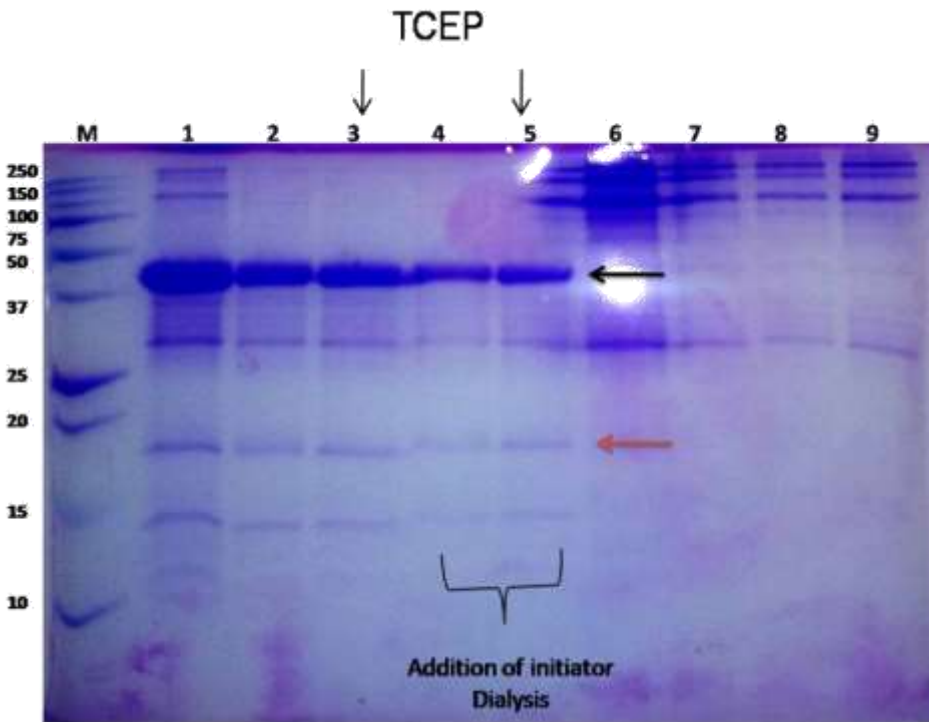


Figure 55: LHCYS protein constructs after the addition of maleimide initiator and TCEP.

Lane M: protein markers

Lane 1: LHCYS protein after purification and dialysis, boiled

Lane 2: LHCYS with the addition of initiator before dialysis, boiled

Lane 3: LHCYS with the addition of initiator and TCEP before dialysis, boiled

Lane 4: LHCYS with the addition of initiator after dialysis, boiled

Lane 5: LHCYS with the addition of initiator and TCEP after dialysis, boiled

Lane 6: LHCYS protein after purification dialysis, unboiled

Lane 7: LHCYS with the addition of initiator before dialysis, unboiled

Lane 8: LHCYS with the addition of initiator after dialysis, unboiled

Lane 9: LHCYS with the addition of initiator and TCEP after dialysis, unboiled

The protein was treated with the maleimide initiator and TCEP. Protein samples treated with the initiator and further dialysed to remove the excess of the initiator seem to have increased molecular weights as observed in the Lanes 4 & 5 (arrows). The increase is clearly distinguishable at their degradation products (red arrow). Despite the treatments

the protein was able to trimerize correctly as observed from the migration of protein bands at higher molecular weights at lanes 6-9.

Incubation with styrene monomers and polymerization

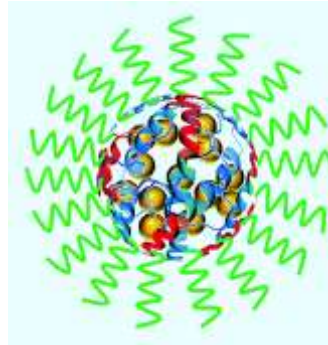


Figure 56: Potential final polymerization product where the therapeutic molecules are encapsulated within the polymer and the protein is exposed on the surface, potentially guiding the polymer for cell internalization.

The proteins with the initiator were treated with styrene monomers under optimal conditions at the laboratory of Prof. Kelly Velonia and dialysed for the removal of excess styrene. The protein-polymer was electrophoresed with SDS 2% sample buffer to examine its permeability of the polyacrylamide gel and stability.

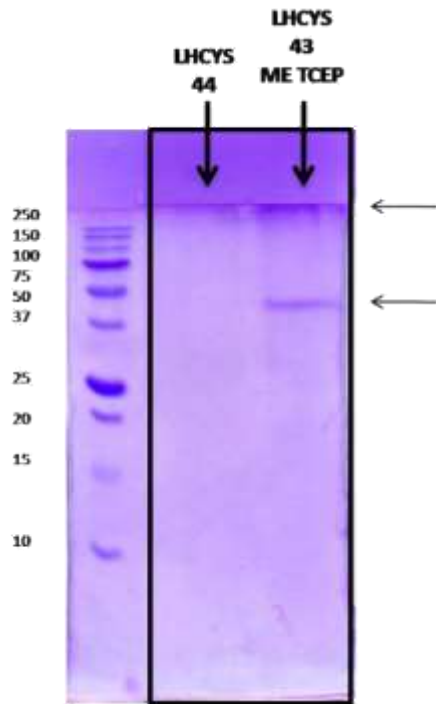


Figure 57: 12% SDS-PAGE of the LHCYS-polymer. From left to right: protein markers, Protein-polymer, protein-polymer with TCEP.

The protein polymer was unable to internalize the polyacrylamide gel, due to accumulation of styrene monomers during the polymer assembly and the subsequent increase of its size and amphiphilicity. The stained protein-polymer is gathered between the stacking and separating gel parts (upper arrow) unable to migrate through the polyacrylamide pores of the separating gel. This indicates the effective grafting of the polymer from the protein macroinitiator. For the protein-polymer sample treated with TCEP (right), an accumulation of protein material between the two gel parts is observed again but additionally a protein band is observed that was able to migrate through the gel (arrow below). This could correspond to protein molecules that were not co-polymerized effectively but were connected by disulfide bonds with other protein molecules. The polymerization efficiency certainly needs further investigation.

2. 5. CONCLUSIONS

Stable and fibrous beta structured proteins forming nanorods are promising templates for protein biomaterial design and engineering. These proteins can be manipulated for exhibiting intrinsic functionalities useful for drug delivery, tissue engineering and gene therapy purposes. Materials fabricated for such applications should not trigger cytotoxic and immunological responses. Moreover, they should attain a well-defined conformation in addition to a stable and resistant to harsh conditions folding state. In this study the chimeric protein constructs were fabricated by substituting the natural -difficult to handle due to its size- globular head at the C-terminus with an alternative and smaller trimerization motif, the fibrin 'foldon' domain. The newly constructed proteins retain their ability to self-assemble into their trimeric and nanorod formation as observed under EM microscopy. Furthermore, they can be overexpressed in big quantities in heterologous *E.coli* bacterial strains, in contrast to the natural fiber sequence with the globular head, an advantage that renders the production of these materials cost-effective. The resulting degradation products most probably truncated from the fiber sequence due to the protease action, were eliminated by the addition of a 6x His-tag at the N-terminal end of the protein constructs (Linker-H and NoLinker-H) that additionally massively increased the efficiency of the purification process through a one-step Ni-NTA affinity column. The His-tag tails are also considered to facilitate the escape of the protein from the endosome entrapment that occurs shortly after cell internalization.⁹⁵ The shorter version of the protein shaft with the foldon domain (StabL-H) enabled the localization after overexpression of part of the protein material in the cytosol and not its aggregation into the inclusion bodies. This facilitates even further the isolation of the protein by avoiding the handling process of denaturation of the inclusion bodies containing the aggregated protein with chaotropic agents such urea and the subsequent protein renaturation. The biotinylation site added in the chimeric protein Linker-His-Biotin

(LHB) enables the addition of a biotin molecule in the cell, during the overexpression process. The streptavidin-biotin strong non-covalent bond allows to carry and transfer biotinylated moieties into the cell for therapeutic applications. To this end, the chimeric protein LHB was chosen for internalization studies into mammalian cells. Although the protein does not contain the CAR receptor binding motif located in the natural globular head of the fiber, it can internalize cell lines such as HeLa, fibroblasts and HEK293T cells. This indicates that another mechanism is operating for cell internalization of the proteins that needs further investigation. The same protein construct LHB was able to transfer into mammalian cells a streptavidin conjugated gold nanoparticle with an attached fluorophore, therefore confirming its ability as a carrier. The insertion of a cysteine residue in an exposed loop of the protein renders it with the function of creating disulfide bridges with molecules or binding gold nanoparticles. In this study the designed LHCYS protein was used for the synthesis of a protein-polymer particle through styrene grafting from the relevant LHCYS macroinitiator. The resulting self-assembled nanoparticles is expected to bear proteins exposed at its surface for guiding the particle into cells. Such nanoparticles could potentially allow the encapsulation and delivery of therapeutic molecules into cells.

Generally, a series of constructs were fabricated to examine possible parameters concerning the design and engineering of an optimal therapeutic molecule carrier. The experimental results show that the proteins designed are non-cytotoxic, stable and exhibit diverse functionalities that can be rationally engineered onto the initial protein structural framework. The work presented in this thesis aimed at establishing the proof-of-principle. Future experimental avenues would also include the elucidation of the internalization mechanism and confirmation experiments for the transfection efficacy of the proteins into cells with potentially therapeutic biotinylated moieties. Moreover, crystallization studies could be undertaken for unravelling the newly constructed

proteins as well as further polymerization experiments with polymers responsive to environmental conditions such as temperature and pH (Figure 58).

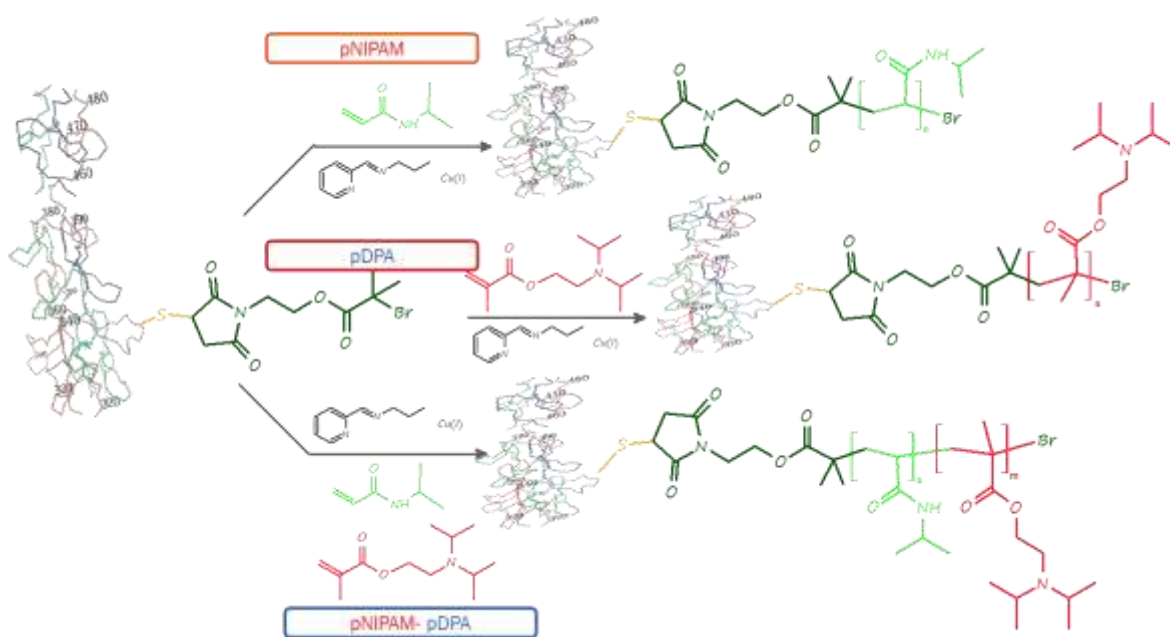


Figure 58: Outlook of polymerization experiments with responsive polymers

Chapter 3

A Novel Amyloid Designable Scaffold and Potential Inhibitor Inspired by GAIIG of Amyloid Beta and the HIV-1 V3 Loop

My own contribution in this paper consisted in consolidating and confirming previously scattered observations made during previous diploma theses in the Biomaterials Laboratory concerning the GAIIG and YATGAIIGNII building blocks, as well as the inhibition of fibrillization by the GAIPIG peptide.

3. 1. Introduction

Naturally occurring peptide sequences extracted from amyloid proteins or beta-sheet protein regions can self- assemble outside the context of the entire sequence into amyloid beta-sheets and can serve as scaffolds for novel materials.^{24, 68-70, 103-110} GAIIGL¹¹¹ and NSGAIIG²³ are two peptide sequences similar in sequence, which are part of the amyloid-b (Ab) peptide, linked to Alzheimer's disease, and the adenovirus fiber shaft,¹¹²⁻¹¹³ respectively. Both GAIIGL and NSGAIIG form amyloid b-sheets outside the context of the entire peptide or protein. According to experimental X-ray and computational molecular dynamics (MD) simulation studies, in both peptides, residues outside the GAIIG or GAIIG sequences are not part of the amyloidogenic b-sheet core: the C-terminal leucine, and the N-terminal asparagine and serine residues in the two peptides, respectively, are exposed. The latter provided impetus²³ for the discovery of a series of amyloid materials with several applications^{24, 68-70} by modifying the NS-residues.

While aromatic residues are key components of amyloid self-assembly (as pioneered by Gazit and colleagues¹¹⁴⁻¹¹⁶), patterns of aliphatic residues are also key self-assembly

components,^{22, 117-118} contributing to the amyloid properties of GAIIGL.¹¹¹ In this study, we carried out experimental and computational studies that show that the shorter GAIIG peptide (amidated at the C-terminus) self-assembles into amyloid b-sheets. This sequence is common to the amyloid-b (Ab) peptide (residues 29–33) and to HIV gp120 (residues 24–28 in a typical 35-residue long V3 loop), according to the HIV sequence database (<https://www.hiv.lanl.gov/>). We also show that the longer YAT-GAIIGNII sequence from the V3 loop self-assembles into amyloid fibrils of which the first and last three residues are outside the amyloid GAIIG core. Finally, we report on the single crystal structure of the beta- breaker peptide GAIPIG and the computational investigation of its binding properties to Ab and the V3 loop. We discuss potential implications for material design and structure-based inhibitor design.

3. 2. Materials and Methods

Peptides and chemicals

The following peptides were studied: NH₃⁺-GAIIG-CONH₂, NH₃⁺-GAIPIG-CONH₂ and NH₃⁺-YATGAIIGNII-COO⁻. The peptides were purchased from Genecust (Luxemburg) and possessed a degree of purity higher than 95%. The Aβ₁₋₄₀ peptide was purchased from Bachem (Switzerland). Phosphate-buffered saline and Thioflavin T were from Sigma, and sodium azide from Serva.

Transmission Electron Microscopy (TEM): Samples for TEM analysis were prepared by depositing 8 μl of the sample on carbon-coated formvar copper grids (Agar Scientific), left aside for two minutes, dried with a filter paper and then the same procedure was repeated with the stain. The samples were negatively stained with 8 μl 1% (w/v) phosphotungstic acid for two minutes for GAIIG and with 8 μl 2% (w/v) uranyl acetate for YATGAIIGNII. The TEM experiments were performed using a JEOL JEM 2100 High Resolution microscope, operating at 80 kV.

X-Ray Fiber Diffraction: A droplet of a peptide fibril solution was placed between two glass rods that were supported by two plasticine balls and allowed to dry while pulling to induce shear alignment as previously described.¹¹⁹ The X-rays were focused on the aligned fibers at right angles and the diffraction patterns were recorded.

Single-Crystal X-ray Diffraction

Crystallization trials were carried out by sitting-drop vapor diffusion in MRC crystallization plates (Molecular Dimensions, Newmarket, Suffolk, England). Crystals were obtained in wells with different concentrations of ammonium sulfate and pH values. Optimization was performed using 50 μL of reservoir solution and drops consisting of 2 μL of GAIPIG peptide aqueous solution at 38 mg/mL mixed with 2 μL of reservoir solution. Crystals appeared after a period of more than 3 months, only after removing the covering tape in five occasions for 3 to 5 minutes during the month previous to appearance of the needle-shaped crystals. The dataset used for structure solution was collected from a crystal grown when 0.1 M Tris-HCl pH 7.5, 1 M ammonium sulphate was used as reservoir solution. A crystal was mounted in a LithoLoop (Molecular Dimensions) and vitrified in liquid nitrogen for native data collection at 100 K.

The X-ray fiber diffraction pattern of the peptides GAIIG and YATGAIIGNII were conducted by Drs. Estelle Mossou and Trevor Forsyth at ILL and ESRF, France. The Single-Crystal X-ray Diffraction of the GAIPIG peptide were conducted by Mateo Seoane Blanco, Dr Antonio L. Llamas-Saiz and Dr Mark van Raij at CSIC, Madrid. The experimental methods are extensively analyzed in the corresponding paper in ref⁷⁶.

Thioflavin T assay

Synthetic lyophilized peptide A β ₁₋₄₀ (Bachem) was dissolved in DMSO to a concentration of 100 μM , aliquoted and stored at -20°C. A β ₁₋₄₀ aliquots were thawed, sonicated in ice

cold water for 20 s to prevent pre-aggregation and immediately diluted with 10 mM phosphate-buffered saline containing 10% (v/v) DMSO and 0.05% (w/v) sodium azide [150mM NaCl (pH 7.4)] to a final concentration of 10 μ M. The A β ₁₋₄₀ solution was immediately mixed with the GAIPIG stock solution (1 mM) to a final A β ₁₋₄₀ concentration of 5 μ M and GAIPIG concentration of 50 μ M. A 10 μ M A β ₁₋₄₀ control solution was mixed with the equivalent amount of 10 mM phosphate-buffered saline to a final concentration of 5 μ M. A solution of the GAIPIG peptide at the same final concentration (50 μ M) without A β ₁₋₄₀ was also prepared. The samples were incubated without agitation at 37 °C, and the fibrillogenesis rate was monitored by using ThT fluorescence analysis. 40 μ l of each sample was taken and mixed with 360 μ L of 4 μ M ThT. The respective excitation and emission wavelengths were 450 nm (5nm slit) and 480 nm (5 nm slit). The fluorescence of ThT was measured using a SPEX FluoroMax fluorimeter.

Computational Methods

Computational methods were conducted by the group of Asst. Prof. Tamamis at Texas A&M and are analyzed in the supplementary information document of the corresponding paper published in FEBS LETTERS. Ref⁷⁶

3.3. Results and Discussion

Self-assembly of the GAIIG and YATGAIIGNII sequences

According to 16 μ s replica exchange MD simulations and a subsequent computational analysis performed analogously to previous studies^{25, 120-123} GAIIG primarily self-assembles into antiparallel off-register β -sheets which possess a high degree of order and alignment of peptides. The β -sheet core of the peptide is predominantly composed of the two isoleucine residues Ile3 and Ile4. A representative structure of a highly-ordered and well-aligned β -sheet composed by four peptide strands is presented in **Figure 59A**. Compared to the antiparallel β -sheets formed by GAIIGL, our analysis suggests that the presence of an additional leucine at the end of GAIIG is not necessary for self-assembly. The complete methods and analysis are included in the Supplementary Information of ref⁶. Experiments validated the amyloidogenic properties of GAIIG, revealing that the peptide forms non-branched fibrils with diameters of around ten nm and lengths reaching the order of microns as revealed by Transmission Electron Microscopy (**Figure 60A**). Fibrous rods of the peptide display the characteristic cross-beta signature in X-ray fiber diffraction: a 4.6 Å meridional reflection that corresponds to the distance between β -strands, and a 10.1 Å equatorial reflection that corresponds to the distance between β -sheets (**Figure 60B**).

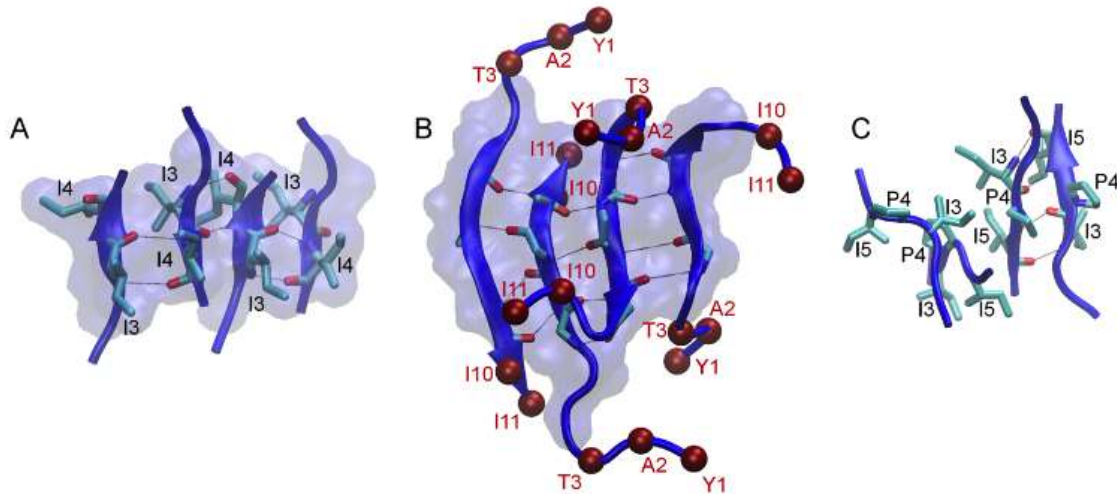


Figure 59: Molecular graphics images of representative highly ordered and well aligned 4-stranded β -sheet fibrils of A) GAIIG and B) YATGAIIGNII peptides and an example of the disordered structure of C) GAIPIG peptides. A) Residues Ile3 and Ile4, shown in licorice representation, form β -bridge interactions, indicated with black dotted lines, and make up the β -sheet core. B) β -sheet interactions within the GAIIG motif of the YATGAIIGNII peptides, indicated using dotted black lines, are preserved while the N- and C-terminal ends are exposed and flexible. The three N-terminal residues, Tyr1, Ala2, and Thr3 as well as the two C-terminal residues Ile10 and Ile11 are indicated with maroon spheres. C) Pro4 of the GAIPIG peptides prevents the formation of ordered β -sheet structures Pro4 of the GAIPIG peptides prevents the formation of ordered β -sheet structures and disrupts the formation of extended β -sheet conformations (e.g., see the left and middle pairs of peptides forming single β -bridge interactions in contrast to the right pair of peptides where an extended β -sheet conformation is formed).

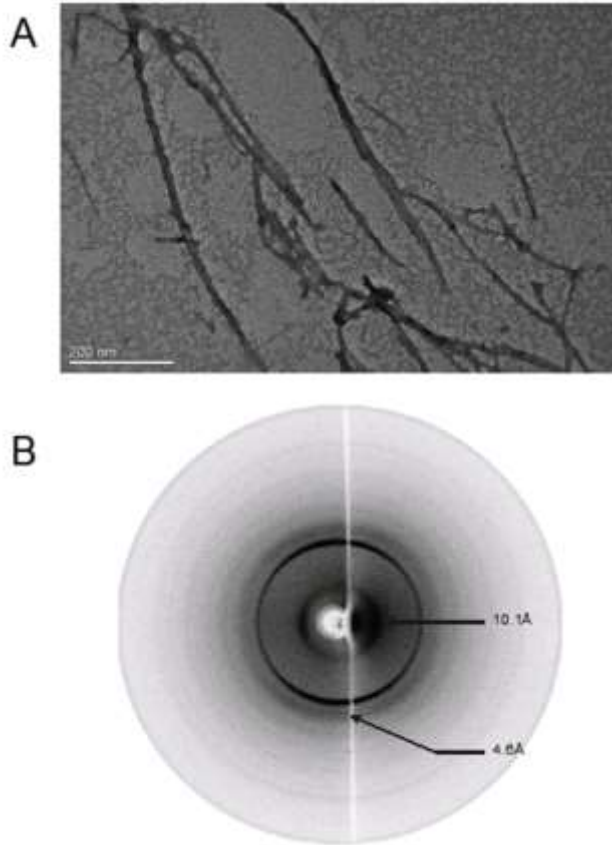


Figure 60: **A)** TEM micrograph of a 20 mg/ml solution of the GAIIG peptide following 62 days of incubation in phosphate buffer pH 7, negatively stained with phosphotungstic acid 1%. **B)** X-ray fiber diffraction pattern of rods formed from a 7 mg/ml solution in phosphate buffer following aging for 40 days.

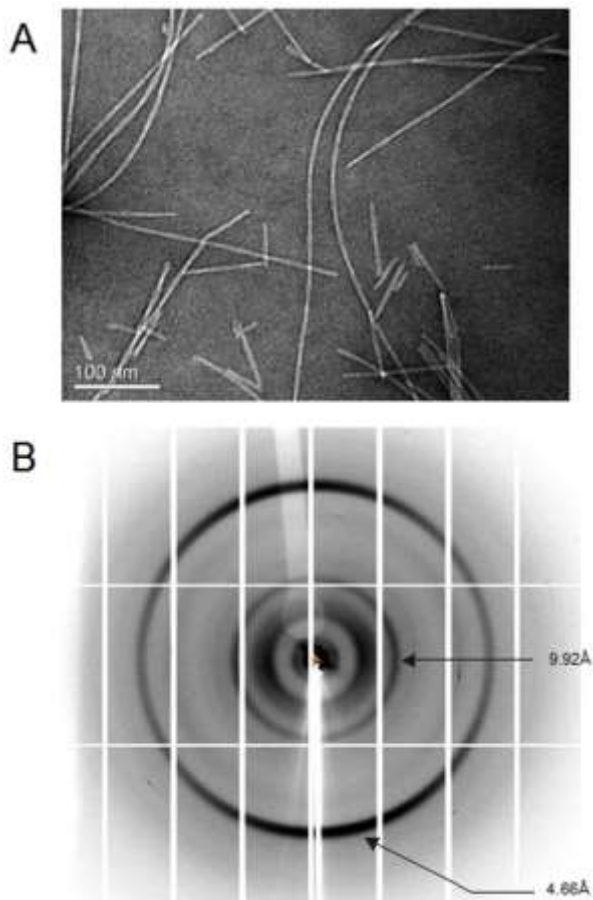


Figure 61: A) TEM micrograph of a 5 mg/ml solution of the YATGAIIGNII peptide following 5 days of incubation in water, negatively stained with uranyl acetate 2%. B) X-ray fiber diffraction pattern of rods formed from a 3 mg/ml solution in water after 2 hours of incubation.

The recent experimentally resolved structures of entire A β fibrils^{61, 63, 124} show that the last glycine of GAIIG introduces a turn into the amyloid β -sheets. The aforementioned information suggests that GAIIG can be a sufficiently short amyloidogenic core of larger amyloid forming peptides containing additional (e.g. 2-3) residues at both termini which can be outside the amyloid β -sheet, as glycine residues can act as β -turn promoters halting β -sheet elongation. The discovery of such amyloid peptide scaffolds can serve as

a source of inspiration for the discovery of amyloid materials with advanced properties, as the exposed residues can be modified accordingly depending on the desired application.

Previous computational studies¹²⁵⁻¹²⁶ showed that the HIV-1 gp120 V3 loop adopts a structure in which the opposite stems of the loop form a β -sheet in its interaction with chemokine receptors CXCR4 and CCR5. Interestingly, we observed that a GAIIG sequence fragment (or other homologous fragments including GQIIG, GQIVG) is part of one of the two stems, comprising residues 24-28 in a typical 35-residue long V3 loop, according to the HIV sequence database (<https://www.hiv.lanl.gov/>). This observation further supported our aforementioned suggestion and led us to postulate that such variable sequences derived from the HIV-1 gp120 V3 loop containing GAIIG as an amyloid core and additional (e.g. 2-3) residues at both termini could serve as a source of inspiration for novel amyloid material scaffolds. Additionally, this led us to a second postulation that sequence fragments including GAIPIG, which are homologous to GAIIG but are not amyloidogenic due to the presence of a proline beta-breaker²², could potentially bind to GAIIG fragments of HIV-1 gp120 V3 loop and to A β .

As for the first postulation, in this study, we focused on one such sequence: YATGAIIGNII derived from a V3 loop¹²⁷ (without any modifications at the termini). Similarly to GAIIG, according to 16 μ s replica exchange MD simulations and a subsequent computational analysis, which was performed analogously to previous studies^{23, 25, 120-123}, the YATGAIIGNII peptide primarily self-assembles into antiparallel off-register β -sheets, which possess a high degree of order and alignment of peptides. The β -sheet core of the peptide is predominantly composed of residues Gly4 to Asn9, encompassing the GAIIG domain. A representative structure of a highly-ordered and well-aligned β -sheet composed by four peptide strands is presented in **Figure 59B**. Interestingly, we observe that both glycine residues act as β -turn promoters, which halt

the elongation of the β -sheet core outside the domain. Thus, N-terminal residues Tyr1, Ala2, Thr3, as well as C-terminal residues Ile10 and Ile11 are rarely involved in β -sheet formation and are outside the amyloid zipper-like region formed within the GAIIG domain and Asn9. As a result, the amyloid scaffolds formed by YATGAIIGNII can be considered as excellent designable scaffolds for the synthesis of functional amyloid materials. This can be achieved by introducing suitably selected mutations at the non β -sheet forming terminal residue positions 1, 2, 3, 10 and 11, which would not disrupt the amyloid self-assembly properties and at the same time would allow the newly designed amyloid fibrils to bind to ions, molecules or surfaces. The complete methods and analysis are included in the Supplementary Information of ref⁷⁶. Experiments validated the amyloidogenic properties of YATGAIIGNII. TEM micrographs of YATGAIIGNII fibrils reveal a typical amyloid-type conformation (**Figure 61A**) and X-ray fiber diffraction of rods display the characteristic cross- β signature with a 4.67 Å reflection at the meridian and 9.92 Å at the equator (**Figure 61B**). Additional computer simulation runs with a longer 13-residue peptide extracted from the same HIV-1 gp120 V3 loop with sequence AFYATGAIIGNII show that the inclusion of additional residues results in the formation of U-shaped β -sheets (preliminary results not shown) similarly to β -sheets formed by LSFDNSGAIIG^{22, 122}. On the contrary, 11-residue peptides containing 3 residues before and after the GAIIG domain can be optimal designable amyloid scaffolds containing the maximum number of mutable positions and at the same time comprising linear shaped peptides at which the non- β -sheet residues are exposed for functionalization purposes.

Additional peptide sequences containing the GAIIG amyloid core plus 2-3 residues at both termini, and inspired by either the HIV-1 V3 loop sequence variability or other naturally occurring proteins encompassing the amyloid GAIIG, may also be designable amyloid scaffolds that could be further investigated. Interestingly, this can be supported by the fact that GAIIG domain can be found in amyloid or β -sheet rich regions of proteins

of known structure, including A β (₂₉GAIIG₃₃ in PDB ID: 5OQV¹²⁴), α -tubulin acetyl transferase (₉₁GAIIG₉₅ in PDB ID: 4PK2¹²⁸ Chain A), *Mycobacterium smegmatis* alpha-ketoglutarate decarboxylase homodimers (₂₇₅GAIIG₂₇₉ in PDB ID: 2XT6¹²⁹ Chain A), and Tryparedoxin from *Trypanosoma brucei* (₁₂₀GAIIG₁₂₄ in PDB ID: 1073)¹³⁰.

X-ray and computational analysis of the GAIPIG peptide

While GAIIG is an amyloid peptide and as a domain it comprises the amyloid core of the larger peptide YATGAIIGNII, our previous experiments showed that the insertion of a proline between the two isoleucine residues (GAIPIG peptide) results in the disruption of amyloid formation²². Here, we performed additional X-ray and computational analyses on the structures formed by GAIPIG. A crystallographic structure reveals that two extended molecules of the GAIPIG peptide interact with each other to form an anti-parallel dimer, reminiscent of a small beta-sheet. In the crystal, these dimers associate in helical fashion around a 3₁ symmetry axis. The center of the helix is hydrophobic, while the outside is hydrophilic (**Figure 62 A, B, C, D**).

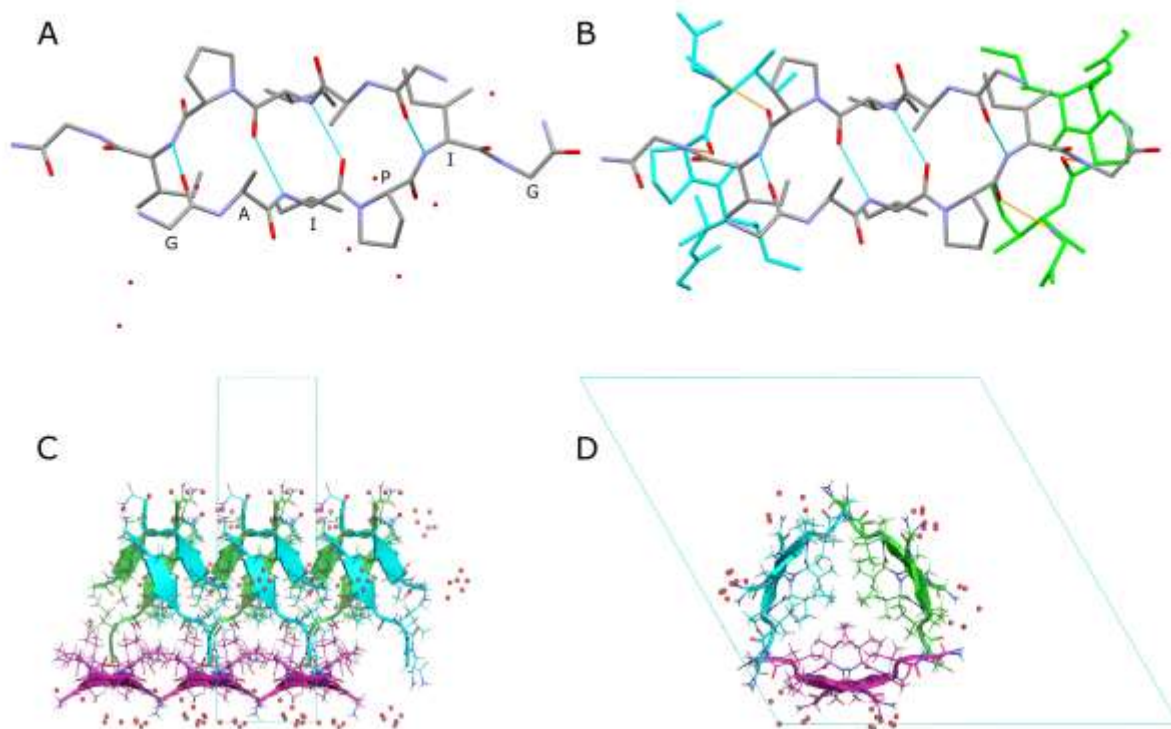


Figure 62: **A)** Hydrogen bonded dimer formed by the two peptide molecules in the crystallographic asymmetric unit (AU). Single-letter amino acid code is displayed for one peptide. **B)** Same as **A)** including two additional symmetry related molecules (cyan and green) that extend the hydrogen bonded helical assembly. Hydrogen bonds for symmetry related molecules in orange. Water molecules omitted for clarity. **C)** Ribbon representation of the helical hydrogen bonded assembly of GAIPG molecules displayed along crystallographic a axis and **D)** along c axis. Side chains are showed in wireframe representation and solvent water molecules as red dots. The antiparallel β -strand corresponding with the crystallographic AU is colored in green; in cyan and purple are the 3-fold screw symmetry related ones. Figures were generated with MERCURY¹³¹ **A)** and **B)** and PyMOL **C)** and **D)** (PyMOL 1.9: The PyMOL Molecular Graphics System, Schrodinger, LLC.)

The computational analysis depicts that the peptide forms β -sheet rich structures and the interactions occur frequently within the AIPI moiety of the peptide which primarily involve β -isolated bridges formed between Ile5 residues, in line with our X-ray studies. Yet, the presence of proline at the middle of the core disallows the formation of highly-ordered and well-aligned β -sheets (**Figure 59C**). This in contrast to GAIIG, providing evidence for the inability of the GAIPIG peptide to self-assemble into amyloid cross- β -sheets. Additionally, in the simulations we observed the infrequent formation of complex conformations in which a peptide on one side forms nearly in-register antiparallel β -sheets while, on the opposite side, its proline side chain disallows the formation of an in-register β -sheet. Instead off-register antiparallel β -sheet interactions are formed, which result in breaking of the symmetry required for cross β -sheet interactions. These conformations, which are part of the complex conformations in our analysis¹²³ (**Figure 63A**), are reminiscent of the elementary structural units observed in the X-ray studies (**Figure 63B**).

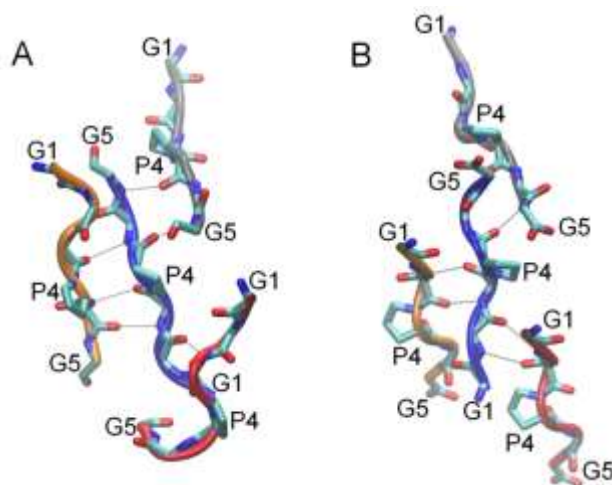


Figure 63: Molecular graphics images of the elementary structural unit of GAIPIG peptides. (A) A snapshot extracted from the self-assembly simulations of GAIPIG peptides which reproduces features of the elementary structural unit as depicted in (B) the experimentally resolved X-ray structure of GAIPIG.

Computational investigation of binding properties of GAIPIG to A β and the V3 loop

As for the second postulation, driven by the non-amyloid character of GAIPIG and our present results, we computationally investigated the binding properties to the sequentially similar GAIIG domains of A β and the HIV-1 gp120 V3 loop, and its ability to potentially inhibit A β fibril elongation or prevent the binding of the HIV-1 gp120 V3 loop to chemokine receptors. Of note, according to experiments, in the presence of elevated concentrations of GAIPIG, an increase in the length of the lag phase was as well as a reduction in the quantity of fibril formation by A β was observed; a 10-fold molar excess of GAIPIG led to about 25-30 % reduction in fibril formation after 168 hours (7 days) of incubation (**Figure 66**).

Simulations of A β fibrils in the presence of GAIPIG peptides provide insights for the experimentally observed inhibition, depicting that GAIPIG peptides bind to and form β -sheet interactions with ${}_{19}\text{FFA}_{21}$ and ${}_{30}\text{AII}_{32}$ of the VFFA and GAIIG motifs of A β respectively in such a way that the proline side chain is facing outwards from the fibril (**Figure 64**). Additional details are provided in Supplementary Information of ref⁷⁶. In addition, according to simulations of a specific HIV-1 gp120 V3 loop in the presence of GAIPIG peptides, GAIPIG peptides predominantly bind and form β -sheet interactions with residues within the GAIIG motif of loop and, to a lesser extent, residues on the opposite site of the loop comprising the GIHIG motif (**Figure 65**). Furthermore, as GAIPIG peptides favor interactions to the II motif of GAIIG and the GXIIG motif is abundant (e.g. GAIIG, GQIIG, GEIIG, GKIIG, etc.) despite the high variability of the HIV-1 gp120 V3 loop¹³², the future study and design of peptides acquiring a GAIPIG- based core and designed extensions (e.g., analogously to ref.¹³³) targeting V3 loop sequences can be of interest. GAIPIG-based peptide analogues could constitute seeds for potential HIV-1 gp120 V3 loop entry inhibitors, preventing its binding to chemokine receptors, similarly to polyanionic HIV-inhibitors¹³⁴⁻¹³⁵.

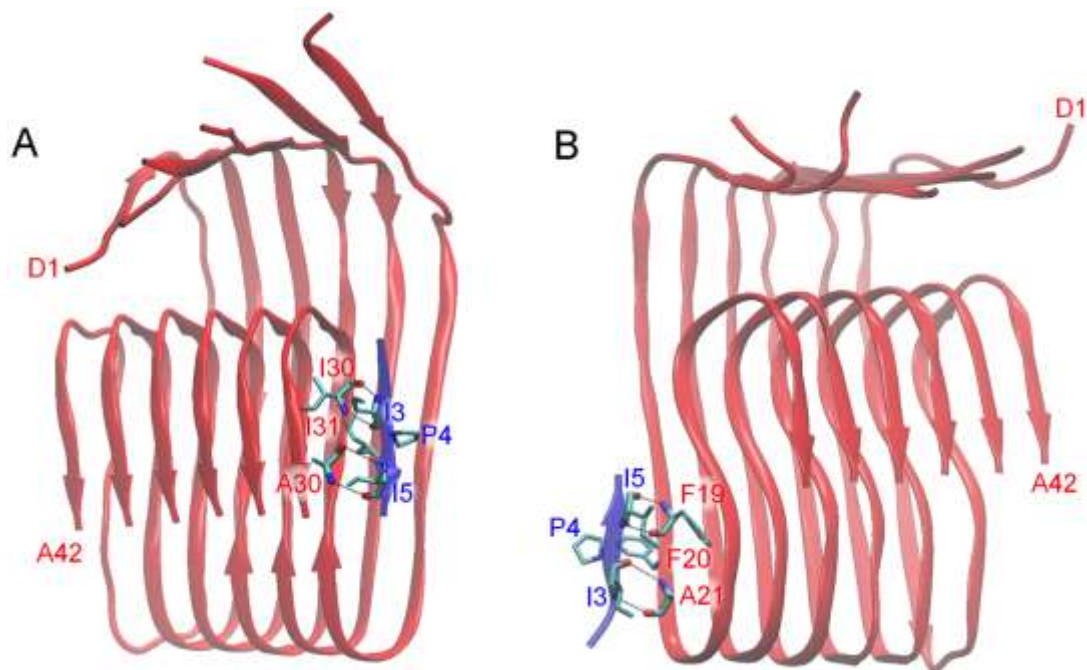


Figure 64: Molecular graphics images of representative structures of GAIPIG peptides, shown in blue cartoon representation, binding to A β fibrils, shown in red cartoon representation. GAIPIG peptides form β -sheet interactions, indicated with black dotted lines, with residues within the (A) GAIIG and (B) VFFA motifs.

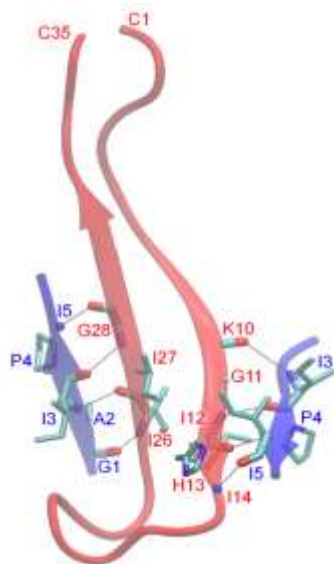


Figure 65: Molecular graphics images of representative structures of GAIPIG peptides, shown in blue cartoon representation, binding to V3 loop, shown in red cartoon representation. GAIPIG peptides form β -sheet interactions, indicated with black dotted lines.

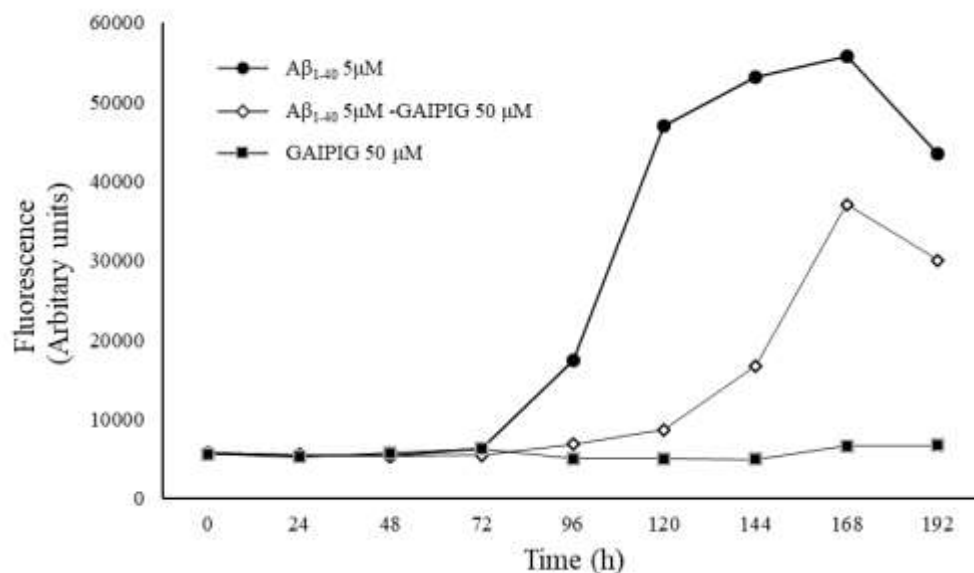


Figure 66: Kinetics of the A β_{1-40} peptide fibril formation (5 μ M) as assessed by Thioflavin-T binding assay in the absence (full circles) or in the presence of 50 μ M (open diamonds) GAIPIG peptide. Full squares, 50 μ M of GAIPIG peptide alone. One representative experiment from four independent ones is shown.

GAIIG as another A β core recognition sequence?

Of the residues belonging to the core of the amyloid fibril, the stretch comprising residues 16-21, KLVFFA, comprising the aromatic dipeptide motif FF has been most investigated as a core recognition sequence in Alzheimer's disease.¹³⁶ The beta-breaker peptide LPFFD was designed and studied both theoretically and experimentally.¹³⁷⁻¹⁴⁰ Moreover, endomorphin analogues comprising aromatic amino acids along with proline residues were recently studied as inhibitors of β -amyloid oligomerization.¹⁴¹ In addition to the role of the KLVFFA stretch, a number of different approaches were pointing at an important role of the GAIIG stretch in A β aggregation and fibril elongation. Residues ³⁰AIIIG³³, were

identified as part of the aggregation-prone region 30-42 of the A β peptide using a predictive algorithm of aggregation propensities developed by Dobson and colleagues.¹⁴² Thorough proline¹⁴³ and alanine-scanning¹⁴⁴ mutagenesis studies carried out by Wetzel and colleagues suggested that residues ₃₁IIG₃₃ were highly sensitive to proline and alanine replacements. Both replacements were increasing the ΔG of elongation equilibrium of the fibrils, indicating a destabilization of the fibril (reviewed in ref.¹⁴⁵). The peptide sequence NKGAI comprising residues 27-32 of A β , was also recently identified as one of the “hot regions” for self-and cross-interaction between A β and IAPP.¹⁴⁶ By using an *in vivo* reporter system, Ventura and colleagues calculated experimental aggregation propensities of the 20 amino acids with isoleucine ranking highest, followed by phenylalanine,¹⁴⁷ and identified the ₃₀AIIGLM₃₅ stretch as a “hot spot” for aggregation.¹⁴⁸ Moreover, according to theoretical studies, Ile is avoided in protein interfaces, has a high propensity to be involved in amyloid formation, and molecular dynamics studies of Nussinov and colleagues pointed to a stable Ile-Ile cluster holding the structure of the A β 25-35 region.¹⁴⁹ The Ile-Ile dipeptide motif might constitute a core recognition motif, analogous to the dipeptide motif Phe-Phe extracted from the KLVFFA sequence. Taking this into account, the GAIPIG peptide was studied and the computational results as well as the single crystal structure presented here confirm that proline insertion between the two isoleucines disrupts amyloid formation. Most efforts on discovering peptide inhibitors inspired by the sequence of A β focused primarily on modified peptides homologous to the sequence fragment KLVFFA.¹⁵⁰⁻¹⁵¹ Interestingly, our computational results show that the inhibition of GAIPIG to A β can be attributed to its capacity to bind to both sequence fragments KLVFFA and GAIIG of A β , suggesting that modified GAIPIG peptides are worthy of further investigation for A β inhibition.

3. 4. Conclusion

The theoretical and experimental studies presented here point to the GAIIG sequence as an amyloid-forming building block that merits further investigation as a potential core recognition sequence in A β . By introducing suitably selected mutations at the non β -sheet forming terminal residue positions of the longer sequence YATGAIIGNIL, novel materials could be designed. Furthermore, our computational results suggest interaction of the beta-breaker GAIPIG peptide with A β and experiments showed that the peptide delays the aggregation of the peptide A β_{1-40} *in vitro*. A natural peptide like GAIPIG cannot be envisaged as a potential therapeutic *per se*, due to degradation and stability issues *in vivo*, however non-natural analogues and peptidomimetics structurally related to the parent peptide can be developed¹⁵². Thus, the single-crystal structural information on the beta-breaker GAIPIG peptide could be exploited as a minimal framework for future structure-based design of A β inhibitors. Our computational results also suggested interaction of GAIPIG with the GAIIG sequence of gp120 V3 loop, especially with the II motif common to the GXIIG sequence of the V3 loop. Although we have not performed experimental investigations of inhibition of the V3 loop binding to chemokine receptors, the computational and single-crystal information presented in this paper can be of interest for the future design of V3 loop entry inhibitors in the future.

Chapter 4:

Designer Amyloid Cell Penetrating Peptides for Potential Use as Gene Transfer Agents

4. 1. Introduction

The development of biocompatible, efficient and stable carriers for the delivery of nucleic acids into eukaryotic cells for the restoration or correction of deficient gene products to normal expression levels has garnered increased interest in the field of gene therapy. Optimal carriers should package the DNA molecule efficiently into a stable complex that can bind and access cells, avoid degradation and release nucleic acids to the nucleus for gene expression or in the cytosol for gene regulation.^{153,154,155} Common hurdles are the inefficient delivery of nucleic acids in their naked form into the cells, due to their strong negative charge that inhibits their internalization, and their susceptibility to nucleolytic enzymes. This led to the development of a variety of non-viral vectors that can incorporate genetic material and efficiently deliver it into the cells.¹⁵⁶ One such vector comprising short cationic peptides called cell-penetrating peptides (CPPs) has recently emerged. CPPs have the capacity to effectively cross cellular membranes, have limited toxicity and could function as transfection carriers for nucleic acid cargos including siRNAs and plasmids.¹⁵⁷

CPPs typically consist of 5-30 amino acids rich in arginine and lysine amino acid groups, which are positively charged due to their protonation at neutral pH. Various energy-dependent or - independent¹⁵⁸ internalization mechanisms have been proposed,¹⁵⁹ including the interaction of the positively charged residues with the negatively charged phospholipids of the cell membrane to facilitate direct internalization and endosomal uptake via endocytic pathways.^{160, 161} Due to their ability to penetrate cellular membranes, CPPs could enhance the transportation of conjugated bioactive cargos, which in turn could initiate the expression or function of specific intracellular targets. These bioactive cargos can be conjugated with the CPPs through a covalent bond or through a non-covalent complex formation.¹⁵⁶

The mechanism proposed for a non-covalent complex formation and subsequent DNA transduction involves the complexation through electrostatic interaction of the positively charged amino acids of the peptide with the negatively charged nucleic acids and the further internalization of the newly constructed complex into the cell. The complexation of the CPPs with DNA and the subsequent transportation of the peptide-DNA complex through the cell membrane suggests the enhancement of gene transfer and also the protection of DNA against enzymatic degradation.³⁸

Extended lists of peptide carriers or enhancers of the expression of a gene of interest into cells have been proposed that facilitate the non-covalent peptide-DNA complex formation. Among others are the highly cationic TAT peptide that can directly penetrate the plasma membrane as polyelectrolytic complex upon interacting with plasmid DNA,³⁸ the amphipathic α -helical peptide NF55^{162,163} and the PepFect14 peptide vector.¹⁶⁴ Highly cationic peptides, especially polyarginine (nonaarginine, R9) and the T22 peptide (RRWCYRKCYKGYCYRKCR), when fused to the N-terminus of GFP along with a His-tag at the C-terminus were recently reported to mediate self-association into nanosized particles that penetrate cells.^{155,157,158} These nanosized particles can be exploited for the targeted delivery of both nucleic acids and protein drugs. Very recently, a novel category

of promising AMPs was reported, based on a number of bacterial aggregation prone regions (APRs) which are not toxic to mammalian cells but can induce protein aggregation in the bacterial cell, leading to loss of the bacterial proteostasis and eventual bacterial cell death.^{30,165} It seems therefore that properly designed protein and peptide aggregates in either synthetic or recombinant form could be amenable to rational design targeted for cell penetration and drug or DNA delivery. Cationic, amyloid forming peptides are also considered promising nanomaterials for boosting gene transduction by utilizing the positive charges on the fibrillar nanosheet formed by the peptides to capture nucleic acids and virion particles and subsequently promote their cell attachment and fusion.^{28, 67, 71, 166, 29}

Amyloid aggregation of initially correctly folded proteins is driven by short amyloidogenic sequence domains within the protein full sequence that self-assemble into fibrils.¹⁶⁷⁻¹⁶⁸ Amyloid formation was thought to be associated solely with amyloid diseases such as Alzheimer's and Parkinson's diseases.^{169,170,171,172} However, numerous studies demonstrated that amyloids could also be exploited as promising bionanomaterials^{105, 159, 173} or even assume physiologically relevant roles.^{174,161}

We have previously demonstrated that the ultrashort and homologous peptide sequences GAITIG and GAIIG can spontaneously self-assemble into amyloid fibrils^{22,76}. The GAITIG sequence is part of the adenovirus fiber shaft segment that in the absence of its natural trimerization motif aggregates into amyloid-type fibrils. By employing a reductionist approach, the sequence GAITIG was previously shown to be a minimal self-assembling building block.^{23,22} Similarly, the sequence GAIIG which is part of the amyloid beta peptide (residues 29-33) and also part of the HIV-1 gp120 V3 loop (residues 24-28) can also spontaneously form a beta-sheet amyloid core.⁷⁶ Exposed residues, outside the β -sheet GAITIG or GAIIG core, could be accessible and available for suitable selected modifications, rendering the resulting rationally designed sequences available for applications in biomedicine and technology.^{24, 25, 26} Thus, both peptides were previously

used as starting sequences for the computational and experimental design of functional scaffolds.²⁴⁻²⁶

In the present study we sought to rationally design self-assembling amyloid peptide sequences that could display cationic residues targeted for cell penetrating properties and eventual DNA binding ability. We employed computational methods, starting with scaffolds YATGAIIGNII and RGDSGAITIGC and mutated key non- β -sheet positions at the termini of the scaffolds, namely residues 1,2,3 and 11. We replaced these exposed residue positions with a combination of positively charged residues (Arg, and Lys) and tyrosine residues,¹⁷⁵ to mimic the cell penetrating properties and DNA binding ability of CPPs. The computational and experimental studies of the two rationally designed amyloid peptides, KYKGAIIGNIK and KYRSGAITIGY (hereinafter referred to as KK and KY, respectively) allowed us to conclude on the following concerning their properties: They i) can spontaneously self-assemble into amyloid fibrils ii) can interact electrostatically with plasmid DNA to form complexes and iii) can transfer pDNA into mammalian cells and promote protein expression of the gene of interest. Moreover, formulated peptide/DNA complexes exhibit long term stability, very limited cytotoxicity and the cationic peptides display strong bactericidal effect against *Escherichia coli*.

4. 2. Materials and Methods

Materials

KYKGAIIGNIK and KYRSGAITIGY peptides were custom synthesized by GenScript with C-terminal amidation. The purity of the peptides was over 95%. pGL3 plasmid with the SV40 promoter containing the gene for expressing luciferase was obtained from Addgene. HEK293T cell line was cultured at 37°C, 5%CO₂ in DMEM(Gibco) supplemented with 10% fetal bovine serum (Gibco) and 50 μ g/ml gentamycin. OPTI-

MEM (Gibco) was used to obtain a reduced environment for the optimal transfection conditions. Thiazolyl Blue Tetrazolium Bromide (MTT) and Congo Red were purchased from Sigma-Aldrich. Quant-IT PicoGreen dsDNA assay kit was purchased from ThermoFisher Scientific. Proteostat Aggresome detection kit was from Enzo.

Computational methods

The computational methods were conducted from Dr. Tamamis group at Texas A&M and are analyzed extensively in the submitted CPPs paper and in Sai Vamshi Jonnalagadda's PhD thesis.

In summary the two peptide sequences NH₃⁺-KYRSGAITIGY-CONH₂ and NH₃⁺-KYKGAIIGNIK-CONH₂ were rationally designed and computationally investigated using Replica Exchange Molecular Dynamics (REMD). Initially simulations were performed for the two peptides to investigate their conformational and self-assembly properties. The extracted highly ordered and well-aligned β -sheet structures were investigated for the key interactions formed between the amino acids within the structures and the solvent accessibility of the designed residues to assess the peptides' functionality was calculated.

Amyloid Fibril formation

Peptide powders were dissolved in sterile filtered double distilled water in a final concentration of 6mg/ml. The resulting peptide solutions were incubated in room temperature for 3 days. Formation of fibrils was confirmed by FESEM, TEM and Congo red staining as previously described.²⁵

Field Emission Scanning Electron Microscopy (FESEM)

After the 3 day incubation period, 10 μ L of each peptide sample, diluted 1:6, was deposited on a cover glass and was air-dried overnight. Dried samples were covered with 10 nm Au/Pd sputtering. Observation experiments were performed using a JEOL JSM-7000F microscope operating at 15 kV.

Transmission Electron Microscopy (TEM)

Each sample (5 μ l) was deposited directly onto a formvar/carbon coated electron microscopy grid for 2min. Excess was carefully removed with a filter paper and the sample was stained with 2% w/v uranyl acetate for 2 min. The observations were conducted with a JEOL JEM-2100 Transmission Electron Microscope at 80 kV.

Congo Red staining

Each peptide solution (20 μ l) was thoroughly mixed with 5 μ l of a fresh Congo Red assay solution (10mM Congo Red, 2.5mM NaOH in 50% ethanol). A drop of the mixture was deposited on a glass coverslip and was examined before or after it was dried, at room temperature, with a Zeiss Stemi 2000-C microscope with and without the use of a crossed polarizer.

Formulation of Cationic Peptides and pDNA complexes

The pGL3-SV40 luciferase expressing plasmid was mixed with the self-assembled peptides at various ratios, in a total volume of 50 μ l double distilled sterile water. Formulations were allowed to assemble for at least 1 hour in room temperature before cell transfection.

Gel retardation assay

The formation and DNA condensation of the CPP-DNA complexes was verified by electrophoresis on a 0.5% agarose gel in TAE 1x buffer and imaged by staining of the gel with Gel-Red (Biotium). Complexes were formed as previously described. 0.5µg of pGL3-SV40 was mixed with 10, 25, 50, 100, 200 µg of each peptide for 1 hour. 4µL loading buffer was mixed with the samples before the electrophoresis.

PicoGreen fluorescence quenching experiments

pDNA (0.5 µg) was labelled with 30µL of the PicoGreen reagent (1:150w/v) in TE buffer for 30min at room temperature. The labelled pDNA was mixed with 10, 25, 50, 100, 200 µg of the self-assembled peptides for 1 hour in room temperature. PicoGreen binds to the grooves of the DNA backbone and strongly fluoresces when excited at 488nm. Quenching of the fluorescence indicates packaging of the nucleic acid. The quenched fluorescence was analyzed in a BioRad CFX Connect Real-Time System and the naked pDNA labelled with PicoGreen fluorescence signal was used to normalize the signal detected from the peptide-DNA signal. Values are expressed as quenching percentage.

Zeta potential measurement

pDNA-peptide complexes were formulated in a final volume of 200µl filtered double distilled water in different DNA : peptide concentration ratios (1:312, 1:625, 1:1250, 1:2500 and 1:5000). An additional dilution with 1mM NaCl to up to 1ml volume followed before measurement. Measurements were performed in a ZetaSizer Malvern instrument, using the Smoluchowski model, set to a number of 5 runs.

Cell internalization of the amyloid forming peptides

5x10⁴ HEK293T Human embryonic kidney cells were seeded for 24h in a 24 well plate after addition of a 13mm TC Coverslip at the bottom of the well. The culture medium (DMEM) was replaced and 25µg of the fibrillar peptide sequence, diluted in 0.5ml

DMEM, was added for overnight incubation. Culture media was aspirated and the cells were carefully washed two times with PBS 1x. The cells were fixed with 4% formaldehyde for 30min, washed with PBS 1x and permeabilized for 5 min with 0.5% Triton X-100, 3mM EDTA, pH:8. After washing twice with PBS 1x the cells were treated with the staining solution containing the Proteostat aggregates staining and Hoechst nuclear dye. Additional washes with PBS 1X followed, the coverslip was mounted on a microscope coverslip and the internalization efficacy of the peptides was assessed in a Leica SP8 inverted confocal microscope at ex/em 500/600nm for the Proteostat dye and ex/em 350/461nm for Hoechst 33342.

MTT cell proliferation assay

Cell viability in the presence of the peptides was studied by monitoring the conversion of Thiazolyl Blue Tetrazolium Bromide reagent (MTT) into formazan by the mitochondrial dehydrogenases of the living cells. HEK293T cells with concentrations of 7×10^3 cells/well were cultured in a 96-plate for 24h. Removal of the medium was followed by treatment of the cells with increasing concentrations (10, 25, 50, 100, 200 μ g) of the self-assembled peptide, suspended in a total volume of 200 μ l of culture medium. Cells which were not treated with the peptide, served as control. After 48h incubation, the medium was carefully removed and replaced with 100 μ l of fresh medium and 10 μ l of MTT (5mg/ml) dissolved in PBS 1x. The cells were incubated for 4 h to allow the development of the purple formazan products and the MTT-culture medium was substituted with 100 μ l of isopropanol-DMSO 1:1 solution. The formazan crystals were allowed to dissolve for 15min at 37°C. The absorbance was measured at 570nm in a Synergy HTX BioTEK Plate Reader.

Plasmid transfection and luciferase assay

HEK293T cells were seeded in a 24-wellplate at a density of 6×10^4 cells per well and grown until 60% confluency. The cultured medium was smoothly removed and 500 μ l of OPTI-MEM medium containing 50 μ l of the preformed pDNA : peptide complexes in ratios (1:312, 1:625, 1:1250, 1:2500 and 1:5000 after sequential dilutions) were carefully added into the wells. After a 4hour at 37° C incubation period, the medium was removed, 1 ml of fresh DMEM supplemented with FBS and gentamycin was added and the cells were incubated for 48h to allow the reporter gene expression. Luciferase activity was measured by using a luciferase assay system according to the manufacturer's guidelines (Bright-Glo, Promega) in a Synergy HTX BioTEK Plate Reader. Protein concentration in cell lysates was assessed by the Bradford assay.

Antimicrobial testing

The antimicrobial activity of the peptides was assessed by following the broth microdilution method¹⁷⁶ adjusted to the guidelines of CLSI (*Clinical and Laboratory Standards Institute. Performance standards for antimicrobial susceptibility testing; sixteenth informational supplement. CLSI document M100-S16* CLSI, Wayne, PA (2006) and EUCAST (*European Committee for Antimicrobial Susceptibility Testing (EUCAST) of the European Society of Clinical Microbiology and Infectious Diseases (ESCMID)*). Bacteria were grown in Luria Bertani broth (LB) in a shaking incubator at 37°C overnight, using individual colonies retrieved from a fresh overnight BL21 DE3 plate. The bacterial suspension was adjusted to 10^6 CFU/mL in LB according to the MacFarlane standard. 50 μ l of the bacterial inoculum was mixed in 96-well plates with the twofold diluted peptide solutions (50 μ l) to reach final concentrations of peptides ranging from 3mg/ml to 0.005mg/ml, including two inhibition controls (kanamycin 50 μ g/ml and ampicillin 100 μ g/ml), a sterility, and a growth control. Each peptide concentration was tested in triplicate. The plate was incubated for 24h at 37°C and the optical density was measured at 600nm (OD600) in a Synergy HTX BioTEK Plate Reader.

pDNA internalization and sub-cellular localization

7x10⁴ HEK293T Human embryonic kidney cells were seeded for 24h in a 24 well plate after addition of a 13mm TC Coverslip at the bottom of the well. The following day 50ng of pGL3-SV40 plasmid was incubated for 30min with the PicoGreen dye (1:150 dilution) and it was further mixed with 250µg of the KK or KY peptide for 1 hour. The medium was carefully removed and 50µl of the pre-stained pGL3-SV40-peptide complex diluted in 500µl OPTI-MEM was added to the well. After 4h incubation at 37°C, the culture media was aspirated and the cells were carefully washed two times with PBS 1x. The cells were fixed with 4% formaldehyde for 15min, washed with PBS 1x and permeabilized for 5 min with 0.1%Triton X-100. After washing twice with PBS 1x and incubate for 30min with BSA 2%-PBS 1x, the cells were treated with the staining solution containing the AlexaFluor 680 Phalloidin dye. Two additional washing steps with PBS 1x followed before the coverslip was mounted on a microscope coverslip containing a drop of the DAPI nuclear staining dye. The internalization and subcellular localization of the stained pDNA was assessed in a Leica SP8 inverted confocal microscope at ex/em 679/702 nm for the AlexaFluor 680 Phalloidin dye, ex/em 488/520nm for the PicoGreen dye and ex/em 360/460nm for DAPI nucleus stain.

4. 3. Results

Computational Results

The computational results were carried out by Dr. Tamamis group at Texas A&M and are analyzed extensively in the submitted CPPs paper and Sai Vamshi Jonnalagadda's PhD thesis.

In summary, the simulations verified the self-assembly properties for both peptides after observing

the frequent formation of intermolecular β -sheets. Moreover, both the designed peptides formed antiparallel as their dominant configuration in line with the configuration of the designable scaffolds from which each of them was designed (**Figure 67**). The functionality of the residues at the C- and N-terminal part of the peptide sequences KYRSGAITIGY and KYKGAIIGNIK indicate potential functionality, since they are outside the predicted amyloid core. The β -sheet forming cores of the peptides were predicted to be GAITIG and GAIIGN, respectively. Subsequently, the designed residues were predicted to be sufficiently solvent exposed suggesting their potential functionality for cell-penetration and DNA binding properties (**Table 4**).

Table 4: Degree of solvent accessibility of the four designed residues in the two designed peptides KYRSGAITIGY and KYKGAIIGNIK. The degree of solvent accessibility is calculated for the sidechains of the designed residues based on the definitions provided in the refs ^{25, 26}

Peptide	Residue Position 1	Residue Position 2	Residue Position 3	Residue Position 11
NH ₃ ⁺ -KYRSGAITIGY- CONH ₂	0.58 ± 0.06	0.45 ± 0.10	0.49 ± 0.08	0.43 ± 0.11
NH ₃ ⁺ -KYKGAIIGNIK- CONH ₂	0.63 ± 0.06	0.42 ± 0.09	0.53 ± 0.06	0.53 ± 0.07

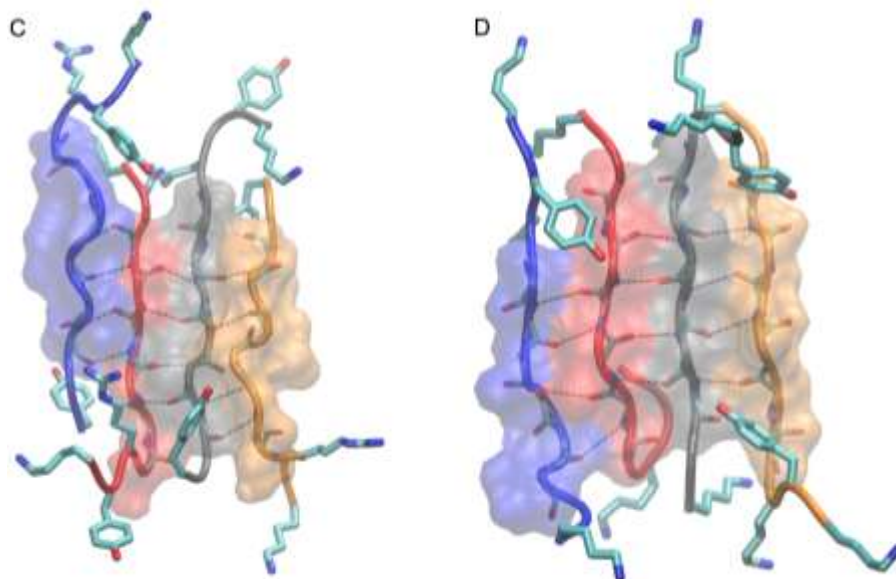


Figure 67: Panels C and D correspond to molecular graphic images of representative highly ordered and well-aligned conformations of peptides KYRSGAITIGY, and KYKGAIIGNIK in antiparallel arrangement, respectively. The peptides' backbone is shown in tube representation and the backbone atoms forming β -bridges are shown in thin licorice representation and are colored by name, and the β -bridge associated hydrogen bonds are shown using black dashed lines. The peptides are colored in blue, red, gray and orange from left to right. Residue moieties 4-9 in each of the two designed peptides form amyloid-zipper like patterns and are shown in transparent surface representation. Side chain atoms of residues at positions 1, 2, 3, and 11 are shown in thick licorice representation.

Designer peptides KK and KY self-assemble into positively charged amyloid fibrils

Both peptides $\text{NH}_3^+\text{KYKGAIIGNIK-CONH}_2$ (KK) and $\text{NH}_3^+\text{KYRSGAITIGY-CONH}_2$ (KY) were designed to contain a beta-sheet forming core, GAIIG and GAITIG respectively, that is being reported to self-assemble into amyloid fibrils in vivo and in vitro.^{22, 76} To assess whether our beta-sheet-containing sequences correspond to amyloid like morphologies after self-assembly, FESEM and TEM observations were performed. We further validated that the peptides can self-assemble into amyloid fibrils with Congo Red, one of the most

commonly used dyes for amyloid detection. Both peptide powders after being dissolved in sterile deionized water, acquired a fibrillar conformation of long, straight, randomly oriented fibrils with widths in the range of 10–20 nm as observed under FESEM (**Figure 68A, Figure 69A**) and TEM (**Figure 72A, Figure 73A**) Moreover, addition of Congo Red stain to the incubated peptides uncovered the amyloid nature of the fibrils due to the yellow-green birefringence of the peptides under a crossed polarizer (**Figure 68B, Figure 69B**). A combination of positively charged residues (Arg, and Lys) at the designable positions on both scaffolds resulted in a positive z-potential indicating the cationic peptide KK at 32.3 ± 0.91 mV and KY at 31.2 ± 2.19 mV (**Table 6**)

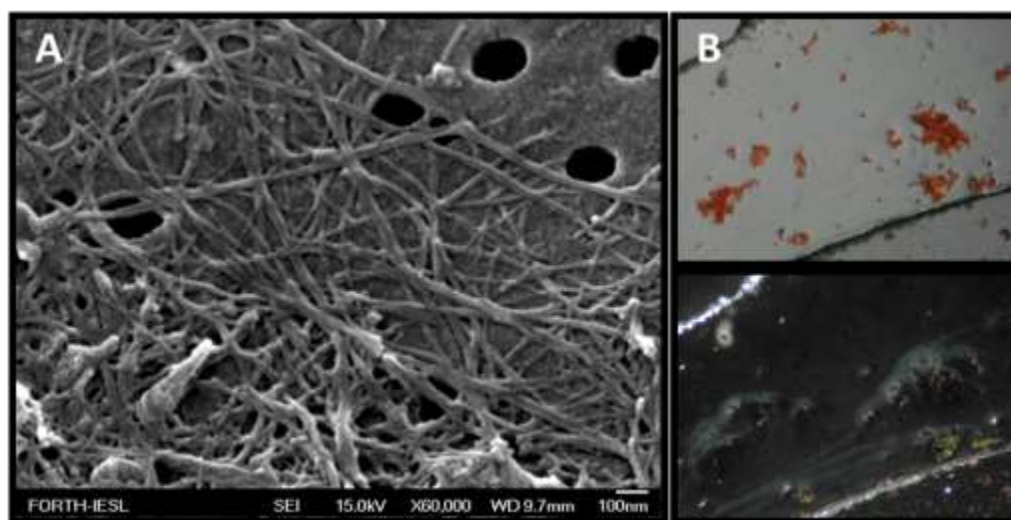


Figure 68: **A:** FESEM picture of the self-assembled peptide $\text{NH}_3^+ \text{KYKGAIIGNIK-CONH}_2$ (KK) after incubation in sterile double distilled water for 3 days. Distinct fibrillar conformation is observed. **B:** Congo Red staining confirms the formation of amyloid fibrils due to the yellow/green birefringence under crossed polarizer. Top: without and Bottom: with the use of a crossed polarizer. FESEM scale bar is 100 nm

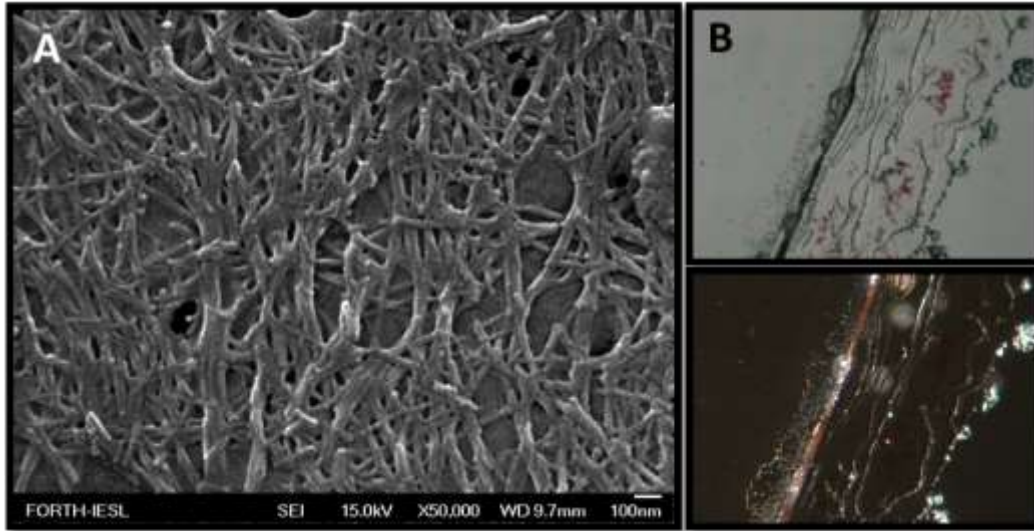


Figure 69: **A:** FESEM picture of the self-assembled peptide $\text{NH}_3^+ \text{KYRSGAITIGY-CONH}_2$ (KY) after incubation in sterile double distilled water for 3 days. Distinct fibrillar conformation is observed. **B:** Congo Red staining confirms the formation of amyloid fibrils due to the yellow/green birefringence under crossed polarizer. Top: without and Bottom: with the use of a crossed polarizer. FESEM scale bar is 100 nm.

Amyloid cationic peptides package pDNA by forming stable fibrillar complexes

To examine the binding and condensation ability of our amyloid peptides with pDNA, Gel retardation, PicoGreen fluorescence assay and TEM observations were performed.

pDNA complexes were prepared with the two cationic peptides at DNA/peptide ratios ranging from 1:20 to 1:400. After 1h incubation they were analyzed for changes in their mobility by a 0.5% agarose gel electrophoresis. Both peptides bound and completely retarded pDNA in the wells (**Figure 70**). It should also be noted a slight decrease in the intensity of the GelRed stain fluorescence in the highest concentrations of the KK peptide complexes suggesting further fluorescence quenching due to the additional pDNA association. The aim of this experiment is to identify the DNA condensation capacity of the peptides since plasmid DNA has a highly negative charge and each of the peptide monomers can contribute positive charges attributed to the arginine and lysine residues and also to the unprotected amino group at the N-terminal end. Concluding the above results, we have verified that our peptides can fully package pDNA.

As an additional confirmation for the binding of the peptides to pDNA, a PicoGreen fluorescent quenching assay was conducted. In the following assay, pDNA was mixed with the PicoGreen dye that emits a strong fluorescent signal when excited at 488nm. Quenching of this signal indicates packaging of the DNA and subsequent binding. Comparing the remaining fluorescence after the complex formation with the fluorescence of the naked pDNA, the percentage of the fluorescence loss corresponds on the level of DNA packaging by the peptides. Complexes of pDNA with the peptides achieved maximal quenching of the PicoGreen signal in all of the DNA-peptide ratios tested (**Figure 71**) , which confirms that even in low concentrations our amyloid cationic peptides possess a high binding capacity, a result that is in agreement with the Gel retardation assay experiment.

Table 5: Summary of the peptide and pDNA concentrations used for the formation of the complexes.

pDNA/peptide ratio	Peptide concentration (µg/ml)	pDNA concentration (ng/µl)
1:5000	250	50
1:2500	125	50
1:1250	52.5	50
1:625	31.2	50
1:312	15.6	50

Table 6: The average zeta potential of the cationic amyloid peptides.

<i>Zeta potential (mV)</i>

pDNA/peptide ratio	NH ₃ ⁺ KYKGAIIIGNIK- CONH ₂	NH ₃ ⁺ KYRSGAITIGY- CONH ₂
Peptide only	32.3 ± 0.91	31.2 ± 2.19
1:5000	27.45 ± 0.9	28.8 ± 0.21
1:2500	26.9 ± 0.67	24.1 ± 1.25
1:1250	24.9 ± 0.66	14.8 ± 1.72
1:625	22.1 ± 2.92	13.7 ± 2.75
1:312	1.95 ± 1.02	4.2 ± 0.74

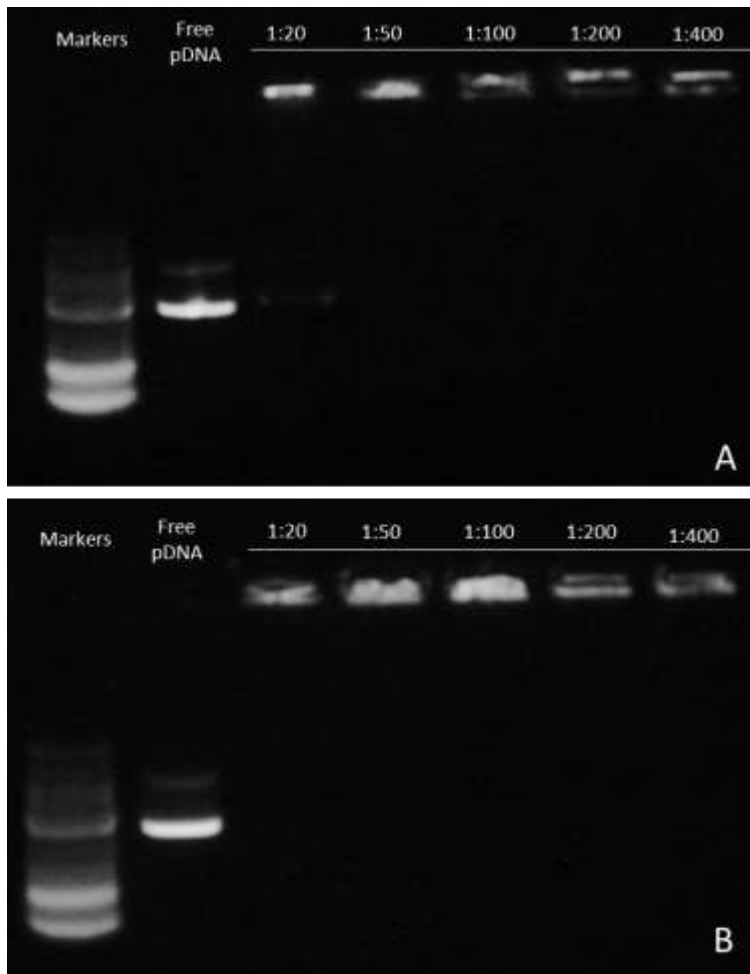


Figure 70: Gel retardation assay for the binding efficiency of the amyloid peptides with pDNA. Peptides **A)** KK and **B)** KY were complexed with 500ng of pGL3-SV40 in

pDNA/peptide ratios varying from 1:20 to 1:400 for 30min. Formed complexes were run in a 0.5% agarose gel. Free pDNA was used as control.

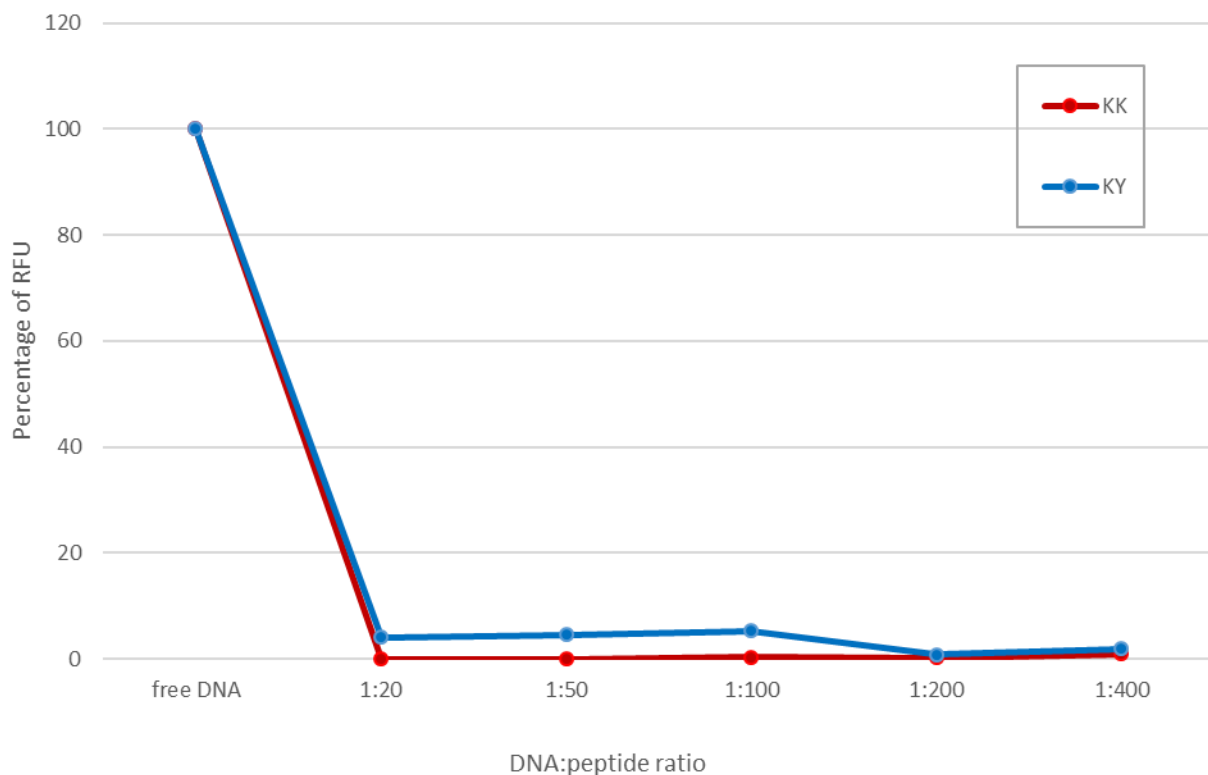


Figure 71: Percentage of Pico Green fluorescence quenching due to pDNA binding to the amyloid peptides. NH_3^+ KYKGAIIGNIK- CONH_2 (red) and NH_3^+ KYRSGAITIGY- CONH_2 (blue) are mixed with a constant concentration of pDNA (500ng) in various ratios for 30min. Complexes are further stained with the PicoGreen dsDNA dye. The fluorescence intensity of the complexes was then measured and normalized with the naked pDNA and the percentage of free and unbound pDNA is measured according to the fluorescence quenching level. Low fluorescence percentages indicate DNA binding with the peptides and subsequent quenching of the fluorescence signal.

DNA binding alters the conformation of the fibrils

We next investigated the effect of DNA binding to the conformation of the fibrils after incubation. Interestingly, while amyloid peptides KK and KY exhibit a randomly

oriented architecture (**Figure 72A, Figure 73A**), when these peptides are incubated with the pDNA molecules they seem to adhere with each other affording a more aligned assembly (**Figure 72B, Figure 73B**). This bundling of the fibrils could be mediated by the electrostatic attraction between negatively charged pDNA molecules and cationic residues belonging to adjacent fibrils/beta sheets.

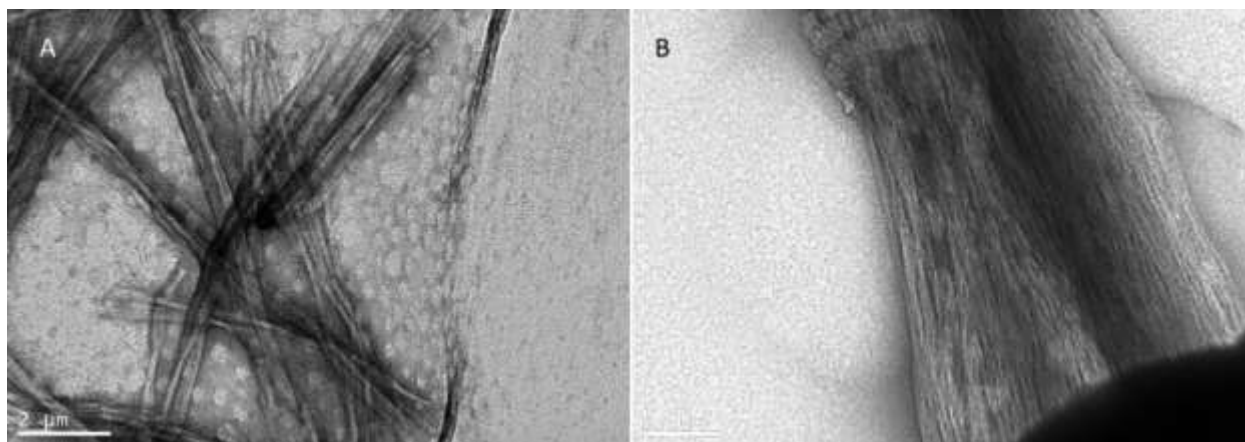


Figure 72: TEM micrographs of the NH_3^+ KYKGAIIGNIK- CONH_2 peptide's fibrils negatively stained with 2% uranyl acetate **A**) before incubation with pDNA **B**) after incubation with pDNA for 1hour in a 1:1000 DNA/peptide ratio. Change in the conformation of the fibrils after binding with pDNA, pDNA, from a random orientation to a more aligned configuration with adherent fibrils suggests DNA binding. Scale bar is $2\mu\text{m}$.

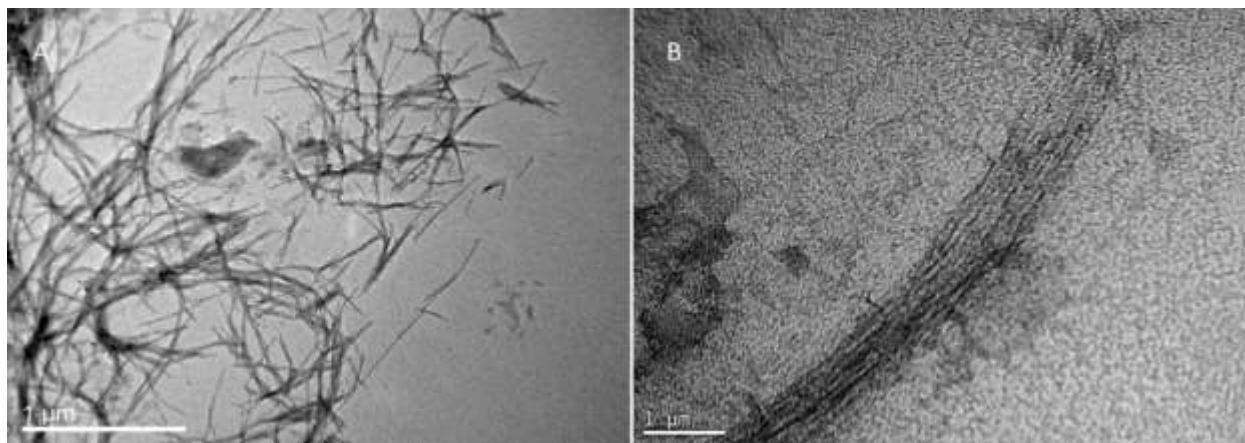


Figure 73: TEM micrographs of the NH_3^+ KYRSGAITIGY- CONH_2 peptide's fibrils negatively stained with 2% uranyl acetate **A**) before incubation with pDNA **B**) after

incubation with pDNA for 1hour in a 1:1000 DNA/peptide ratio. Change in the conformation of the fibrils after binding with pDNA, from a random orientation to a more aligned configuration with adherent fibrils suggests DNA binding. Scale bar is 1 μ m.

Long term stability of the pDNA/peptide complexes

Moreover, KK-DNA and KY-DNA complexes displayed excellent stability in long term storage (over 4 months) at room temperature or in refrigerated conditions without the use of any additives. Furthermore, after lyophilization of the peptide-DNA complex solutions and subsequent resuspension in water, no apparent loss of their binding capability and stability was observed, after being tested with the aforementioned methods. (results not shown).

Internalization of the cationic peptides and pDNA-peptide complexes and their subcellular localization

As concluded in the computational analysis of the two peptides, the designed cationic residues have a high probability of being exposed and accessible for cell penetration and DNA binding. We examined the cell internalization propensity of the two peptides by employing the Proteostat staining assay. The PROTEOSTAT® dye is a red fluorescent molecular rotor dye, which specifically intercalates into the cross-beta spine of protein and peptide structures. This binding inhibits the dye rotation and leads to a strong fluorescence emission.¹⁷⁷ Peptides KK and KY were incubated with HEK293T cells and were subsequently stained with the Proteostat dye. Cells were also stained with the nuclear Hoechst dye to better distinguish the cell nucleus location. Both peptides seem to internalize in the cell and to localize in the cytoplasm. (**Figure 74**). For additional internalization detection studies concerning the pDNA-peptide complexes, kidney embryonic cells HEK293T were incubated with the pre-stained peptide-pGL3 DNA complexes for 4 hours and subsequently imaged in a confocal fluorescent microscope. We detected the prestained with Picogreen plasmid mainly in the nuclear area (**Figure 75**), indicating successful transfection and transition of pDNA in the nucleus within 4 h

hours with the use of the peptide carriers. In **Figure 75A** is shown only the PicoGreen stain control. PicoGreen although is able to stain free dsDNA, is not considered a cell permeable dye. To confirm that the green fluorescence is attributed predominantly to the prestained pDNA inserted in the nucleus, and not PicoGreen interference, cells were incubated for 4h only with the PicoGreen stain in the same concentrations used for staining of the pDNA. Only a dim green fluorescence was observed in the cell nucleus, indicated that PicoGreen unspecific staining will not interfere with our observations. Cells incubated with the prestained pDNA/peptide complex are shown in **Figure 75B** where only the cell nucleus (blue) and actin (red) were visualized, whereas in **Figure 75C** the PicoGreen (green) and actin (red) filters were applied. An intense green fluorescence signal in the nucleus is detected in **Figure 75C** and is indicative of the effective internalization and transfer of the prestained SV40-pDNA into the nuclear area. Eventually, when all the filters were applied, the cell nucleus acquires a blue/green color attributed to the mixed color of the DAPI and PicoGreen fluorescence signals. (**Figure 75D**).

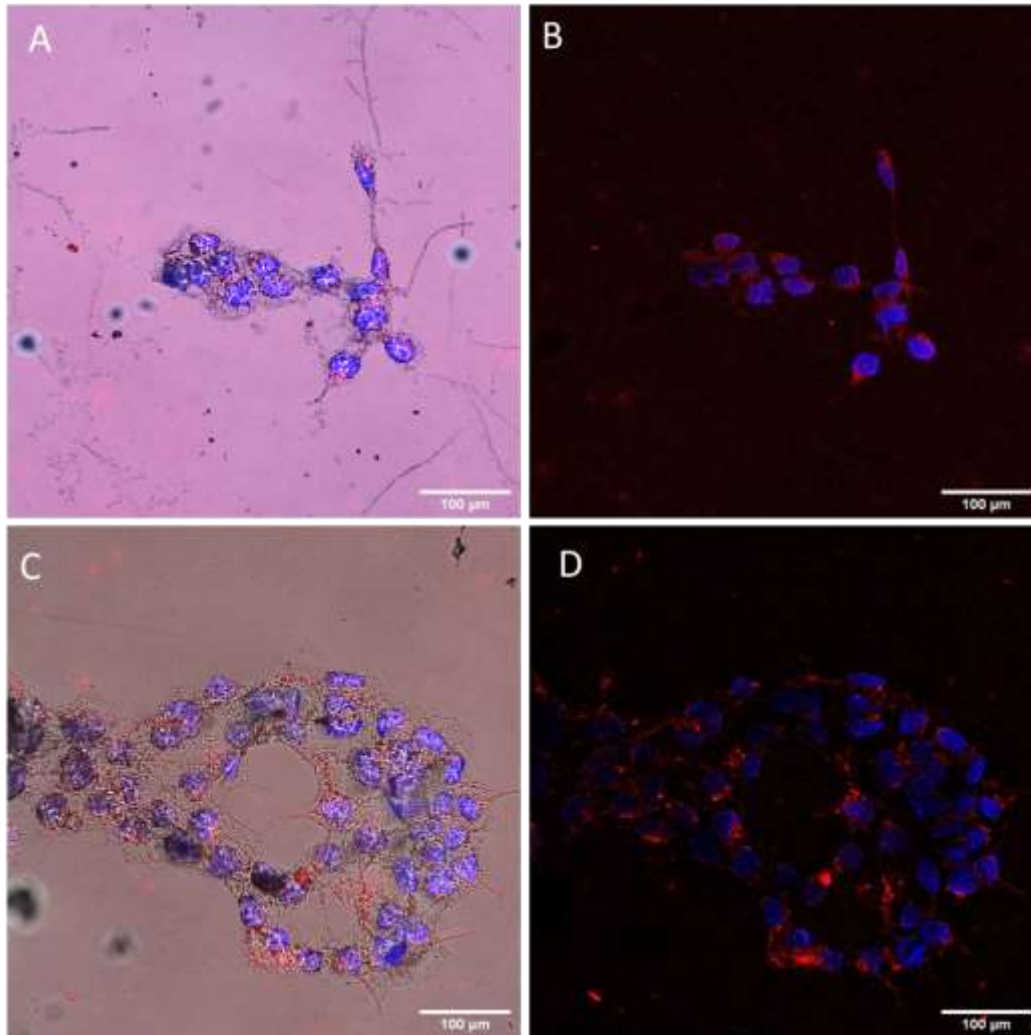


Figure 74 : Cellular uptake of the cationic amyloid peptides. HEK293T cells were exposed to 25 μ g of KK and KY peptide, followed by a 24h incubation. For confocal microscopy observations, cells were washed and stained with a mixture of the Proteostat dye that binds to the amyloid fibrils and Hoechst 33342 for nuclear stain. Pictures **A** and **B** correspond to KK peptide and **C** and **D** to KY peptide. For pictures **A** and **C** the brightfield illumination form was applied additionally, to circumscribe the limits of the cell membranes. Moreover, z-stacks for each peptide was obtained to ensure the internalization and not the external cell adhesion of the peptides (results not shown). Scale bar:100 μ m

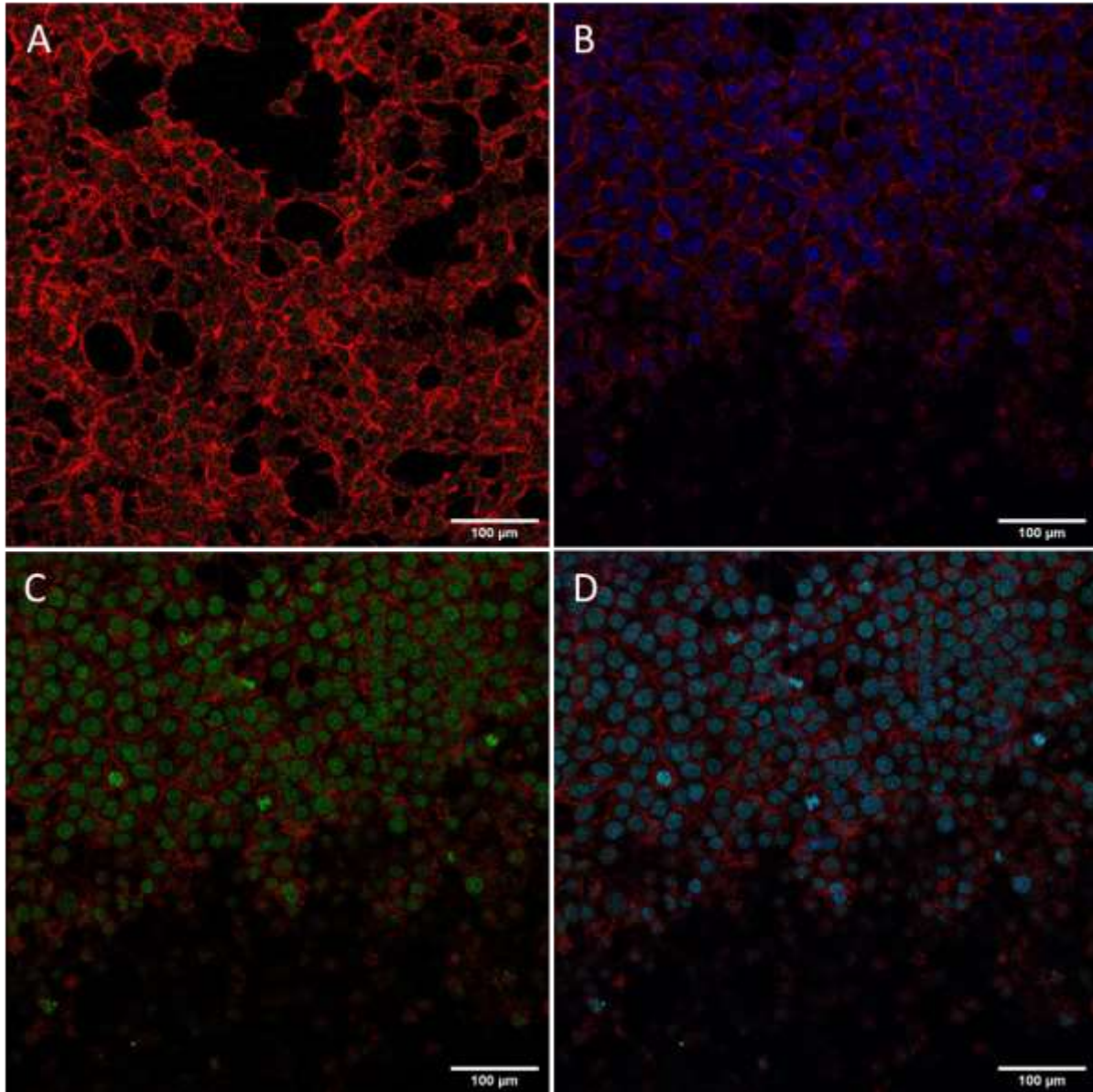


Figure 75: pGL3-SV40 delivery into the nucleus with the aid of the KK peptide. HEK293T cells were treated for 4h with a prestained with PicoGreen pDNA/KK complex at a 1:5000 ratio. PicoGreen dye without adding the DNA/peptide complex was used as a control. Cells were washed and stained with AlexaFluor680-Phalloidin for visualizing cell membranes (red) and DAPI for visualizing the nucleus (blue). Confocal image of the cells **A)** incubated only with the PicoGreen stain control. **B)** after incubation for 4h with the complex applying only the DAPI (blue) and Phalloidin (red) filter **C)** with the PicoGreen filter for pDNA visualization (green) and Phalloidin (red). **D)** A merged picture with the three stains (all filters applied) confirms the successful transportation of the pGL3-SV40 into the nucleus due to the SV40 nuclear localization signal. KY rendered similar results. Scale bar: 100 μm

Transfection studies of the cell penetrating amyloid peptide - pDNA complexes

We investigated the ability of our amyloid peptides to deliver the luciferase expressing plasmid pGL3-SV40 into the cells and trigger effective gene expression. For gene expression studies, kidney embryonic cells HEK293T were incubated with the peptide/DNA complexes (**Table 5**) for 48h followed by a luciferase activity detection assay. The KK-pDNA and KY-pDNA complexes mediated detectable and satisfactory transfection levels of the pGL3-SV40 plasmid as detected by the luciferase expression levels (**Figure 76**). KK-DNA and KY-DNA complexes have their highest transfection efficacy at a DNA/peptide ratio of 1:5000, while decreasing the peptide concentration down to a 1:312 ratio led to decreased transfection efficacy for both peptides. This can be attributed to the higher overall positive charge of the complexes in ratios where the peptide concentration is increased. As depicted in **Table 6**, KK and KY complexes start from a 1:5000 DNA/peptide ratio with a positive zeta potential of 27.45 ± 0.9 mV and 28.8 ± 0.21 mV accordingly. Keeping a constant DNA concentration of 50 ng and gradually decreasing the peptide concentration from 250 μ g to 15.6 μ g, we come down to a DNA/peptide ratio of 1:312 and a decreased zeta potential of 1.95 ± 1.02 mV and 4.2 ± 0.74 mV for the KK-pDNA and KY-pDNA complexes accordingly. The results indicate that there is a direct correlation between the amount of higher positively charged peptide complexes and the transfection levels. Moreover, it should be noted that KY-DNA complexes achieved higher luciferase gene expression level compared to KK-DNA complexes.

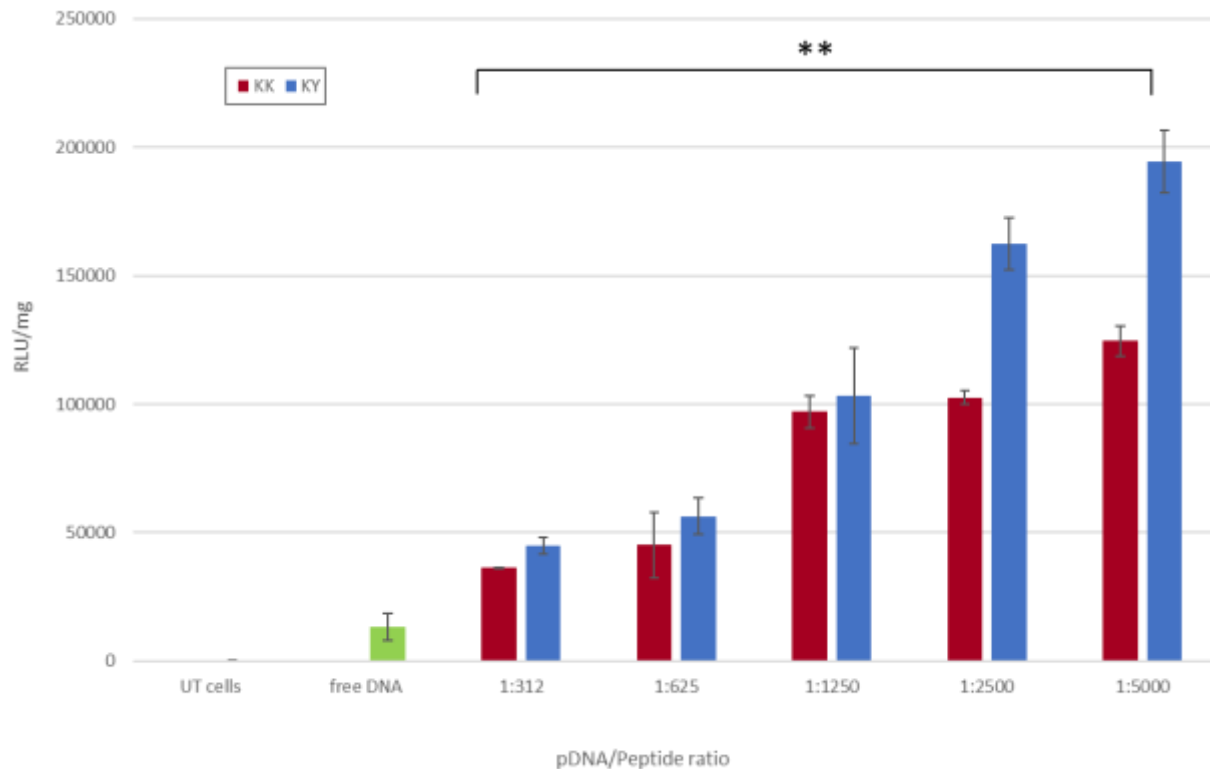


Figure 76: Levels of expression of the luciferase protein in the HEK293T cells after transfection with the pGL3-SV40/KK and pGL3-SV40/KY complexes at different ratios for 4hours and a following incubation for 48hours. Untreated cells and free pDNA were used as controls. ** denotes the significant difference in the RLU/mg between the untreated cells and the transfected cells ($p < 0.01$).

Designed peptides are toxic to bacteria but not to mammalian cells

An ideal gene delivery vehicle should exhibit very limited or no cytotoxicity to the cells being transfected. Indications of a toxic carrier are initially assessed by cell viability assays such as the MTT test. To validate this, we carried out transfections with the KK and KY peptides at increasing concentrations and measured the impact on the cell line by using MTT assay. Results indicate that, no significant cytotoxicity related with KK and KY peptides was observed and therefore the peptides can be considered non-toxic to the cell line and at the conditions tested (**Figure 77**). We further examined the antimicrobial

potency of our cationic amyloid peptides against a common Gram-negative bacterial specie, *Escherichia coli* BL21 DE3. It should be noted that both cationic peptides KK and KY inhibited bacterial population growth. However, KY has better antimicrobial activity by reducing bacterial population at 50% at concentrations around 0,375mg/ml compared to KK that required higher concentrations (1.5mg/ml) for the same result. (Figure 78).

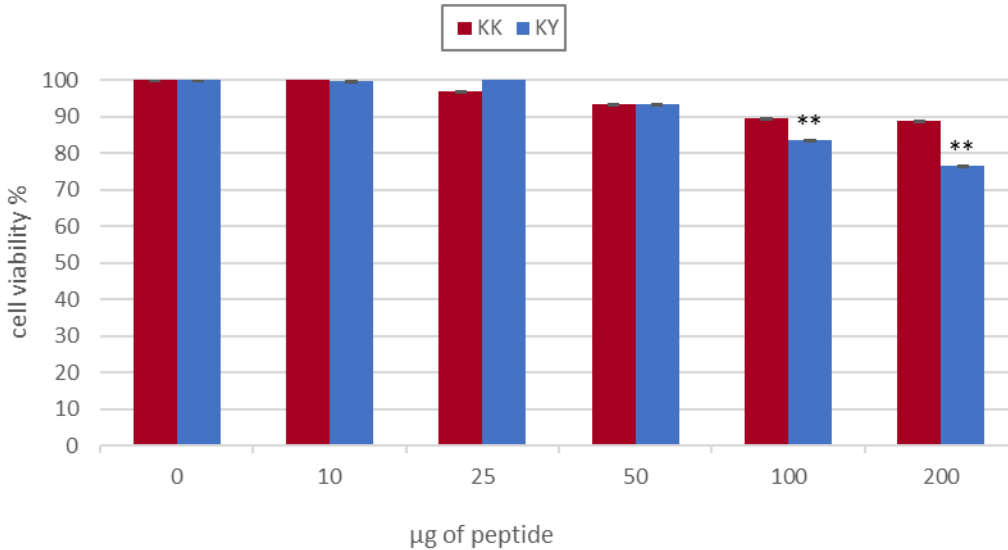


Figure 77: MTT cell viability assay results of the amyloid peptides incubated for 48h in HEK293T cells. KK peptide is represented with red and KY with blue. Various concentrations of the peptides were used varying from 10 to 200µg. Results are expressed as a percentage value of control cells cultured without the addition of peptides (control = 100%). ** denotes the significant difference in cell viability between the untreated cells and the transfected cells with the peptides ($p < 0.01$).

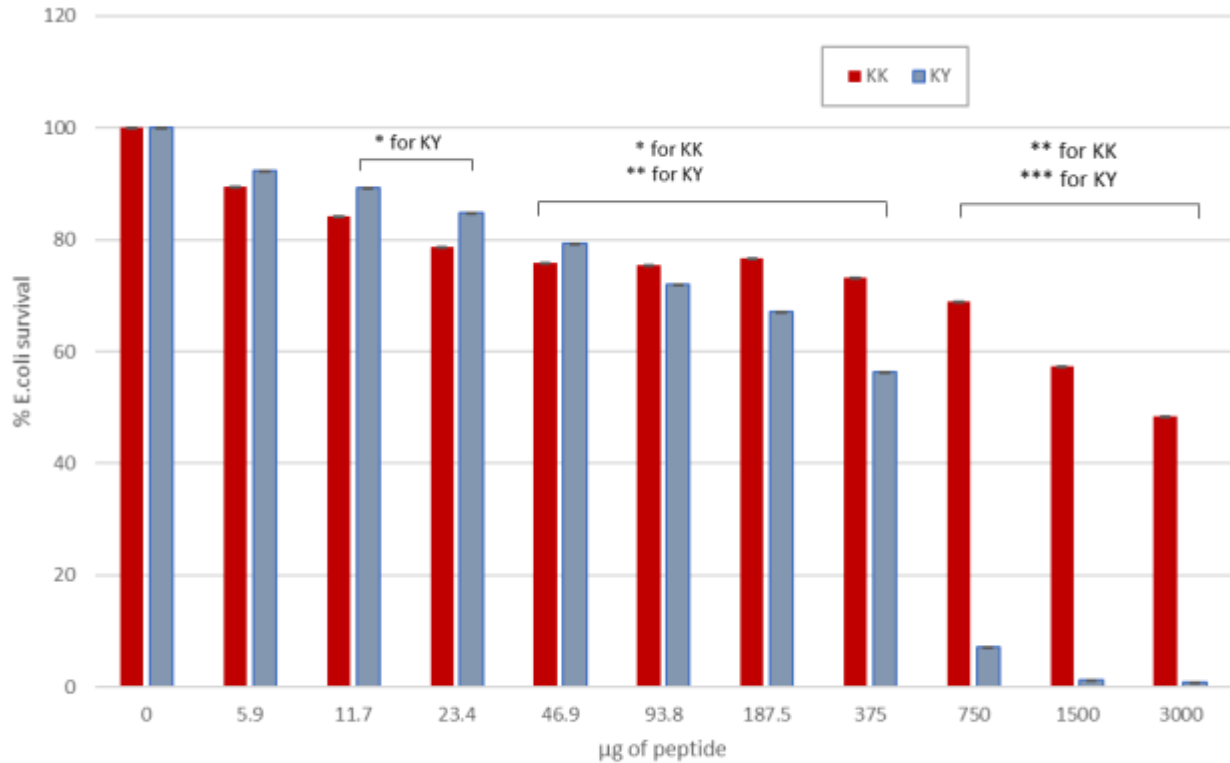


Figure 78: Antimicrobial activity of peptides KK (red) and KY (blue) against Escherichia coli bacteria after treatment with increasing concentrations of the peptides. The cultures of bacteria were treated for 24 hours in 37°C followed by absorbance measurements at 600nm. Untreated cultures (0µg of peptide) were used as control and the measurements were performed in triplicates. * for p<0.05, ** for p < 0.01, ***p<0.0001.

4. 4. DISCUSSION

In the present study we employed computational methods towards the design of amyloid cell penetrating biomaterials with DNA binding functionalities. The computational design was based on the amyloid scaffolds YATGAIIGNII⁷⁶ and RGDSGAITIGC²⁵ which contain the β -sheet cores GAIIG and GAITIG and which were further mutated at key non- β -sheet positions at their termini namely at residues 1,2,3 and 11. We speculated that inserting positively charged residues (Arg, and Lys) at these specific positions would favor cell penetration and DNA binding as was recorded in similar studies¹⁷⁸⁻¹⁷⁹. We purposely left the N-terminal end unprotected for potential involvement of the positively charged amino group to the electrostatic interactions of the peptide. Moreover, aromatic residues in the order Y>W>F are abundant in proteins interacting with DNA¹⁷⁵. Thus, we hypothesized that tyrosine residues at key positions would additionally favor DNA interaction with our scaffolds.

To elucidate if the novel peptide sequences NH₃⁺KYKGAIIGNIK-CONH₂ and NH₃⁺KYRSGAITIGY-CONH₂ (KK and KY for abbreviation) have the requested self-assembly properties we used independent REMD simulations where we concluded that they can spontaneously self-assemble predominantly in antiparallel beta-sheets. Importantly, the altered residues in both scaffolds are not involved in β -bridge interactions, suggesting that these residues are exposed and could possess cell penetration and DNA binding properties. The amyloid nature was further experimentally verified when the peptides were dissolved in sterile double distilled H₂O and formed the characteristic amyloid fibrils as assessed by TEM, FESEM and Congo Red staining.

Utilizing positively charged peptides for transferring cargo into the cells and especially for gene therapy purposes, some important characteristics should be taken into

consideration: 1) effective binding of the oligonucleotide of interest, 2) efficient cellular membrane translocation of the peptide 3) transfer of the CPP-conjugate into the cell and subsequent release of the oligonucleotide and 4) very limited or no cytotoxicity at all.

The common characteristic of cationic CPPs is their positive net charge which originates from their basic residues arginine and lysine. Both play a pivotal role in mediating the internalization of the naked peptide and also of a variety of therapeutic cargoes, into mammalian cells. Tat derived peptide¹⁸⁰, synthetic polyarginines³⁶ and penetratin¹⁸¹ are among the best representatives of the cationic class cell penetrating peptides. Both designer peptides exhibited a positive z-potential of 32.3 ± 0.91 mV for the KK and of 31.2 ± 2.19 mV for the KY peptide respectively, confirming the exposure of the arginine and lysine residues and also classifying the peptide assemblies as positively charged.

CPPs internalization can be attributed to various mechanisms. Routes can be divided into two broad categories: direct penetration of the plasma membrane through interaction of the positively charged peptides with the negatively charged membrane components and phospholipid bilayer¹⁵⁸ or through energy-dependent endocytic pathways, especially when peptides are associated with cargo molecules. Moreover, the internalization process can be dependent on various factors, for example concentration of the peptide, properties of the cargo molecules or the cell line.¹⁵⁶ Amyloid fibrils possess cell adhesive properties and can mimic the fibrillar conformation of the extracellular matrix through functionalization with cell adhesive ligands^{182,183}. Moreover, amyloid nanosheets with positive charge can be also be used as a “docking station” for DNA condensation and retroviral transduction enhancement.^{28,29,67}. However, due to their extending fibrillar conformation they were not considered until now as possible candidates for cell internalization and gene carriers. In the present study the designed peptides successfully achieved non cytotoxic internalization into the HEK293T cells after incubation for 24h as

revealed by MTT and Proteostat aggresome staining. However the exact cell uptake mechanisms remain to be elucidated.

For a facile gene transfer application, the peptide carrier should be able to bind and protect effectively the genetic material. Positively charged peptides can interact with the negatively charged phosphate backbone of DNA through electrostatic interactions leading to condensation of the nucleic acid biomolecules¹⁸⁴. DNA-condensing, cell penetrating peptides must retain their condensation abilities following cell internalization, in order to prolong the life of the carried nucleic acid¹⁸⁵ and prevent DNA degradation by cytosolic nucleases¹⁸⁶. Generally following endocytosis, a significant amount of internalized DNA is targeted to the lysosomes where it will be degraded¹⁸⁷. Even the remaining “free” DNA has a life expectancy of 50-90 min in the cytoplasm since it is subject to degradation by nucleases¹⁸⁵. The presence of a carrier that can protect the DNA integrity is essential for safe pDNA transition into the nucleus. Cationic peptides KK and KY, were incubated with the luciferase carrying plasmid and their DNA binding abilities were assessed by Gel retardation, PicoGreen assay and TEM. Since amyloid fibrils cannot diffuse through the agarose pores during electrophoresis due to their conformation, any observed delay in the pDNA migration reflects the extent of the peptide DNA binding ability. In order to test the DNA binding capacity of the peptides, we used high pDNA concentration relative to the peptide concentration. Full retardation of the plasmid band was observed in all of the DNA/peptide ratios tested. Furthermore, the PicoGreen quenching assay showed that when peptides were mixed with the pre-stained pDNA in the same complex ratios, full quenching of the fluorescent signal was observed. Thus, both the gel retardation and fluorescence quenching evidence point to DNA condensation ability of the peptides. Interestingly, TEM observation of the peptide-pDNA revealed a change in the arrangement of the fibrils from a randomly oriented fibrillary conformation to bundled assemblies that seem to be connected to each other.

We speculate that this alteration is a result of electrostatic interactions between the negatively charged DNA and the positively charged residues emanating from different fibrillar moieties.

Peptide transfection studies showed efficient gene delivery results by the pDNA/KK and pDNA/KY complexes in HEK293T cells after a minimal incubation period of 4h. The delivery efficiency was significantly increased with the increase of the peptide concentration. For both peptides the z-potential of the complexes increased from 1.95 ± 1.02 to 27.45 ± 0.9 for pDNA/KK and 4.2 ± 0.74 to 28.8 ± 0.21 for pDNA/KY (corresponding to DNA/peptide ratios from 1:312 to 1:5000). Therefore, as the added peptide in the complex is increasing, the DNA negative charge is completely neutralized and positive charges are in excess. Concurrently, the transfection efficiency increased along with the increase in the overall charge complex from 1:312 to 1:5000. It is reported that the excess of positive charge in the transfecting DNA/peptide complex leads to a more efficient gene transfer. The positive charges may in part serve for the electrostatic binding and condensation of DNA¹⁸⁸ and in part for the translocation through the negatively charged anionic phospholipids and/or for the neutralization of various charge factors on the cell surface. It is plausible to conclude that as the negative charge of the complexes was reduced, the transduction efficiency increased, resulting in a direct correlation of the pDNA/peptide complex charge and the gene delivery efficacy. Furthermore, KY-DNA complexes achieved higher luciferase gene expression levels compared to KK-DNA complexes. This cannot be attributed solely to the difference in overall charge, since the zeta potential measurements fluctuate in the same levels. Arginine-containing sequences may have an advantage in rapid cell penetration due to its guanidine head that forms bidentate hydrogen bonds with the negatively charged membrane constituents¹⁸⁹. Recent theoretical and experimental studies also point to an important role of arginines in CPP peptides¹⁹⁰. The confocal observations of cells treated with the prestained SV40-pGL3

plasmid show that it enters the nucleus in a period of 4 hours as observed from the blue/green overlay on the nuclear area.

Generally, CPPs are designed for noninvasive cargo transport but they can also possess specific antibacterial activity. Such examples of antimicrobial CPPs are¹⁷⁸: TP-10¹⁹¹, MAP¹⁹², TAT¹⁹³, penetratin^{192, 194}, pVEC¹⁹² and ϵ -poly-L-lysines¹⁹⁵ which can act as antibacterial agents depending on the peptide concentration and the composition of the bacterial membrane. A proposed mechanism of the cell penetrating peptides antimicrobial activity is the carpet-like model, according to which the positively charged domain of the peptides interact and bind to the negatively charged phospholipids on the bacterial membrane, covering the cell surface in a carpet like manner. When a certain concentration of the peptide is reached, the membrane is locally destabilized allowing the passage of the peptides through different perturbation mechanisms¹⁵⁹. Peptides NH₃⁺KYKGAIIGNIK-CONH₂ and NH₃⁺KYRSGAITIGY-CONH₂ are both cationic, cell penetrating and can self-aggregate into amyloid fibrils. They also exhibited bactericidal activity against the *E.coli* strain tested. The peptide NH₃⁺KYRSGAITIGY-CONH₂ required a concentration of 0.375mg/ml to reduce the bacterial population to 50% compared to NH₃⁺KYKGAIIGNIK-CONH₂ that required higher peptide concentration (1,5mg/ml). Cationic aggregating peptides comprising arginine residues along with short aggregation-prone residue stretches were recently identified via bioinformatics approaches in the bacterial proteome and were reported to internalize in mammalian cells. They were also found to be lethal to bacterial cells^{30, 165}. Their specific toxicity towards bacteria only and not mammalian cells involves uptake mechanisms and specific cross-aggregation with bacterial homologous sequences; this cross-aggregation subsequently leads to disruption of bacterial protein homeostasis as a result of the accumulation of protein aggregates^{30, 165}. Elucidating the mechanism of antimicrobial action of the two peptides reported here will be the subject of future studies. It did not

escape our attention that the quasi-homologous sequence SAIIGI was identified with high cross-aggregation score with *E. coli* proteins in ref³⁰ and the designed RSAIIGIIRRPRSAIIGIIRR sequence was predicted to have antibacterial action ³⁰. It is plausible to hypothesize that the antibacterial activity of the two peptides reported here could follow the same mechanism as the one reported in ref³⁰, namely a cell-penetrating activity mediated by positively charged residues and cross-interaction of the amyloid cores with bacterial sequences leading to aggregates that disrupt bacterial proteostasis. However, the exact mechanism remains to be elucidated in future studies.

4. 5. Conclusions

In this study we rationally designed two functional peptides that combine amyloid fibril characteristics and beneficial cell penetrating properties. The novel peptide sequences comprise the fibrillar beta-sheet core of peptides GAIIG and GAITIG and self-assemble spontaneously into amyloid fibrils when dissolved in water. Through incorporation of the positively charged amino acids arginine and lysine and the aromatic residue tyrosine in carefully selected positions we succeeded in mimicking the cell internalization and DNA binding and condensing abilities of previously in-depth tested cell penetrating peptides. More importantly the DNA/peptide fibrillar assemblies were able to transfect and enhance the luciferase protein expression in a charge - and -peptide concentration dependent manner. Moreover, these peptides were able to effectively decrease the *E.coli*'s culture population drastically under the conditions tested.

Amyloid-forming peptides are gaining increasing importance in biomedical applications, including tissue engineering, nanovaccine engineering and biosensing ^{182, 196}. We anticipate that our designer amyloid materials could constitute a stepping stone for

utilizing amyloids as novel biomaterial scaffolds which combine cell penetration and gene transfer with antibacterial properties. Future studies could focus on combining additional properties to the currently designed materials such as transfer of siRNAs and protein therapeutic cargos as well as examining and improving their antimicrobial activity for different bacteria and microbes. Amyloid –forming CPPs present advantages compared to traditional CPPs, such as the possibility to engineer different delivery functionalities onto the same self-assembling scaffold. Moreover, the cross-seeding between the amyloid-forming CPPs and other amyloid peptides, a well-known property of amyloidogenic proteins and peptides¹⁹⁷⁻¹⁹⁹, could potentially be exploited towards multifunctional biomaterial design.

In this study we rationally designed two functional peptides that combine amyloid fibril characteristics and beneficial cell penetrating properties. The novel peptide sequences comprise the fibrillar beta-sheet core of peptides GAIIG and GAITIG and self-assemble spontaneously into amyloid fibrils when dissolved in water. Through incorporation of the positively charged amino acids arginine and lysine and the aromatic residue tyrosine in carefully selected positions we succeeded in mimicking the cell internalization and DNA binding and condensing abilities of previously in-depth tested cell penetrating peptides. More importantly the DNA/peptide fibrillar assemblies were able to transfect and enhance the luciferase protein expression in a charge - and -peptide concentration dependent manner. Moreover, these peptides were able to effectively decrease the *E.coli*'s culture population drastically under the conditions tested.

We anticipate that our designer amyloid materials could constitute a stepping stone for utilizing amyloids as novel biomaterial scaffolds which combine cell penetration and gene transfer with antibacterial properties. Future studies could focus on combining additional properties to the currently designed materials such as transfer of siRNAs and

protein therapeutic cargos as well as examining and improving their antimicrobial activity for different bacteria and microbes.

GENERAL CONCLUSIONS

This PhD study aimed at the development of biocompatible novel protein and peptide materials that were designed and engineered to exhibit functional and applied properties. The protein and peptide sequences were mainly derived from the adenovirus type 2 fiber, Alzheimer's alpha beta peptide and the HIV-1 gp120 V3 loop. Protein constructs and peptide scaffolds can find application as drug and gene delivery agents, and as inspiration for the design of amyloid inhibition materials.

A key role in the rational design of the sequences was played by the computational methods developed and employed by the group of Dr Tamamis at Texas A&M.

The findings of each chapter will be further separately discussed.

Part 1: Adenovirus type 2 engineered fiber constructs for use as biomaterials.

A series of protein constructs were designed by inserting domains or mutating positions of the adenovirus type 2 fiber sequence.

- The chimeric proteins where the natural globular head was substituted with the fibritin foldon trimerization domain exhibited high overexpression levels and were all able to effectively fold into their trimeric state, as observed in SDS-PAGE, and obtain the natural nanorod conformation, as observed with TEM.

-To eliminate the possible degradation products due to the protease actions during protein synthesis in the bacterial cell, a 6x His-tag or an additional foldon domain was inserted at the N-terminal end of the fiber protein (constructs Linker-His, NoLinker-His, Foldon-Linker-Foldon). The His-tag plays a protective role at the N-terminal end, since no degradation products were observed after purification with a Ni-NTA column, subsequent dialysis and Western Blot analysis with an anti-His antibody. Moreover, it is

inferred from previous studies of various groups ⁹⁵ that the histidine-rich protein or peptide sequences could act as endosomal escape agents.

- A smaller version of the fiber protein with the foldon domain as trimerization motif containing approximately 100 amino acids, was expressed in high amounts both in a cytosoluble and aggregated form. This indicates that a smaller protein variant could also be used as an alternative to avoid denaturation and renaturation processes from inclusion bodies with harsh reagents such as urea. Moreover, a predominantly soluble construct can also prove advantageous for crystallization trials.

- The protein construct LHB (Linker-His-Biotin) was chosen for establishing proof-of-concept concerning the use of protein as a therapeutics delivery agent. The LHB construct trimerizes effectively, is non-cytotoxic in the concentrations used and can internalize the mammalian cell lines and localize the cytoplasm and the perinuclear area. The construct due to the absence of the globular head, that acts as CAR receptor binding motif, obviously enters the cells in a CAR- independent mechanism. Its internalization mechanism needs to be investigated in further future experiments. Additionally, LHB comprises a biotinylation site incorporated at its N-terminal end²⁰⁰⁻²⁰¹. This site enables the protein to be biotinylated during its synthesis in the bacterial cell with the addition of the biotin molecule during overexpression. It can be purified both by a Ni-NTA and a streptavidin affinity column. Its intracellular delivery ability was tested by delivery of a streptavidin protein molecule attached to a gold NP and conjugated to a fluorophore. The link was established via the non-covalent bond between biotin and streptavidin. The protein efficiently guided the internalization of the streptavidin-NP cargo into the 293T cell line. Additional molecules could also be tested, such as biotinylated-nucleic acids or proteins for gene or protein therapy applications. The functionalities of the LHB protein are summarized in **Figure 79**.

-The substitution of a serine residue with a cysteine into the protein LHCYS and LHBCYS sequence allows the interaction of the protein through disulfide bonds. The LHCYS protein interacted with a maleimide initiator while retaining its trimeric folding. Furthermore, styrene polymerization was triggered. This preliminary assembly opens new possibilities toward the assembly of a responsive protein-polymer, which could encapsulate moieties of interest for cell targeting applications. Future experiments entail the morphological characterization of the protein-polymer with EM methods and further polymerization of the protein with responsive polymers.

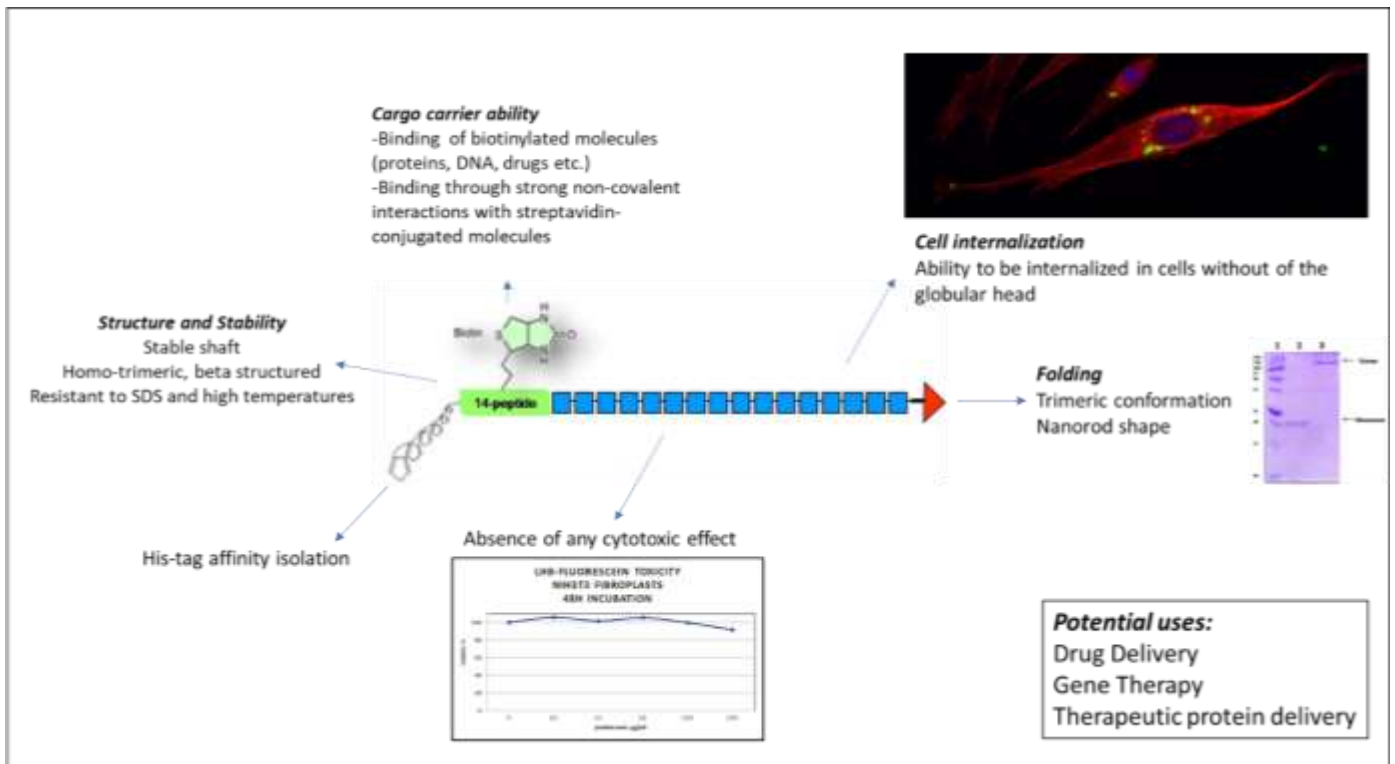


Figure 79: Design, Expression and Properties Characterization of Hybrid shaft proteins

Part 2: "GAIPIG" A novel amyloid designable scaffold and potential inhibitor inspired by GAIIG of amyloid beta and the HIV-1 V3 loop

In this part the amyloid peptides derived from natural amyloidogenic sequences were examined for the development of materials that act as functional scaffolds or as inspiration for specifically targeted amyloid fibrillization inhibitors (**Figure 80**). In summary:

- The GAIIG sequence was detected in both the Alzheimer's A β peptide and the V3 loop sequence of HIV-1 gp120. It is considered a key determinant for beta-sheet formation as it can self-assemble spontaneously outside the sequence of origin.
- GAIIG sequence self-assembles into amyloid fibrils as observed under TEM and FESEM and displays the characteristic amyloid X-ray diffraction pattern. It was also postulated that the longer sequence YATGAIIGNII with the GAIIG sequence as an amyloid core and with suitably selected modifications at the flexible positions, a designable scaffold for novel amyloid-based materials could be developed.
- Inspired by the homologous beta-sheet key determinants GAIIG and adenovirus fiber's GAITIG sequence, a new peptide, GAIPIG was examined for its self-assembling properties. The GAIPIG peptide contains the proline residue that is generally considered to be a beta-breaker residue. The peptide indeed fails to self-assemble into amyloid fibrils.
- Single crystal X-ray analysis of the beta-breaker peptide GAIPIG indicate that the peptide molecules interact with each other toward the formation antiparallel dimer that is only a reminiscent of a small beta-sheet.
- Computational simulation analysis concluded that the GAIPIG peptide has binding properties to Ab and the V3 loop recognition sites but its proline side chain protrudes and is facing outwards from the fibril, therefore disallows the further beta-sheet fibrillar elongation.

- Experimental fibrillization studies (Thioflavin binding assay) of the A β peptide in the presence of the GAIPIG peptide show fibril formation inhibition. It was observed an increase in the length of the lag phase as well as a 30% reduction in the fibril formation by A β after 168 h (7 days) of incubation.

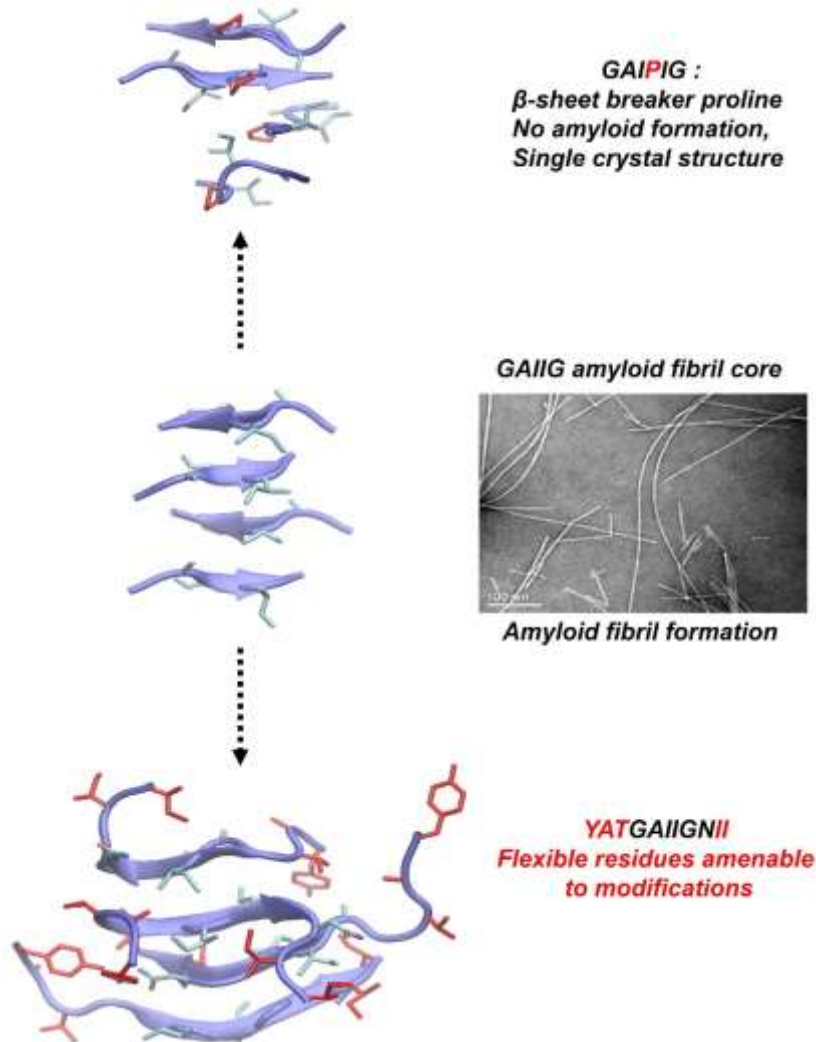


Figure 80: Illustration of the molecular linkage between an amyloid forming core, material scaffold and beta-breaker peptide. The GAIIG amyloid forming core (center) surrounded by flexible residues (in red color, bottom panel) becomes amenable to modifications that can target a variety of materials. When a proline residue (in red, upper panel) is introduced between the two isoleucines the resulting GAIPIG peptide does not

form amyloids and crystallizes yielding a single crystal structure. Isoleucine residues are in cyan color.

Part 2 Chapter 4: Designer Amyloid Cell Penetrating Peptides for Potential Use as Gene Transfer Agents

This study was focused on two rationally and computationally designed peptides comprised of natural beta-sheet cores that can self-assemble into amyloid fibrils and possess cell penetration properties and advantages that allow their use as gene vectors or antimicrobial agents.

More specifically:

-Two novel peptide sequences (KYKGAIIGNIK and KYRSGAITIGY) were rationally designed by inserting mutations on amenable to modifications regions of two previously studied peptides (RGDSGAITIGC and YATGAIIGNII), which contain the amyloid cores GAIIG and GAITIG.

-Both peptides can self-assemble into amyloid fibrils shortly after being dissolved into water, and also exhibit the amyloid yellow/green characteristic birefringence when observed under a crossed-polarizer.

-Due to the addition of the positively charged residues (lysine and arginine) at designated positions the peptide assemblies are characterized by a positive charge that allows their interaction with strong negatively charged nucleic acids and the interaction with the negative phospholipid membranes of the cells.

-Peptides were able to form complexes with the pDNA molecule encoding the luciferase gene and condense it, which allows its protection and its efficient delivery into the cell. This peptide-DNA conjugate is the result of the positive charge attributed not only to the

lysine and arginine residues but also to carefully positioned aromatic residue tyrosine that is considered to enhance the DNA binding properties of the proteins¹⁷⁵. Furthermore, upon binding of the peptides with pDNA, a rapid change in the conformation of the fibrils was observed, from a branching-like assembly to a more organized configuration with adherent fibrils that clearly indicates effective DNA binding.

-The peptide alone or upon complexing with pDNA were able to penetrate the cell membranes as observed by confocal microscopy. The DNA/peptide fibrillar assemblies were able to transfect and enhance the luciferase protein expression in a charge and peptide concentration dependent manner.

-Peptides KYKGAIIGNIK and KYRSGAITIGY but mainly peptide KYRSGAITIGY exhibited concentration dependent antimicrobial activity against *E.coli* bacterial population. On the contrary they showed no cytotoxic effects towards the mammalian cell line tested. Elucidating the mechanism for the antimicrobial action of the peptides can be the subject for future studies. **Figure 81** summarizes the steps leading to delivery and expression of pDNA by the peptides studied in this work.

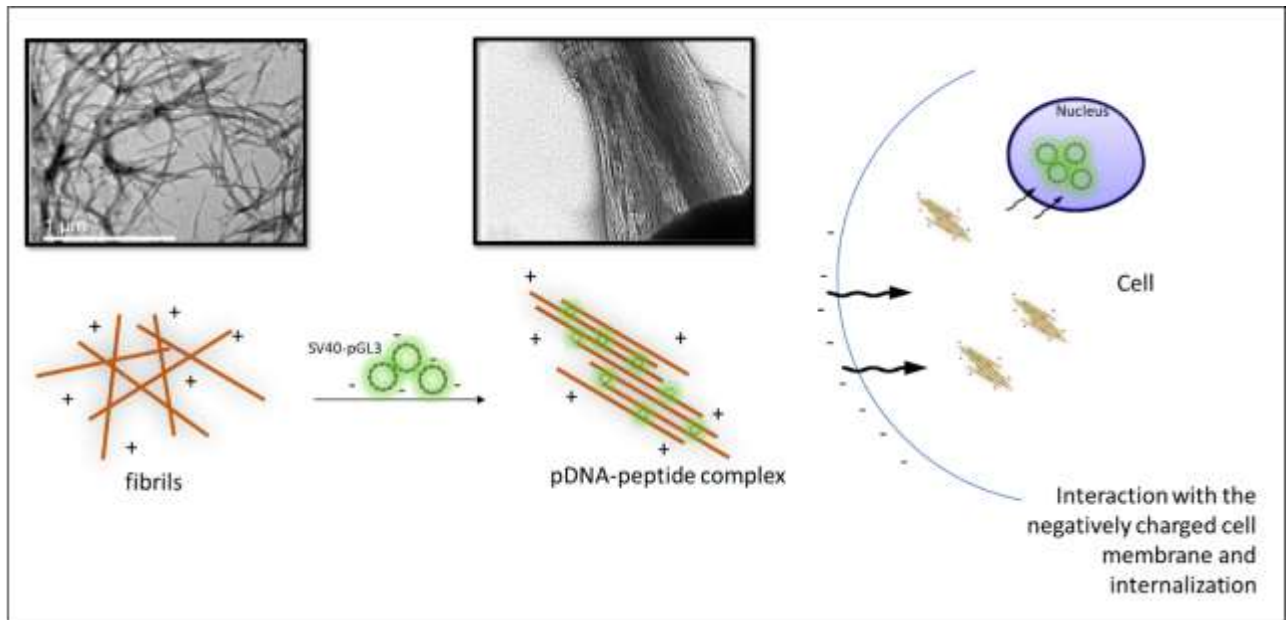


Figure 81: Schematic representation of the pDNA/peptide complex formation and cell uptake through electrostatic interactions. Objects are not drawn to scale.

OUTLOOK

In the present PhD thesis, protein and peptide biomaterials were developed for potential uses in a variety of applications. The proof of principle was proved for the design and engineering of protein constructs that were derived from the adenovirus type 2 fiber and were endowed with useful functionalities.

The proteins fabricated can be cost-effectively produced in bacterial strains and have the advantage of the in-vivo biotinylation. The advantages offered by the recombinant protein scaffolds include the possibility of incorporating long amino acid sequences, or even entire domains. In this way, modular protein scaffolds comprising various domains can be envisaged. For example, the fibritin domain can act as trimerization motif for different fibrous folds, such as coiled coils, triple beta spiral sequences and collagenous domains. One can easily imagine modular fibrous constructs comprising these different motifs. However, bacterial expression also entails concerns of traces impurities that might cause immunogenicity and complicate regulatory approval.

Peptide biomaterials were inspired from short building blocks of the adenovirus type 2, Alzheimer's A β and HIV-1 V3 loop gp120 and have the advantage of easier manipulation of their sequence in contrast to proteins that their folding is far more complicated. Peptide sequences with the insight offered by molecular dynamics studies can be designed to adopt amyloid conformations with exposed functional groups. A distinctive advantage of the amyloid forming peptides is that through their ability for cross-seeding, multifunctional biomaterials can be developed. However, the possibility of appending functional sequences to peptide scaffolds is limited by the size, ie only short sequences can be appended, depending on the size of the original scaffold, (eg 3 to 4 amino acids in a 7 aa scaffolds in this thesis), since its self-assembling propensity should not be impeded.

In vitro peptide synthesis methods also offer the possibility of incorporating D- amino acids, non-natural amino acids and peptidomimetics, possibilities not offered by the recombinant protein synthesis. This kind of de novo designed, non-natural motifs could lead to novel folds that are also resistant to the action of natural proteases, and therefore open previously unexplored avenues. Since synthetic peptides are chemically well-defined, homogeneity and standardization issues should be more straightforward compared to recombinant protein materials, and therefore make regulatory approval easier.

In conclusion, both protein and peptide scaffolds offer a large spectrum of scientifically very interesting avenues for functionalization towards applications. The choice between a protein or a peptide material should be done by taking into account the desired application and the ensemble of considerations stated above.

List of Publications

- "Designer Amyloid Cell Penetrating Peptides for Potential Use as Gene Transfer Vehicles."
C. Kokotidou, S. V. R. Jonnalagadda, A. A. Orr, G. Vrentzos, A. Kretsovali, P. Tamamis and A. Mitraki, *Biomolecules*, 10(1), 7 (2020)
- 1.
 2. Book Chapter on "Amyloid-like Peptide Aggregates" C. Kokotidou, P. Tamamis, A. Mitraki. *Royal Society of Chemistry*, in preparation.
 3. "Self-Assembling Amyloid Sequences as Scaffolds for Material Design: A Case Study of Building Blocks Inspired From the Adenovirus Fiber Protein" C. Kokotidou, P. Tamamis A. Mitraki. *Macromol. Symp.*,386, 1900005, (2019).
 4. "A self-assembly study of PNA-porphyrin and PNA-BODIPY hybrids in mixed solvent systems." E. Nikoloudakis, K. Karikis, J. Han, C. Kokotidou, A. Charisiadis, F. Folias, A. M. Douvas, A. Mitraki, G. Charalambidis, X. Yan, A. G. Coutsolelos *Nanoscale*, 11(8), 3557-3566.(2019)
 5. "A novel amyloid designable scaffold and potential inhibitor inspired by GAIIG of amyloid beta and the HIV-1 V3 loop." C. Kokotidou*, S.V.R Jonnalagadda *, A.A. Orr *, M. Seoane-Blanco *, C.P. Apostolidou, M.J. van Raaij, M. Kotzabasaki, A. Chatzoudis, J.M. Jakubowski, E. Mossou, V.T. Forsyth, E.P. Mitchell, M.W. Bowler, A.L. Llamas-Saiz., P. Tamamis, A. Mitraki. *FEBS Letters* 592 1777-1788 (2018).
 6. "Computational Design of Functional Amyloid Materials with Cesium Binding, Deposition, and Capture Properties". S. V. R. Jonnalagadda*, C. Kokotidou*, A. A. Orr, E. Fotopoulou, K. J. Henderson, C.H. Choi, W. T. Lim, S. J. Choi, H. K. Jeong, A. Mitraki, and P. Tamamis. *The Journal of Physical Chemistry B* 122 (30), 7555-7568, (2018)
 7. "Self-assembly study of nanometric spheres from polyoxometalate-phenylalanine hybrids, an experimental and theoretical approach." E. Nikoloudakis, K. Karikis, M. Laurans, C. Kokotidou, A. Solé-Daura, J. J. Carbó, A. Charisiadis, G. Charalambidis, G. Izzet, A. Mitraki, A. M. Douvas, J. M. Poblet, A. Proust, A. G. Coutsolelos *Dalton Trans.* 47, 6304–6313 (2018).
 8. "Self-assembly of (boron-dipyrromethane)-diphenylalanine conjugates forming chiral supramolecular materials" K. Karikis, A. Butkiewicz, F. Folias, G. Charalambidis, C. Kokotidou, A. Charisiadis, V. Nikolaou, E. Nikoloudakis, J. Frelek, A. Mitraki and A.G. Coutsolelos. *Nanoscale*,10, 1735-1741 (2018)
 9. "Oleylamine as a beneficial agent for the synthesis of CoFe₂O₄ nanoparticles with potential biomedical uses" V. Georgiadou, C. Kokotidou, B. Le Droumaguet, B. Carbonnier, Th. Choli-Papadopoulou, C. Dendrinou-Samara. *Dalton Trans.* 43: 6377-6388 (2014)
 10. "Copper(I) halide complexes of 5-carbethoxy-2-thiouracil: Synthesis, structure and in vitro cytotoxicity." I. Papazoglou, P.J. Cox, A.G. Hatzidimitriou, C. Kokotidou, T. Choli-Papadopoulou, P. Aslanidis. *European Journal of Medicinal Chemistry* 78: 383-391 (2014)

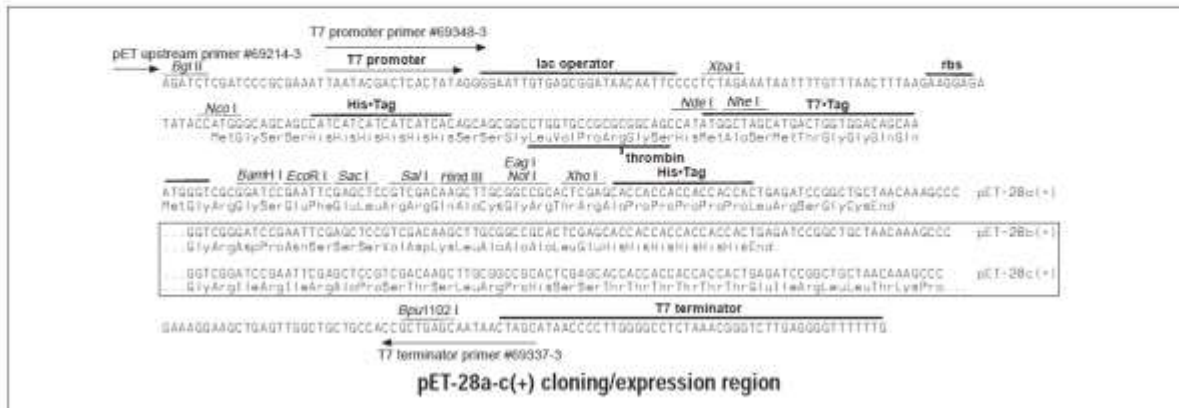
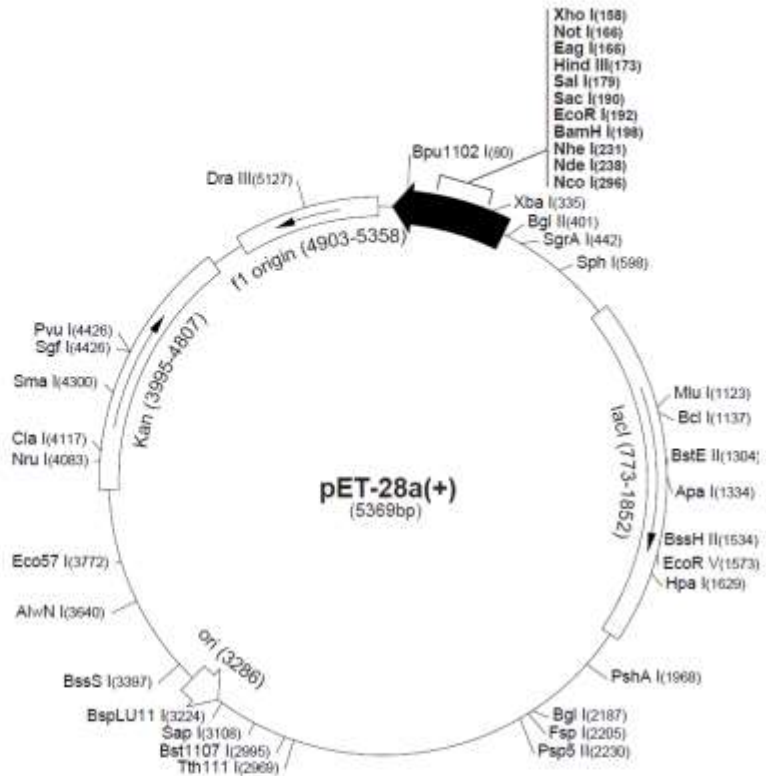
APPENDIX

pET28a plasmid map

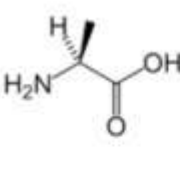
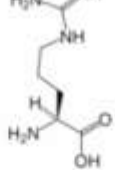
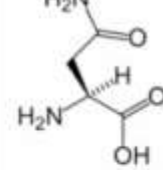
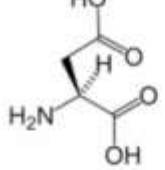
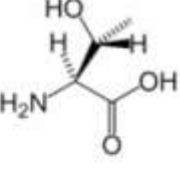
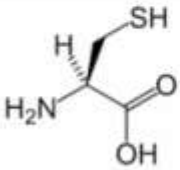
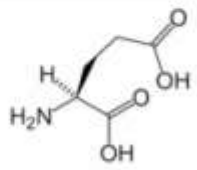
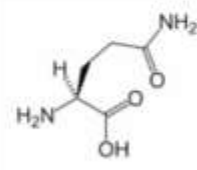
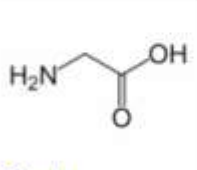
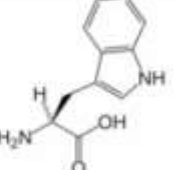
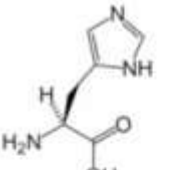
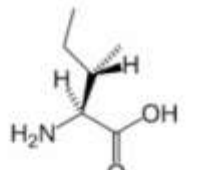
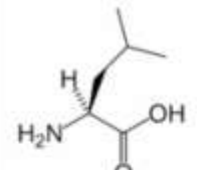
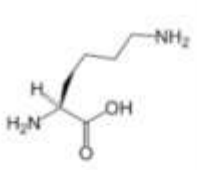
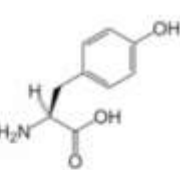
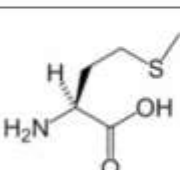
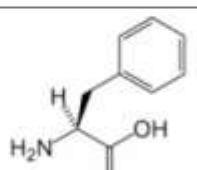
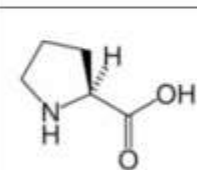
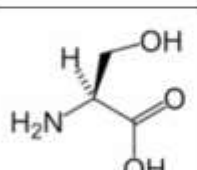
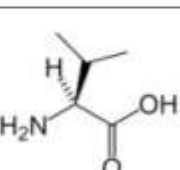
pET-28a(+) sequence landmarks

T7 promoter	370-386
T7 transcription start	369
His•Tag coding sequence	270-287
T7•Tag coding sequence	207-239
Multiple cloning sites (<i>Bam</i> H I - <i>Xho</i> I)	158-203
His•Tag coding sequence	140-157
T7 terminator	26-72
<i>lac</i> I coding sequence	773-1852
pBR322 origin	3286
Kan coding sequence	3995-4807
f1 origin	4903-5358

The maps for pET-28b(+) and pET-28c(+) are the same as pET-28a(+) (shown) with the following exceptions: pET-28b(+) is a 5368bp plasmid; subtract 1bp from each site beyond *Bam*H I at 198. pET-28c(+) is a 5367bp plasmid; subtract 2bp from each site beyond *Bam*H I at 198.



Structures and symbols of the 20 amino acids, which are directly encoded for protein synthesis by the standard genetic code.

 <p>L-Alanine (Ala / A)</p>	 <p>L-Arginine (Arg / R)</p>	 <p>L-Asparagine (Asn / N)</p>	 <p>L-Aspartic acid (Asp / D)</p>	 <p>L-Threonine (Thr / T)</p>
 <p>L-Cysteine (Cys / C)</p>	 <p>L-Glutamic acid (Glu / E)</p>	 <p>L-Glutamine (Gln / Q)</p>	 <p>Glycine (Gly / G)</p>	 <p>L-Tryptophan (Trp / W)</p>
 <p>L-Histidine (His / H)</p>	 <p>L-Isoleucine (Ile / I)</p>	 <p>L-Leucine (Leu / L)</p>	 <p>L-Lysine (Lys / K)</p>	 <p>L-Tyrosine (Tyr / Y)</p>
 <p>L-Methionine (Met / M)</p>	 <p>L-Phenylalanine (Phe / F)</p>	 <p>L-Proline (Pro / P)</p>	 <p>L-Serine (Ser / S)</p>	 <p>L-Valine (Val / V)</p>

REFERENCES

1. Lee, C. S.; Bishop, E. S.; Zhang, R.; Yu, X.; Farina, E. M.; Yan, S.; Zhao, C.; Zheng, Z.; Shu, Y.; Wu, X.; Lei, J.; Li, Y.; Zhang, W.; Yang, C.; Wu, K.; Wu, Y.; Ho, S.; Athiviraham, A.; Lee, M. J.; Wolf, J. M.; Reid, R. R.; He, T. C., Adenovirus-Mediated Gene Delivery: Potential Applications for Gene and Cell-Based Therapies in the New Era of Personalized Medicine. *Genes Dis* **2017**, *4* (2), 43-63. DOI: 10.1016/j.gendis.2017.04.001.
2. Nemerow, G. R.; Stewart, P. L.; Reddy, V. S., Structure of human adenovirus. *Current Opinion in Virology* **2012**, *2* (2), 115-121. DOI: 10.1016/j.coviro.2011.12.008.
3. Fender, P.; Ruigrok, R. W.; Gout, E.; Buffet, S.; Chroboczek, J., Adenovirus dodecahedron, a new vector for human gene transfer [see comments]. *Nat.Biotechnol.* **1997**, *15*, 52-56.
4. Fuschiotti, P.; Schoehn, G.; Fender, P.; Fabry, C. M. S.; Hewat, E. A.; Chroboczek, J.; Ruigrok, R. W. H.; Conway, J. F., Structure of the dodecahedral penton particle from human adenovirus type 3. *Journal of Molecular Biology* **2006**, *356* (2), 510-520. DOI: 10.1016/j.jmb.2005.11.048.
5. Schoehn, G.; Fender, P.; Chroboczek, J.; Hewat, E. A., Adenovirus 3 penton dodecahedron exhibits structural changes of the base on fibre binding. *EMBO J.* **1996**, *15*, 6841-6846.
6. Rentsendorj, A.; Agadjanian, H.; Chen, X.; Cirivello, M.; Macveigh, M.; Kedes, L.; Hamm-Alvarez, S.; Medina-Kauwe, L. K., The Ad5 fiber mediates nonviral gene transfer in the absence of the whole virus, utilizing a novel cell entry pathway. *Gene therapy* **2005**, *12* (3), 225-37. DOI: 10.1038/sj.gt.3302402.
7. Nicklin, S. A.; Wu, E.; Nemerow, G. R.; Baker, A. H., The influence of adenovirus fiber structure and function on vector development for gene therapy. *Molecular therapy : the journal of the American Society of Gene Therapy* **2005**, *12* (3), 384-93. DOI: 10.1016/j.ymthe.2005.05.008.
8. Nicklin, S. A.; Dishart, K. L.; Buening, H.; Reynolds, P. N.; Hallek, M.; Nemerow, G. R.; Von Seggern, D. J.; Baker, A. H., Transductional and transcriptional targeting of cancer cells using genetically engineered viral vectors. *Cancer Letters* **2003**, *201* (2), 165-173. DOI: <https://doi.org/10.1016/j.canlet.2003.07.003>.
9. Dmitriev, I.; Kashentseva, E.; Rogers, B. E.; Krasnykh, V.; Curiel, D. T., Ectodomain of coxsackievirus and adenovirus receptor genetically fused to epidermal growth factor mediates adenovirus targeting to epidermal growth factor receptor-positive cells. *J. Virol.* **2000**, *74* (15), 6875-84. DOI: 10.1128/jvi.74.15.6875-6884.2000.
10. Dmitriev, I. P.; Kashentseva, E. A.; Curiel, D. T., Engineering of adenovirus vectors containing heterologous peptide sequences in the C terminus of capsid protein IX. *J. Virol.* **2002**, *76* (14), 6893-9. DOI: 10.1128/jvi.76.14.6893-6899.2002.
11. Hemminki, A.; Belousova, N.; Zinn, K. R.; Liu, B.; Wang, M.; Chaudhuri, T. R.; Rogers, B. E.; Buchsbaum, D. J.; Siegal, G. P.; Barnes, M. N.; Gomez-Navarro, J.; Curiel, D. T.; Alvarez, R. D., An adenovirus with enhanced infectivity mediates molecular chemotherapy of ovarian cancer

- cells and allows imaging of gene expression. *Molecular therapy : the journal of the American Society of Gene Therapy* **2001**, 4 (3), 223-31. DOI: 10.1006/mthe.2001.0446.
12. Beatty, M. S.; Curiel, D. T., Chapter two--Adenovirus strategies for tissue-specific targeting. *Advances in cancer research* **2012**, 115, 39-67. DOI: 10.1016/B978-0-12-398342-8.00002-1.
 13. van Beusechem, V. W.; van Rijswijk, A. L. C. T.; van Es, H. H. G.; Haisma, H. J.; Pinedo, H. M.; Gerritsen, W. R., Recombinant adenovirus vectors with knobless fibers for targeted gene transfer. *Gene Ther.* **2000**, 7 (22), 1940-1946. DOI: 10.1038/sj.gt.3301323.
 14. Papanikolopoulou, K.; Teixeira, S.; Belrhali, H.; Forsyth, V. T.; Mitraki, A.; van Raaij, M. J., Adenovirus fibre shaft sequences fold into the native triple beta-spiral fold when N-terminally fused to the bacteriophage T4 fibritin foldon trimerisation motif. *J. Mol. Biol.* **2004**, 342 (1), 219-27.
 15. Krasnykh, V.; Belousova, N.; Korokhov, N.; Mikheeva, G.; Curiel, D. T., Genetic targeting of an adenovirus vector via replacement of the fiber protein with the phage T4 fibritin. *J. Virol.* **2001 May**, 75 (9), 4176-83.
 16. Liu, H. R.; Jin, L.; Koh, S. B. S.; Atanasov, I.; Schein, S.; Wu, L.; Zhou, Z. H., Atomic Structure of Human Adenovirus by Cryo-EM Reveals Interactions Among Protein Networks. *Science* **2010**, 329 (5995), 1038-1043. DOI: 10.1126/science.1187433.
 17. Reddy, V. S.; Natchiar, S. K.; Stewart, P. L.; Nemerow, G. R., Crystal Structure of Human Adenovirus at 3.5 angstrom Resolution. *Science* **2010**, 329 (5995), 1071-1075. DOI: 10.1126/science.1187292.
 18. Mitraki, A.; Barge, A.; Chroboczek, J.; Andrieu, J. P.; Gagnon, J.; Ruigrok, R. W., Unfolding studies of human adenovirus type 2 fibre trimers Evidence for a stable domain. *Eur. J. Biochem.* **1999**, 264 (2), 599-606.
 19. van Raaij, M. J.; Mitraki, A.; Lavigne, G.; Cusack, S., A triple beta-spiral in the adenovirus fibre shaft reveals a new structural motif for a fibrous protein. *Nature* **1999**, 401 (6756), 935-938.
 20. Papanikolopoulou, K.; Forge, V.; Goeltz, P.; Mitraki, A., Formation of highly stable chimeric trimers by fusion of an adenovirus fiber shaft fragment with the foldon domain of bacteriophage t4 fibritin. *The Journal of biological chemistry* **2004**, 279 (10), 8991-8.
 21. Papanikolopoulou, K. PhD Thesis. 2004.
 22. Papanikolopoulou, K.; Schoehn, G.; Forge, V.; Forsyth, V. T.; Riekkel, C.; Hernandez, J. F.; Ruigrok, R. W. H.; Mitraki, A., Amyloid fibril formation from sequences of a natural beta-structured fibrous protein, the adenovirus fiber. *J. Biol. Chem.* **2005**, 280 (4), 2481-2490. DOI: 10.1074/jbc.M406282200.
 23. Tamamis, P.; Kasotakis, E.; Mitraki, A.; Archontis, G., Amyloid-Like Self-Assembly of Peptide Sequences from the Adenovirus Fiber Shaft: Insights from Molecular Dynamics Simulations. *Journal of Physical Chemistry B* **2009**, 113 (47), 15639-15647. DOI: 10.1021/jp9066718.

24. Kasotakis, E.; Mossou, E.; Adler-Abramovich, L.; Mitchell, E. P.; Forsyth, V. T.; Gazit, E.; Mitraki, A., Design of Metal-Binding Sites Onto Self-Assembled Peptide Fibrils. *Biopolymers* **2009**, *92* (3), 164-172. DOI: 10.1002/bip.21163.
25. Deidda, G.; Jonnalagadda, S. V. R.; Spies, J. W.; Ranella, A.; Mossou, E.; Forsyth, V. T.; Mitchell, E. P.; Bowler, M. W.; Tamamis, P.; Mitraki, A., Self-Assembled Amyloid Peptides with Arg-Gly-Asp (RGD) Motifs As Scaffolds for Tissue Engineering. *ACS Biomaterials Science & Engineering* **2017**, *3* (7), 1404-1416. DOI: 10.1021/acsbomaterials.6600570.
26. Jonnalagadda, S. V. R.; Kokotidou, C.; Orr, A. A.; Fotopoulou, E.; Henderson, K. J.; Choi, C. H.; Lim, W. T.; Choi, S. J.; Jeong, H. K.; Mitraki, A.; Tamamis, P., Computational Design of Functional Amyloid Materials with Cesium Binding, Deposition, and Capture Properties. *The journal of physical chemistry. B* **2018**, *122* (30), 7555-7568. DOI: 10.1021/acs.jpcc.8b04103.
27. Tao, Y.; Strelkov, S. V.; Mesyanzhinov, V. V.; Rossmann, M. G., Structure of bacteriophage T4 fibritin: a segmented coiled coil and the role of the C-terminal domain. *Structure* **1997 Jun 15**, *5* (6), 789-98.
28. Dai, B.; Li, D.; Xi, W.; Luo, F.; Zhang, X.; Zou, M.; Cao, M.; Hu, J.; Wang, W.; Wei, G.; Zhang, Y.; Liu, C., Tunable assembly of amyloid-forming peptides into nanosheets as a retrovirus carrier. *Proc. Natl. Acad. Sci. U. S. A.* **2015**, *112* (10), 2996-3001. DOI: 10.1073/pnas.1416690112.
29. Kirti, S.; Patel, K.; Das, S.; Shrimali, P.; Samanta, S.; Kumar, R.; Chatterjee, D.; Ghosh, D.; Kumar, A.; Tayalia, P.; Maji, S. K., Amyloid Fibrils with Positive Charge Enhance Retroviral Transduction in Mammalian Cells. *ACS Biomaterials Science & Engineering* **2019**, *5* (1), 126-138. DOI: 10.1021/acsbomaterials.8b00248.
30. Khodaparast, L.; Gallardo, R.; Louros, N. N.; Michiels, E.; Ramakrishnan, R.; Ramakers, M.; Claes, F.; Young, L.; Shahrooei, M.; Wilkinson, H.; Desager, M.; Tadesse, W. M.; Nilsson, K. P. R.; Hammarstrom, P.; Aertsen, A.; Carpentier, S.; Van Eldere, J.; Rousseau, F.; Schymkowitz, J., Aggregating sequences that occur in many proteins constitute weak spots of bacterial proteostasis. *Nat. Commun.* **2018**, *9*. DOI: <https://doi.org/10.1038/s41467-018-03131-0>.
31. Medina-Kauwe, L. K., Development of adenovirus capsid proteins for targeted therapeutic delivery. *Therapeutic delivery* **2013**, *4* (2), 267-77. DOI: 10.4155/tde.12.155.
32. Rueda, F.; Cespedes, M. V.; Conchillo-Sole, O.; Sanchez-Chardi, A.; Seras-Franzoso, J.; Cubarsi, R.; Gallardo, A.; Pesarrodon, M.; Ferrer-Miralles, N.; Daura, X.; Vazquez, E.; Garcia-Fruitos, E.; Mangues, R.; Unzueta, U.; Villaverde, A., Bottom-Up Instructive Quality Control in the Biofabrication of Smart Protein Materials. *Adv Mater* **2015**, *27* (47), 7816-22. DOI: 10.1002/adma.201503676.
33. Ferrer-Miralles, N.; Rodriguez-Carmona, E.; Corchero, J. L.; Garcia-Fruitos, E.; Vazquez, E.; Villaverde, A., Engineering protein self-assembling in protein-based nanomedicines for drug delivery and gene therapy. *Crit Rev Biotechnol* **2015**, *35* (2), 209-21. DOI: 10.3109/07388551.2013.833163.

34. Ferrer-Miralles, N.; Vazquez, E.; Villaverde, A., Membrane-active peptides for non-viral gene therapy: making the safest easier. *Trends Biotechnol.* **2008**, *26* (5), 267-75. DOI: 10.1016/j.tibtech.2008.02.003.
35. Vazquez, E.; Ferrer-Miralles, N.; Villaverde, A., Peptide-assisted traffic engineering for nonviral gene therapy. *Drug Discov Today* **2008**, *13* (23-24), 1067-74. DOI: 10.1016/j.drudis.2008.08.008.
36. Futaki, S.; Suzuki, T.; Ohashi, W.; Yagami, T.; Tanaka, S.; Ueda, K.; Sugiura, Y., Arginine-rich peptides - An abundant source of membrane-permeable peptides having potential as carriers for intracellular protein delivery. *J. Biol. Chem.* **2001**, *276* (8), 5836-5840. DOI: DOI 10.1074/jbc.M007540200.
37. Saccardo, P.; Villaverde, A.; Gonzalez-Montalban, N., Peptide-mediated DNA condensation for non-viral gene therapy. *Biotechnol. Adv.* **2009**, *27* (4), 432-438. DOI: 10.1016/j.biotechadv.2009.03.004.
38. Ignatovich, I. A.; Dizhe, E. B.; Pavlotskaya, A. V.; Akifiev, B. N.; Burov, S. V.; Orlov, S. V.; Perevozchikov, A. P., Complexes of plasmid DNA with basic domain 47-57 of the HIV-1 Tat protein are transferred to mammalian cells by endocytosis-mediated pathways. *The Journal of biological chemistry* **2003**, *278* (43), 42625-36. DOI: 10.1074/jbc.M301431200.
39. Vazquez, E.; Roldan, M.; Diez-Gil, C.; Unzueta, U.; Domingo-Espin, J.; Cedano, J.; Conchillo, O.; Ratera, I.; Veciana, J.; Daura, X.; Ferrer-Miralles, N.; Villaverde, A., Protein nanodisk assembling and intracellular trafficking powered by an arginine-rich (R9) peptide. *Nanomedicine* **2010**, *5* (2), 259-268. DOI: 10.2217/Nnm.09.98.
40. Tuunnemann, G.; Ter-Avetisyan, G.; Martin, R. M.; Stoochl, M.; Herrmann, A.; Cardoso, C., Live-cell analysis of cell penetration ability and toxicity of oligo-arginines. *J. Pept. Sci.* **2008**, *14* (4), 469-476. DOI: 10.1002/psc.968.
41. Chiti, F.; Dobson, C. M., Protein Misfolding, Amyloid Formation, and Human Disease: A Summary of Progress Over the Last Decade. *Annual review of biochemistry* **2017**, *86*, 27-68. DOI: 10.1146/annurev-biochem-061516-045115.
42. Nizynski, B.; Dzwolak, W.; Nieznanski, K., Amyloidogenesis of Tau protein. *Protein science : a publication of the Protein Society* **2017**, *26* (11), 2126-2150. DOI: 10.1002/pro.3275.
43. Kaye, R.; Bernhagen, J.; Greenfield, N.; Sweimeh, K.; Brunner, H.; Voelter, W.; Kapurniotu, A., Conformational transitions of islet amyloid polypeptide (IAPP) in amyloid formation in vitro. *Journal of molecular biology* **1999**, *287* (4), 781-96. DOI: 10.1006/jmbi.1999.2646.
44. Jaikaran, E. T.; Clark, A., Islet amyloid and type 2 diabetes: from molecular misfolding to islet pathophysiology. *Biochimica et biophysica acta* **2001**, *1537* (3), 179-203. DOI: 10.1016/s0925-4439(01)00078-3.
45. Conway, K. A.; Harper, J. D.; Lansbury, P. T., Jr., Fibrils formed in vitro from alpha-synuclein and two mutant forms linked to Parkinson's disease are typical amyloid. *Biochemistry* **2000**, *39* (10), 2552-63. DOI: 10.1021/bi991447r.

46. Fowler, D. M.; Koulov, A. V.; Alory-Jost, C.; Marks, M. S.; Balch, W. E.; Kelly, J. W., Functional amyloid formation within mammalian tissue. *PLoS biology* **2006**, *4* (1), e6. DOI: 10.1371/journal.pbio.0040006.
47. Bissig, C.; Rochin, L.; van Niel, G., PMEL Amyloid Fibril Formation: The Bright Steps of Pigmentation. *International journal of molecular sciences* **2016**, *17* (9). DOI: 10.3390/ijms17091438.
48. Watt, B.; van Niel, G.; Raposo, G.; Marks, M. S., PMEL: a pigment cell-specific model for functional amyloid formation. *Pigment cell & melanoma research* **2013**, *26* (3), 300-15. DOI: 10.1111/pcmr.12067.
49. Audas, T. E.; Audas, D. E.; Jacob, M. D.; Ho, J. J.; Khacho, M.; Wang, M.; Perera, J. K.; Gardiner, C.; Bennett, C. A.; Head, T.; Kryvenko, O. N.; Jorda, M.; Daunert, S.; Malhotra, A.; Trinkle-Mulcahy, L.; Gonzalzo, M. L.; Lee, S., Adaptation to Stressors by Systemic Protein Amyloidogenesis. *Developmental cell* **2016**, *39* (2), 155-168. DOI: 10.1016/j.devcel.2016.09.002.
50. Maji, S. K.; Perrin, M. H.; Sawaya, M. R.; Jessberger, S.; Vadodaria, K.; Rissman, R. A.; Singru, P. S.; Nilsson, K. P.; Simon, R.; Schubert, D.; Eisenberg, D.; Rivier, J.; Sawchenko, P.; Vale, W.; Riek, R., Functional amyloids as natural storage of peptide hormones in pituitary secretory granules. *Science* **2009**, *325* (5938), 328-32. DOI: 10.1126/science.1173155.
51. Hamodrakas, S. J.; Paulson, J. R.; Rodakis, G. C.; Kafatos, F. C., X-ray diffraction studies of a silkworm chorion. *International journal of biological macromolecules* **1983**, *5* (3), 149-153. DOI: [https://doi.org/10.1016/0141-8130\(83\)90029-6](https://doi.org/10.1016/0141-8130(83)90029-6).
52. Iconomidou, V. A.; Hamodrakas, S. J., Natural protective amyloids. *Current Protein & Peptide Science* **2008**, *9* (3), 291-309.
53. Fitzpatrick, A. W.; Debelouchina, G. T.; Bayro, M. J.; Clare, D. K.; Caporini, M. A.; Bajaj, V. S.; Jaroniec, C. P.; Wang, L.; Ladizhansky, V.; Muller, S. A.; MacPhee, C. E.; Waudby, C. A.; Mott, H. R.; De Simone, A.; Knowles, T. P.; Saibil, H. R.; Vendruscolo, M.; Orlova, E. V.; Griffin, R. G.; Dobson, C. M., Atomic structure and hierarchical assembly of a cross-beta amyloid fibril. *Proc. Natl. Acad. Sci. U. S. A.* **2013**, *110* (14), 5468-73. DOI: 10.1073/pnas.1219476110.
54. Astbury, W. T.; Dickinson, S.; Bailey, K., The X-ray interpretation of denaturation and the structure of the seed globulins. *Biochem. J.* **1935**, *29* (10), 2351-2360. DOI: 10.1042/bj0292351.
55. Makin, O. S.; Atkins, E.; Sikorski, P.; Johansson, J.; Serpell, L. C., Molecular basis for amyloid fibril formation and stability. *Proc. Natl. Acad. Sci. U. S. A.* **2005**, *102* (2), 315-20. DOI: 10.1073/pnas.0406847102.
56. Sawaya, M. R.; Sambashivan, S.; Nelson, R.; Ivanova, M. I.; Sievers, S. A.; Apostol, M. I.; Thompson, M. J.; Balbirnie, M.; Wiltzius, J. J.; McFarlane, H. T.; Madsen, A. O.; Riek, C.; Eisenberg, D., Atomic structures of amyloid cross-beta spines reveal varied steric zippers. *Nature* **2007**, *447* (7143), 453-7. DOI: 10.1038/nature05695.

57. Jimenez, J. L.; Nettleton, E. J.; Bouchard, M.; Robinson, C. V.; Dobson, C. M.; Saibil, H. R., The protofilament structure of insulin amyloid fibrils. *Proc. Natl. Acad. Sci. U. S. A.* **2002**, *99* (14), 9196-201. DOI: 10.1073/pnas.142459399.
58. Sunde, M.; Blake, C., The structure of amyloid fibrils by electron microscopy and X-ray diffraction. *Adv. Protein Chem.* **1997**, *50*, 123-59.
59. LeVine, H., 3rd, Quantification of beta-sheet amyloid fibril structures with thioflavin T. *Methods Enzymol.* **1999**, *309*, 274-84.
60. Yakupova, E. I.; Bobyleva, L. G.; Vikhlyantsev, I. M.; Bobylev, A. G., Congo Red and amyloids: history and relationship. *Bioscience reports* **2019**, *39* (1). DOI: 10.1042/BSR20181415.
61. Colvin, M. T.; Silvers, R.; Ni, Q. Z.; Can, T. V.; Sergeev, I.; Rosay, M.; Donovan, K. J.; Michael, B.; Wall, J.; Linse, S.; Griffin, R. G., Atomic Resolution Structure of Monomorphic A beta(42) Amyloid Fibrils. *J. Am. Chem. Soc.* **2016**, *138* (30), 9663-9674. DOI: 10.1021/jacs.6b05129.
62. Fitzpatrick, A. W. P.; Falcon, B.; He, S.; Murzin, A. G.; Murshudov, G.; Garringer, H. J.; Crowther, R. A.; Ghetti, B.; Goedert, M.; Scheres, S. H. W., Cryo-EM structures of tau filaments from Alzheimer's disease. *Nature* **2017**, *547* (7662), 185-190. DOI: 10.1038/nature23002.
63. Walti, M. A.; Ravotti, F.; Arai, H.; Glabe, C. G.; Wall, J. S.; Bockmann, A.; Guntert, P.; Meier, B. H.; Riek, R., Atomic-resolution structure of a disease-relevant A beta(1-42) amyloid fibril. *Proc. Natl. Acad. Sci. U. S. A.* **2016**, *113* (34), E4976-E4984. DOI: 10.1073/pnas.1600749113.
64. Holmes, T. C.; de Lacalle, S.; Su, X.; Liu, G.; Rich, A.; Zhang, S., Extensive neurite outgrowth and active synapse formation on self-assembling peptide scaffolds. *P. Natl. Acad. Sci.* **2000**, *97* (12), 6728. DOI: 10.1073/pnas.97.12.6728.
65. Ellis-Behnke, R. G.; Schneider, G. E., Peptide amphiphiles and porous biodegradable scaffolds for tissue regeneration in the brain and spinal cord. *Methods in molecular biology* **2011**, *726*, 259-81. DOI: 10.1007/978-1-61779-052-2_17.
66. Gelain, F.; Unsworth, L. D.; Zhang, S., Slow and sustained release of active cytokines from self-assembling peptide scaffolds. *J. Controlled Release* **2010**, *145* (3), 231-239. DOI: <https://doi.org/10.1016/j.jconrel.2010.04.026>.
67. Yolamanova, M.; Meier, C.; Shaytan, A. K.; Vas, V.; Bertocini, C. W.; Arnold, F.; Zirafi, O.; Usmani, S. M.; Muller, J. A.; Sauter, D.; Goffinet, C.; Palesch, D.; Walther, P.; Roan, N. R.; Geiger, H.; Lunov, O.; Simmet, T.; Bohne, J.; Schrezenmeier, H.; Schwarz, K.; Standker, L.; Forssmann, W. G.; Salvatella, X.; Khalatur, P. G.; Khokhlov, A. R.; Knowles, T. P.; Weil, T.; Kirchhoff, F.; Munch, J., Peptide nanofibrils boost retroviral gene transfer and provide a rapid means for concentrating viruses. *Nature nanotechnology* **2013**, *8* (2), 130-6. DOI: 10.1038/nnano.2012.248.
68. Kasotakis, E.; Mitraki, A., Designed Self-Assembling Peptides as Templates for the Synthesis of Metal Nanoparticles. In *Protein Nanotechnology: Protocols, Instrumentation, and Applications, Second Edition*, Gerrard, J. A., Ed. Humana Press: Totowa, NJ, 2013; pp 195-202. DOI: 10.1007/978-1-62703-354-1_11.

69. Kasotakis, E.; Mitraki, A., Silica biotemplating by self-assembling peptides via serine residues activated by the peptide amino terminal group. *Biopolymers* **2012**, *98* (6), 501-509. DOI: 10.1002/bip.22091.
70. Terzaki, K.; Kalloudi, E.; Mossou, E.; Mitchell, E. P.; Forsyth, V. T.; Rosseeva, E.; Simon, P.; Vamvakaki, M.; Chatzinikolaidou, M.; Mitraki, A.; Farsari, M., Mineralized self-assembled peptides on 3D laser-made scaffolds: a new route toward 'scaffold on scaffold' hard tissue engineering. *Biofabrication* **2013**, *5* (4). DOI: 10.1088/1758-5082/5/4/045002.
71. Li, D.; Jones, E. M.; Sawaya, M. R.; Furukawa, H.; Luo, F.; Ivanova, M.; Sievers, S. A.; Wang, W.; Yaghi, O. M.; Liu, C.; Eisenberg, D. S., Structure-based design of functional amyloid materials. *J. Am. Chem. Soc.* **2014**, *136* (52), 18044-51. DOI: 10.1021/ja509648u.
72. Rufo, C. M.; Moroz, Y. S.; Moroz, O. V.; Stohr, J.; Smith, T. A.; Hu, X.; DeGrado, W. F.; Korendovych, I. V., Short peptides self-assemble to produce catalytic amyloids. *Nat Chem* **2014**, *6* (4), 303-9. DOI: 10.1038/nchem.1894.
73. Bewley, M. C.; Springer, K.; Zhang, Y. B.; Freimuth, P.; Flanagan, J. M., Structural analysis of the mechanism of adenovirus binding to its human cellular receptor, CAR. *Science* **1999**, *286* (5444), 1579-83. DOI: 10.1126/science.286.5444.1579.
74. Bergelson, J. M.; Cunningham, J. A.; Droguett, G.; Kurt-Jones, E. A.; Krithivas, A.; Hong, J. S.; Horwitz, M. S.; Crowell, R. L.; Finberg, R. W., Isolation of a common receptor for Coxsackie B viruses and adenoviruses 2 and 5. *Science* **1997**, *275* (5304), 1320-3. DOI: 10.1126/science.275.5304.1320.
75. Kasotakis, E.; Kostopoulou, A.; Spuch-Calvar, M.; Androulidaki, M.; Pelekanos, N.; Kanaras, A. G.; Lappas, A.; Mitraki, A., Assembly of quantum dots on peptide nanostructures and their spectroscopic properties. *Appl. Phys. A-Mater. Sci. Process.* **2014**, *116* (3), 977-985. DOI: 10.1007/s00339-014-8538-5.
76. Kokotidou, C.; Jonnalagadda, S. V. R.; Orr, A. A.; Seoane-Blanco, M.; Apostolidou, C. P.; van Raaij, M. J.; Kotzabasaki, M.; Chatzoudis, A.; Jakubowski, J. M.; Mossou, E.; Forsyth, V. T.; Mitchell, E. P.; Bowler, M. W.; Llamas-Saiz, A. L.; Tamamis, P.; Mitraki, A., A novel amyloid designable scaffold and potential inhibitor inspired by GAIIG of amyloid beta and the HIV-1 V3 loop. *FEBS Lett.* **2018**, *592* (11), 1777-1788. DOI: 10.1002/1873-3468.13096.
77. Chemerovski-Glikman, M.; Frenkel-Pinter, M.; Mdah, R.; Abu-Mokh, A.; Gazit, E.; Segal, D., Inhibition of the Aggregation and Toxicity of the Minimal Amyloidogenic Fragment of Tau by Its Pro-Substituted Analogues. *Chem. -Eur. J.* **2017**, *23* (40), 9618-9624. DOI: 10.1002/chem.201701218.
78. Bergelson, J. M.; Cunningham, J. A.; Droguett, G.; Kurt-Jones, E. A.; Krithivas, A.; Hong, J. S.; Horwitz, M. S.; Crowell, R. L.; Finberg, R. W., Isolation of a common receptor for Coxsackie B viruses and adenoviruses 2 and 5. *Science* **1997 Feb 28**, *275* (5304), 1320-3.
79. M.J., v. R.; Louis, N.; Chroboczek, J.; Cusack, S., Structure of the human adenovirus serotype 2 fiber head domain at 1.5 Å resolution. *Virology* **1999**, *262*, 333-343.

80. van Raaij, M. J.; Louis, N.; Chroboczek, J.; Cusack, S., Structure of the human adenovirus serotype 2 fiber head domain at 1.5 Å resolution. *Virology* **1999**, *262* (2), 333-43.
81. Letarov, A. V.; Londer, Y. Y.; Boudko, S. P.; Mesyanzhinov, V. V., The carboxy-terminal domain initiates trimerization of bacteriophage T4 fibritin. *Biochemistry (Mosc)* **1999**, *64* (7), 817-23.
82. van Raaij, M. J.; Schoehn, G.; Jaquinod, M.; Ashman, K.; Burda, M. R.; Miller, S., Identification and crystallisation of a heat- and protease-stable fragment of the bacteriophage T4 short tail fibre. *Biol. Chem.* **2001**, *382* (7), 1049-55.
83. Roelvink, P. W.; Mi Lee, G.; Einfeld, D. A.; Kovesdi, I.; Wickham, T. J., Identification of a conserved receptor-binding site on the fiber proteins of CAR-recognizing adenoviridae. *Science* **1999**, *286* (5444), 1568-71. DOI: 10.1126/science.286.5444.1568.
84. Nemerow, G. R., Cell receptors involved in adenovirus entry. *Virology* **2000**, *274* (1), 1-4. DOI: 10.1006/viro.2000.0468.
85. Magnusson, M. K.; Hong, S. S.; Boulanger, P.; Lindholm, L., Genetic retargeting of adenovirus: novel strategy employing "deknobbing" of the fiber. *J. Virol.* **2001**, *75* (16), 7280-9.
86. Ray, M.; Lee, Y. W.; Scaletti, F.; Yu, R.; Rotello, V. M., Intracellular delivery of proteins by nanocarriers. *Nanomedicine (Lond)* **2017**, *12* (8), 941-952. DOI: 10.2217/nnm-2016-0393.
87. Zochowska, M.; Paca, A.; Schoehn, G.; Andrieu, J.-P.; Chroboczek, J.; Dublet, B.; Szolajska, E., Adenovirus Dodecahedron, as a Drug Delivery Vector. *PLoS One* **2009**, *4* (5), e5569. DOI: 10.1371/journal.pone.0005569.
88. Medina-Kauwe, L. K.; Kasahara, N.; Kedes, L., 3PO, a novel nonviral gene delivery system using engineered Ad5 penton proteins. *Gene Ther.* **2001**, *8* (10), 795-803. DOI: 10.1038/sj.gt.3301448.
89. Rentsendorj, A.; Xie, J.; MacVeigh, M.; Agadjanian, H.; Bass, S.; Kim, D. H.; Rossi, J.; Hamm-Alvarez, S. F.; Medina-Kauwe, L. K., Typical and atypical trafficking pathways of Ad5 penton base recombinant protein: implications for gene transfer. *Gene therapy* **2006**, *13* (10), 821-36. DOI: 10.1038/sj.gt.3302729.
90. Agadjanian, H.; Weaver, J. J.; Mahammed, A.; Rentsendorj, A.; Bass, S.; Kim, J.; Dmochowski, I. J.; Margalit, R.; Gray, H. B.; Gross, Z.; Medina-Kauwe, L. K., Specific delivery of corroles to cells via noncovalent conjugates with viral proteins. *Pharm. Res.* **2006**, *23* (2), 367-77. DOI: 10.1007/s11095-005-9225-1.
91. Carlisle, R. C.; Bettinger, T.; Ogris, M.; Hale, S.; Mautner, V.; Seymour, L. W., Adenovirus hexon protein enhances nuclear delivery and increases transgene expression of polyethylenimine/plasmid DNA vectors. *Molecular therapy : the journal of the American Society of Gene Therapy* **2001**, *4* (5), 473-83. DOI: 10.1006/mthe.2001.0472.
92. Pereboeva, L.; Komarova, S.; Roth, J.; Ponnazhagan, S.; Curiel, D. T., Targeting EGFR with metabolically biotinylated fiber-mosaic adenovirus. *Gene therapy* **2007**, *14* (8), 627-37. DOI: 10.1038/sj.gt.3302916.

93. Papanikolopoulou, K.; van Raaij, M. J.; Mitraki, A., Creation of Hybrid Nanorods From Sequences of Natural Trimeric Fibrous Proteins Using the Fibrin Trimerization Motif. In *Nanostructure Design: Methods and Protocols*, Gazit, E.; Nussinov, R., Eds. Humana Press: Totowa, NJ, 2008; pp 15-33. DOI: 10.1007/978-1-59745-480-3_2.
94. Prigipaki, A.; Papanikolopoulou, K.; Mossou, E.; Mitchell, E. P.; Forsyth, V.; Selimis, A.; Ranella, A.; Mitraki, A., Laser processing of protein films as a method for accomplishment of cell patterning at the microscale. *Biofabrication* **2017**, *9* (4). DOI: 10.1088/1758-5090/aa8859.
95. Ferrer-Miralles, N.; Corchero, J. L.; Kumar, P.; Cedano, J. A.; Gupta, K. C.; Villaverde, A.; Vazquez, E., Biological activities of histidine-rich peptides; merging biotechnology and nanomedicine. *Microb Cell Fact* **2011**, *10*, 101. DOI: 10.1186/1475-2859-10-101.
96. Bhardwaj, A.; Walker-Kopp, N.; Wilkens, S.; Cingolani, G., Foldon-guided self-assembly of ultra-stable protein fibers. *Protein Sci.* **2008**, *17* (9), 1475-85. DOI: 10.1110/ps.036111.108.
97. Li, Y.; Sousa, R., Novel system for in vivo biotinylation and its application to crab antimicrobial protein scygonadin. *Biotechnol. Lett.* **2012**, *34* (9), 1629-35. DOI: 10.1007/s10529-012-0942-3.
98. Predonzani, A.; Arnoldi, F.; López-Requena, A.; Burrone, O. R., In vivo site-specific biotinylation of proteins within the secretory pathway using a single vector system. *BMC Biotechnol* **2008**, *8*, 41-41. DOI: 10.1186/1472-6750-8-41.
99. Freifelder, D., *Microbial genetics*. Jones and Bartlett: Boston, MA, 1987; p xxii, 601 p.
100. Sambrook, J.; Russell, D. W., *Molecular cloning : a laboratory manual*. 3rd ed.; Cold Spring Harbor Laboratory Press: Cold Spring Harbor, N.Y., 2001.
101. Alberts, B., *Molecular biology of the cell*. 4th ed.; Garland Science: New York, 2002; p xxxiv, 1548 p.
102. Prigipaki, A. PhD Thesis. University of Crete, 2017.
103. Knowles, T. P. J.; Mezzenga, R., Amyloid Fibrils as Building Blocks for Natural and Artificial Functional Materials. *Adv. Mater.* **2016**, *28* (31), 6546-6561. DOI: 10.1002/adma.201505961.
104. Ke, P. C.; Sani, M. A.; Ding, F.; Kakinen, A.; Javed, I.; Separovic, F.; Davis, T. P.; Mezzenga, R., Implications of peptide assemblies in amyloid diseases. *Chemical Society Reviews* **2017**, *46* (21), 6492-6531. DOI: 10.1039/c7cs00372b.
105. Wei, G.; Su, Z. Q.; Reynolds, N. P.; Arosio, P.; Hamley, I. W.; Gazit, E.; Mezzenga, R., Self-assembling peptide and protein amyloids: from structure to tailored function in nanotechnology. *Chemical Society Reviews* **2017**, *46* (15), 4661-4708. DOI: 10.1039/c6cs00542j.
106. Dharmadana, D.; Reynolds, N. P.; Conn, C. E.; Valery, C., Molecular interactions of amyloid nanofibrils with biological aggregation modifiers: implications for cytotoxicity mechanisms and biomaterial design. *Interface Focus* **2017**, *7* (4). DOI: 10.1098/rsfs.2016.0160.
107. Iconomidou, V. A.; Vriend, G.; Hamodrakas, S. J., Amyloids protect the silkworm oocyte and embryo. *Febs Letters* **2000**, *479* (3), 141-145.

108. Mitraki, A., Protein aggregation from inclusion bodies to amyloid and biomaterials. *Advances in protein chemistry and structural biology* **2010**, *79*, 89-125. DOI: 10.1016/S1876-1623(10)79003-9.
109. Paci, E.; Gsponer, J.; Salvatella, X.; Vendruscolo, M., Molecular dynamics studies of the process of amyloid aggregation of peptide fragments of transthyretin. *J. Mol. Biol.* **2004**, *340* (3), 555-69. DOI: 10.1016/j.jmb.2004.05.009.
110. Cecchini, M.; Rao, F.; Seeber, M.; Caflisch, A., Replica exchange molecular dynamics simulations of amyloid peptide aggregation. *J. Chem. Phys.* **2004**, *121* (21), 10748-56. DOI: 10.1063/1.1809588.
111. Colletier, J. P.; Laganowsky, A.; Landau, M.; Zhao, M. L.; Soriaga, A. B.; Goldschmidt, L.; Flot, D.; Cascio, D.; Sawaya, M. R.; Eisenberg, D., Molecular basis for amyloid-beta polymorphism. *Proc. Natl. Acad. Sci. U. S. A.* **2011**, *108* (41), 16938-16943. DOI: 10.1073/pnas.1112600108.
112. van Raaij, M. J., and Mitraki, A., Beta-structured viral fibres: assembly, structure and implications for materials design. *Curr. Opin. Solid State Mater. Sci.* **2004**, *8*, 151-156.
113. Mitraki, A.; Papanikolopoulou, K.; Van Raaij, M. J., Natural triple beta-stranded fibrous folds. *Fibrous Proteins: Amyloids, Prions and Beta Proteins* **2006**, *73*, 97-+. DOI: 10.1016/s0065-3233(06)73004-2.
114. Gazit, E., A possible role for pi-stacking in the self-assembly of amyloid fibrils. *FASEB J.* **2002**, *16* (1), 77-83.
115. Gazit, E., Self Assembly of Short Aromatic Peptides into Amyloid Fibrils and Related Nanostructures. *Prion* **2007**, *1* (1), 32-35. DOI: 10.4161/pri.1.1.4095.
116. Tamamis, P.; Adler-Abramovich, L.; Reches, M.; Marshall, K.; Sikorski, P.; Serpell, L.; Gazit, E.; Archontis, G., Self-assembly of phenylalanine oligopeptides: insights from experiments and simulations. *Biophys. J.* **2009**, *96* (12), 5020-9. DOI: 10.1016/j.bpj.2009.03.026.
117. Lakshmanan, A.; Cheong, D. W.; Accardo, A.; Di Fabrizio, E.; Riek, C.; Hauser, C. A. E., Aliphatic peptides show similar self-assembly to amyloid core sequences, challenging the importance of aromatic interactions in amyloidosis. *Proc. Natl. Acad. Sci. U. S. A.* **2013**, *110* (2), 519-524. DOI: 10.1073/pnas.1217742110.
118. Lopez De La Paz, M.; Goldie, K.; Zurdo, J.; Lacroix, E.; Dobson, C. M.; Hoenger, A.; Serrano, L., De novo designed peptide-based amyloid fibrils. *Proc. Natl. Acad. Sci. U. S. A.* **2002**, *99* (25), 16052-7.
119. Luckey, M.; Hernandez, J.; Arlaud, G.; Forsyth, V. T.; Ruigrok, R. W.; Mitraki, A., A peptide from the adenovirus fiber shaft forms amyloid-type fibrils. *FEBS Lett.* **2000**, *468* (1), 23-7.
120. Jonnalagadda, S. V. R.; Ornithopoulou, E.; Orr, A. A.; Mossou, E.; Forsyth, V. T.; Mitchell, E. P.; Bowler, M. W.; Mitraki, A.; Tamamis, P., Computational design of amyloid self-assembling peptides bearing aromatic residues and the cell adhesive motif Arg-Gly-Asp. *Molecular Systems Design & Engineering* **2017**, *2* (3), 321-335. DOI: 10.1039/c7me00016b.

121. Tamamis, P.; Kasotakis, E.; Archontis, G.; Mitraki, A., Combination of Theoretical and Experimental Approaches for the Design and Study of Fibril-Forming Peptides. In *Protein Design: Methods and Applications*, Köhler, V., Ed. Springer New York: New York, NY, 2014; pp 53-70. DOI: 10.1007/978-1-4939-1486-9_3.
122. Tamamis, P.; Archontis, G., Amyloid-like self-assembly of a dodecapeptide sequence from the adenovirus fiber shaft: Perspectives from molecular dynamics simulations. *Journal of Non-Crystalline Solids* **2011**, *357* (2), 717-722. DOI: 10.1016/j.jnoncrysol.2010.05.083.
123. Tamamis, P.; Terzaki, K.; Kassinosopoulos, M.; Mastrogiannis, L.; Mossou, E.; Forsyth, V. T.; Mitchell, E. P.; Mitraki, A.; Archontis, G., Self-Assembly of an Aspartate-Rich Sequence from the Adenovirus Fiber Shaft: Insights from Molecular Dynamics Simulations and Experiments. *Journal of Physical Chemistry B* **2014**, *118* (7), 1765-1774. DOI: 10.1021/jp409988n.
124. Gremer, L.; Scholzel, D.; Schenk, C.; Reinartz, E.; Labahn, J.; Ravelli, R. B. G.; Tusche, M.; Lopez-Iglesias, C.; Hoyer, W.; Heise, H.; Willbold, D.; Schroder, G. F., Fibril structure of amyloid-beta(1-42) by cryo-electron microscopy. *Science* **2017**, *358* (6359), 116-+. DOI: 10.1126/science.aao2825.
125. Tamamis, P.; Floudas, C. A., Molecular recognition of CXCR4 by a dual tropic HIV-1 gp120 V3 loop. *Biophys. J.* **2013**, *105* (6), 1502-14. DOI: 10.1016/j.bpj.2013.07.049.
126. Tamamis, P.; Floudas, C. A., Molecular recognition of CCR5 by an HIV-1 gp120 V3 loop. *PLoS One* **2014**, *9* (4), e95767. DOI: 10.1371/journal.pone.0095767.
127. Troyer, R. M.; Collins, K. R.; Abraha, A.; Fraundorf, E.; Moore, D. M.; Krizan, R. W.; Toossi, Z.; Colebunders, R. L.; Jensen, M. A.; Mullins, J. I.; Vanham, G.; Arts, E. J., Changes in human immunodeficiency virus type 1 fitness and genetic diversity during disease progression. *J. Virol.* **2005**, *79* (14), 9006-18. DOI: 10.1128/JVI.79.14.9006-9018.2005.
128. Szyk, A.; Deaconescu, A. M.; Spector, J.; Goodman, B.; Valenstein, M. L.; Ziolkowska, N. E.; Kormendi, V.; Grigorieff, N.; Roll-Mecak, A., Molecular basis for age-dependent microtubule acetylation by tubulin acetyltransferase. *Cell* **2014**, *157* (6), 1405-15. DOI: 10.1016/j.cell.2014.03.061.
129. Wagner, T.; Bellinzoni, M.; Wehenkel, A.; O'Hare, Helen M.; Alzari, Pedro M., Functional Plasticity and Allosteric Regulation of α -Ketoglutarate Decarboxylase in Central Mycobacterial Metabolism. *Chem. Biol.* **2011**, *18* (8), 1011-1020. DOI: <https://doi.org/10.1016/j.chembiol.2011.06.004>.
130. Alphey, M. S.; Gabrielsen, M.; Micossi, E.; Leonard, G. A.; McSweeney, S. M.; Ravelli, R. B. G.; Tetaud, E.; Fairlamb, A. H.; Bond, C. S.; Hunter, W. N., Tryparedoxins from *Crithidia fasciculata* and *Trypanosoma brucei*: PHOTOREDUCTION OF THE REDOX DISULFIDE USING SYNCHROTRON RADIATION AND EVIDENCE FOR A CONFORMATIONAL SWITCH IMPLICATED IN FUNCTION. *J. Biol. Chem.* **2003**, *278* (28), 25919-25925. DOI: 10.1074/jbc.M301526200.
131. Macrae, C. F.; Bruno, I. J.; Chisholm, J. A.; Edgington, P. R.; McCabe, P.; Pidcock, E.; Rodriguez-Monge, L.; Taylor, R.; van de Streek, J.; Wood, P. A., Mercury CSD 2.0 - new features for the

- visualization and investigation of crystal structures. *Journal of Applied Crystallography* **2008**, *41*, 466-470. DOI: 10.1107/s0021889807067908.
132. López de Victoria, A.; Tamamis, P.; Kieslich, C. A.; Morikis, D., Insights into the structure, correlated motions, and electrostatic properties of two HIV-1 gp120 V3 loops. *PLoS One* **2012**, *7* (11), e49925-e49925. DOI: 10.1371/journal.pone.0049925.
133. Tamamis, P.; Lopez de Victoria, A.; Gorham, R. D., Jr.; Bellows-Peterson, M. L.; Pierou, P.; Floudas, C. A.; Morikis, D.; Archontis, G., Molecular dynamics in drug design: new generations of compstatin analogs. *Chemical biology & drug design* **2012**, *79* (5), 703-18. DOI: 10.1111/j.1747-0285.2012.01324.x.
134. Pirrone, V.; Wigdahl, B.; Krebs, F. C., The rise and fall of polyanionic inhibitors of the human immunodeficiency virus type 1. *Antiviral Res.* **2011**, *90* (3), 168-82. DOI: 10.1016/j.antiviral.2011.03.176.
135. Moulard, M.; Lortat-Jacob, H.; Mondor, I.; Roca, G.; Wyatt, R.; Sodroski, J.; Zhao, L.; Olson, W.; Kwong, P. D.; Sattentau, Q. J., Selective interactions of polyanions with basic surfaces on human immunodeficiency virus type 1 gp120. *J. Virol.* **2000**, *74* (4), 1948-60. DOI: 10.1128/jvi.74.4.1948-1960.2000.
136. Gilead, S.; Gazit, E., Self-organization of short peptide fragments: From amyloid fibrils to nanoscale supramolecular assemblies. *Supramol. Chem.* **2005**, *17* (1-2), 87-92. DOI: 10.1080/10610270412331328943.
137. Bruce, N. J.; Chen, D. L.; Dastidar, S. G.; Marks, G. E.; Schein, C. H.; Bryce, R. A., Molecular dynamics simulations of A beta fibril interactions with beta-sheet breaker peptides. *Peptides* **2010**, *31* (11), 2100-2108. DOI: 10.1016/j.peptides.2010.07.015.
138. Chen, Z. J.; Krause, G.; Reif, B., Structure and orientation of peptide inhibitors bound to beta-amyloid fibrils. *Journal of Molecular Biology* **2005**, *354* (4), 760-776. DOI: 10.1016/j.jmb.2005.09.055.
139. Soto, C.; Sigurdsson, E. M.; Morelli, L.; Kumar, R. A.; Castano, E. M.; Frangione, B., Beta-sheet breaker peptides inhibit fibrillogenesis in a rat brain model of amyloidosis: implications for Alzheimer's therapy. *Nat Med* **1998**, *4* (7), 822-6.
140. Viet, M. H.; Ngo, S. T.; Lam, N. S.; Li, M. S., Inhibition of Aggregation of Amyloid Peptides by Beta-Sheet Breaker Peptides and Their Binding Affinity. *Journal of Physical Chemistry B* **2011**, *115* (22), 7433-7446. DOI: 10.1021/jp1116728.
141. Frydman-Marom, A.; Convertino, M.; Pellarin, R.; Lampel, A.; Shaltiel-Karyo, R.; Segal, D.; Caflisch, A.; Shalev, D. E.; Gazit, E., Structural Basis for Inhibiting beta-Amyloid Oligomerization by a Non-coded beta-Breaker-Substituted Endomorphin Analogue. *Acs Chemical Biology* **2011**, *6* (11), 1265-1276. DOI: 10.1021/cb200103h.
142. Pawar, A. P.; DuBay, K. F.; Zurdo, J.; Chiti, F.; Vendruscolo, M.; Dobson, C. M., Prediction of "aggregation-prone" and "aggregation-susceptible" regions in proteins associated with

- neurodegenerative diseases. *Journal of Molecular Biology* **2005**, 350 (2), 379-392. DOI: 10.1016/j.jmb.2005.04.016.
143. Williams, A. D.; Portelius, E.; Kheterpal, I.; Guo, J. T.; Cook, K. D.; Xu, Y.; Wetzel, R., Mapping A beta amyloid fibril secondary structure using scanning proline mutagenesis. *Journal of Molecular Biology* **2004**, 335 (3), 833-842. DOI: 10.1016/j.jmb.2003.11.008.
144. Williams, A. D.; Shivaprasad, S.; Wetzel, R., Alanine scanning mutagenesis of A beta(1-40) amyloid fibril stability. *Journal of Molecular Biology* **2006**, 357 (4), 1283-1294. DOI: 10.1016/j.jmb.2006.01.041.
145. Wetzel, R.; Shivaprasad, S.; Williams, A. D., Plasticity of amyloid fibrils. *Biochemistry* **2007**, 46 (1), 1-10. DOI: 10.1021/bi0620959.
146. Andreetto, E.; Yan, L. M.; Tatarek-Nossol, M.; Velkova, A.; Frank, R.; Kapurniotu, A., Identification of Hot Regions of the A beta-IAPP Interaction Interface as High-Affinity Binding Sites in both Cross- and Self-Association. *Angew. Chem.-Int. Edit.* **2010**, 49 (17), 3081-3085. DOI: 10.1002/anie.200904902.
147. de Groot, N. S.; Aviles, F. X.; Vendrell, J.; Ventura, S., Mutagenesis of the central hydrophobic cluster in A β 42 Alzheimer's peptide. *The FEBS Journal* **2006**, 273 (3), 658-668. DOI: 10.1111/j.1742-4658.2005.05102.x.
148. de Groot, N. S.; Pallares, I.; Aviles, F. X.; Vendrell, J.; Ventura, S., Prediction of "hot spots" of aggregation in disease-linked polypeptides. *Bmc Structural Biology* **2005**, 5. DOI: 10.1186/1472-6807-5-18.
149. Ma, B.; Nussinov, R., Trp/Met/Phe hot spots in protein-protein interactions: Potential targets in drug design. *Current Topics in Medicinal Chemistry* **2007**, 7 (10), 999-1005. DOI: 10.2174/156802607780906717.
150. Hard, T.; Lendel, C., Inhibition of Amyloid Formation. *Journal of Molecular Biology* **2012**, 421 (4-5), 441-465. DOI: 10.1016/j.jmb.2011.12.062.
151. Kokkoni, N.; Stott, K.; Amijee, H.; Mason, J. M.; Doig, A. J., N-Methylated peptide inhibitors of beta-amyloid aggregation and toxicity. Optimization of the inhibitor structure. *Biochemistry* **2006**, 45 (32), 9906-18. DOI: 10.1021/bi060837s.
152. Adessi, C.; Soto, C., Converting a peptide into a drug: Strategies to improve stability and bioavailability. *Current Medicinal Chemistry* **2002**, 9 (9), 963-978.
153. Kwok, A.; Hart, S. L., Comparative structural and functional studies of nanoparticle formulations for DNA and siRNA delivery. *Nanomedicine* **2011**, 7 (2), 210-9. DOI: 10.1016/j.nano.2010.07.005.
154. Kwok, A.; McCarthy, D.; Hart, S. L.; Tagalakakis, A. D., Systematic Comparisons of Formulations of Linear Oligolysine Peptides with siRNA and Plasmid DNA. *Chemical biology & drug design* **2016**, 87 (5), 747-63. DOI: 10.1111/cbdd.12709.

155. Vaughan, E. E.; Dean, D. A., Intracellular trafficking of plasmids during transfection is mediated by microtubules. *Molecular therapy : the journal of the American Society of Gene Therapy* **2006**, *13* (2), 422-8. DOI: 10.1016/j.ymthe.2005.10.004.
156. Lehto, T.; Ezzat, K.; Wood, M. J. A.; El Andaloussi, S., Peptides for nucleic acid delivery. *Adv Drug Deliv Rev* **2016**, *106* (Pt A), 172-182. DOI: 10.1016/j.addr.2016.06.008.
157. Suhorutsenko, J.; Oskolkov, N.; Arukuusk, P.; Kurrikoff, K.; Eriste, E.; Copolovici, D. M.; Langel, U., Cell-penetrating peptides, PepFects, show no evidence of toxicity and immunogenicity in vitro and in vivo. *Bioconjugate chemistry* **2011**, *22* (11), 2255-62. DOI: 10.1021/bc200293d.
158. Guidotti, G.; Brambilla, L.; Rossi, D., Cell-Penetrating Peptides: From Basic Research to Clinics. *Trends in pharmacological sciences* **2017**, *38* (4), 406-424. DOI: 10.1016/j.tips.2017.01.003.
159. Raucher, D.; Ryu, J. S., Cell-penetrating peptides: strategies for anticancer treatment. *Trends in molecular medicine* **2015**, *21* (9), 560-70. DOI: 10.1016/j.molmed.2015.06.005.
160. Bechara, C.; Sagan, S., Cell-penetrating peptides: 20 years later, where do we stand? *FEBS Lett.* **2013**, *587* (12), 1693-702. DOI: 10.1016/j.febslet.2013.04.031.
161. Wang, F.; Wang, Y.; Zhang, X.; Zhang, W.; Guo, S.; Jin, F., Recent progress of cell-penetrating peptides as new carriers for intracellular cargo delivery. *Journal of controlled release : official journal of the Controlled Release Society* **2014**, *174*, 126-36. DOI: 10.1016/j.jconrel.2013.11.020.
162. Freimann, K.; Arukuusk, P.; Kurrikoff, K.; Vasconcelos, L. D. F.; Veiman, K. L.; Uusna, J.; Margus, H.; Garcia-Sosa, A. T.; Pooga, M.; Langel, U., Optimization of in vivo DNA delivery with NickFect peptide vectors. *Journal of controlled release : official journal of the Controlled Release Society* **2016**, *241*, 135-143. DOI: 10.1016/j.jconrel.2016.09.022.
163. Freimann, K.; Arukuusk, P.; Kurrikoff, K.; Parnaste, L.; Raid, R.; Piirsoo, A.; Pooga, M.; Langel, U., Formulation of Stable and Homogeneous Cell-Penetrating Peptide NF55 Nanoparticles for Efficient Gene Delivery In Vivo. *Molecular therapy. Nucleic acids* **2018**, *10*, 28-35. DOI: 10.1016/j.omtn.2017.10.011.
164. Veiman, K. L.; Mager, I.; Ezzat, K.; Margus, H.; Lehto, T.; Langel, K.; Kurrikoff, K.; Arukuusk, P.; Suhorutsenko, J.; Padari, K.; Pooga, M.; Lehto, T.; Langel, U., PepFect14 peptide vector for efficient gene delivery in cell cultures. *Molecular pharmaceutics* **2013**, *10* (1), 199-210. DOI: 10.1021/mp3003557.
165. Bednarska, N. G.; van Eldere, J.; Gallardo, R.; Ganesan, A.; Ramakers, M.; Vogel, I.; Baatsen, P.; Staes, A.; Goethals, M.; Hammarstrom, P.; Nilsson, K. P.; Gevaert, K.; Schymkowitz, J.; Rousseau, F., Protein aggregation as an antibiotic design strategy. *Molecular microbiology* **2016**, *99* (5), 849-65. DOI: 10.1111/mmi.13269.
166. Munch, J.; Rucker, E.; Standker, L.; Adermann, K.; Goffinet, C.; Schindler, M.; Wildum, S.; Chinnadurai, R.; Rajan, D.; Specht, A.; Gimenez-Gallego, G.; Sanchez, P. C.; Fowler, D. M.; Koulov, A.; Kelly, J. W.; Mothes, W.; Grivel, J. C.; Margolis, L.; Keppler, O. T.; Forssmann, W. G.;

- Kirchhoff, F., Semen-derived amyloid fibrils drastically enhance HIV infection. *Cell* **2007**, *131* (6), 1059-71. DOI: 10.1016/j.cell.2007.10.014.
167. Cherny, I.; Gazit, E., Amyloids: Not only pathological agents but also ordered nanomaterials. *Angew. Chem.-Int. Edit.* **2008**, *47* (22), 4062-4069. DOI: 10.1002/anie.200703133.
168. Chiti, F.; Dobson, C. M., Protein misfolding, functional amyloid, and human disease. *Annu. Rev. Biochem* **2006**, *75*, 333-366. DOI: 10.1146/annurev.biochem.75.101304.123901.
169. Orr, A. A.; Wordehoff, M. M.; Hoyer, W.; Tamamis, P., Uncovering the Binding and Specificity of beta-Wrapins for Amyloid-beta and alpha-Synuclein. *J Phys Chem B* **2016**, *120* (50), 12781-12794. DOI: 10.1021/acs.jpcc.6b08485.
170. Huang, Y.; Mucke, L., Alzheimer mechanisms and therapeutic strategies. *Cell* **2012**, *148* (6), 1204-22. DOI: 10.1016/j.cell.2012.02.040.
171. Lashuel, H. A.; Overk, C. R.; Oueslati, A.; Masliah, E., The many faces of alpha-synuclein: from structure and toxicity to therapeutic target. *Nature reviews. Neuroscience* **2013**, *14* (1), 38-48. DOI: 10.1038/nrn3406.
172. Villar-Pique, A.; Lopes da Fonseca, T.; Outeiro, T. F., Structure, function and toxicity of alpha-synuclein: the Bermuda triangle in synucleinopathies. *Journal of neurochemistry* **2016**, *139 Suppl 1*, 240-255. DOI: 10.1111/jnc.13249.
173. Adler-Abramovich, L.; Gazit, E., The physical properties of supramolecular peptide assemblies: from building block association to technological applications. *Chemical Society Reviews* **2014**, *43* (20), 6881-6893. DOI: 10.1039/c4cs00164h.
174. Jackson, M. P.; Hewitt, E. W., Why Are Functional Amyloids Non-Toxic in Humans? *Biomolecules* **2017**, *7* (4). DOI: 10.3390/biom7040071.
175. Wu, J. S., Y.; Lihua, T.; Dong, H. In *Computational analysis of propensities of amino acids and nucleotides usage at protein-nucleic acid interfaces*, International Conference on Information Science and Technology, 26-28 March 2011; 2011; pp 1342-1349. DOI: 10.1109/ICIST.2011.5765087.
176. Wiegand, I.; Hilpert, K.; Hancock, R. E., Agar and broth dilution methods to determine the minimal inhibitory concentration (MIC) of antimicrobial substances. *Nature protocols* **2008**, *3* (2), 163-75. DOI: 10.1038/nprot.2007.521.
177. Shen, D.; Coleman, J.; Chan, E.; Nicholson, T. P.; Dai, L.; Sheppard, P. W.; Patton, W. F., Novel cell- and tissue-based assays for detecting misfolded and aggregated protein accumulation within aggregates and inclusion bodies. *Cell biochemistry and biophysics* **2011**, *60* (3), 173-85. DOI: 10.1007/s12013-010-9138-4.
178. Copolovici, D. M.; Langel, K.; Eriste, E.; Langel, U., Cell-penetrating peptides: design, synthesis, and applications. *ACS nano* **2014**, *8* (3), 1972-94. DOI: 10.1021/nn4057269.

179. Farkhani, S. M.; Valizadeh, A.; Karami, H.; Mohammadi, S.; Sohrabi, N.; Badrzadeh, F., Cell penetrating peptides: efficient vectors for delivery of nanoparticles, nanocarriers, therapeutic and diagnostic molecules. *Peptides* **2014**, *57*, 78-94. DOI: 10.1016/j.peptides.2014.04.015.
180. Vives, E.; Brodin, P.; Lebleu, B., A truncated HIV-1 Tat protein basic domain rapidly translocates through the plasma membrane and accumulates in the cell nucleus. *The Journal of biological chemistry* **1997**, *272* (25), 16010-7. DOI: 10.1074/jbc.272.25.16010.
181. Derossi, D.; Joliot, A. H.; Chassaing, G.; Prochiantz, A., The third helix of the Antennapedia homeodomain translocates through biological membranes. *The Journal of biological chemistry* **1994**, *269* (14), 10444-50.
182. Das, S.; Jacob, R. S.; Patel, K.; Singh, N.; Maji, S. K., Amyloid Fibrils: Versatile Biomaterials for Cell Adhesion and Tissue Engineering Applications. *Biomacromolecules* **2018**, *19* (6), 1826-1839. DOI: 10.1021/acs.biomac.8b00279.
183. Gras, S. L.; Tickler, A. K.; Squires, A. M.; Devlin, G. L.; Horton, M. A.; Dobson, C. M.; MacPhee, C. E., Functionalised amyloid fibrils for roles in cell adhesion. *Biomaterials* **2008**, *29* (11), 1553-62. DOI: 10.1016/j.biomaterials.2007.11.028.
184. Bloomfield, V. A., DNA condensation. *Current opinion in structural biology* **1996**, *6* (3), 334-41.
185. Lechardeur, D.; Sohn, K. J.; Haardt, M.; Joshi, P. B.; Monck, M.; Graham, R. W.; Beatty, B.; Squire, J.; O'Brodovich, H.; Lukacs, G. L., Metabolic instability of plasmid DNA in the cytosol: a potential barrier to gene transfer. *Gene therapy* **1999**, *6* (4), 482-97. DOI: 10.1038/sj.gt.3300867.
186. Wolfert, M. A.; Seymour, L. W., Chloroquine and amphipathic peptide helices show synergistic transfection in vitro. *Gene therapy* **1998**, *5* (3), 409-14. DOI: 10.1038/sj.gt.3300606.
187. Dean, D. A.; Strong, D. D.; Zimmer, W. E., Nuclear entry of nonviral vectors. *Gene therapy* **2005**, *12* (11), 881-90. DOI: 10.1038/sj.gt.3302534.
188. Zhang, F.; Andreassen, P.; Fender, P.; Geissler, E.; Hernandez, J. F.; Chroboczek, J., A transfecting peptide derived from adenovirus fiber protein. *Gene therapy* **1999**, *6* (2), 171-81. DOI: 10.1038/sj.gt.3300801.
189. Rothbard, J. B.; Jessop, T. C.; Wender, P. A., Adaptive translocation: the role of hydrogen bonding and membrane potential in the uptake of guanidinium-rich transporters into cells. *Adv Drug Deliv Rev* **2005**, *57* (4), 495-504. DOI: 10.1016/j.addr.2004.10.003.
190. Tesei, G.; Vazdar, M.; Jensen, M. R.; Cragnell, C.; Mason, P. E.; Heyda, J.; Skepo, M.; Jungwirth, P.; Lund, M., Self-association of a highly charged arginine-rich cell-penetrating peptide. *Proceedings of the National Academy of Sciences of the United States of America* **2017**, *114* (43), 11428-11433. DOI: 10.1073/pnas.1712078114.
191. Arrighi, R. B.; Ebikeme, C.; Jiang, Y.; Ranford-Cartwright, L.; Barrett, M. P.; Langel, U.; Faye, I., Cell-penetrating peptide TP10 shows broad-spectrum activity against both *Plasmodium falciparum* and *Trypanosoma brucei brucei*. *Antimicrobial agents and chemotherapy* **2008**, *52* (9), 3414-7. DOI: 10.1128/AAC.01450-07.

192. Palm, C.; Netzerea, S.; Hallbrink, M., Quantitatively determined uptake of cell-penetrating peptides in non-mammalian cells with an evaluation of degradation and antimicrobial effects. *Peptides* **2006**, 27 (7), 1710-1716. DOI: 10.1016/j.peptides.2006.01.006.
193. Zhu, W. L.; Shin, S. Y., Effects of dimerization of the cell-penetrating peptide Tat analog on antimicrobial activity and mechanism of bactericidal action. *Journal of peptide science : an official publication of the European Peptide Society* **2009**, 15 (5), 345-52. DOI: 10.1002/psc.1120.
194. Zhu, W. L.; Shin, S. Y., Antimicrobial and cytolytic activities and plausible mode of bactericidal action of the cell penetrating peptide penetratin and its lys-linked two-stranded peptide. *Chemical biology & drug design* **2009**, 73 (2), 209-15. DOI: 10.1111/j.1747-0285.2008.00769.x.
195. Yoshida, T.; Nagasawa, T., epsilon-Poly-L-lysine: microbial production, biodegradation and application potential. *Applied microbiology and biotechnology* **2003**, 62 (1), 21-6. DOI: 10.1007/s00253-003-1312-9.
196. Al-Halifa, S.; Babych, M.; Zottig, X.; Archambault, D.; Bourgault, S., Amyloid self-assembling peptides: Potential applications in nanovaccine engineering and biosensing. *Peptide Science* **2019**, 111 (1). DOI: 10.1002/pep2.24095.
197. Atsmon-Raz, Y.; Miller, Y., Molecular Mechanisms of the Bindings between Non-Amyloid beta Component Oligomers and Amylin Oligomers. *Journal of Physical Chemistry B* **2016**, 120 (41), 10649-10659. DOI: 10.1021/acs.jpcc.6b07731.
198. Atsmon-Raz, Y.; Miller, Y., Non-Amyloid-beta Component of Human alpha-Synuclein Oligomers Induces Formation of New A beta Oligomers: Insight into the Mechanisms That Link Parkinson's and Alzheimer's Diseases. *Acs Chemical Neuroscience* **2016**, 7 (1), 46-55. DOI: 10.1021/acscchemneuro.5b00204.
199. Baram, M.; Atsmon-Raz, Y.; Ma, B. Y.; Nussinov, R.; Miller, Y., Amylin-A beta oligomers at atomic resolution using molecular dynamics simulations: a link between Type 2 diabetes and Alzheimer's disease. *Physical Chemistry Chemical Physics* **2016**, 18 (4), 2330-2338. DOI: 10.1039/c5cp03338a.
200. Men, D.; Zhang, Z. P.; Guo, Y. C.; Zhu, D. H.; Bi, L. J.; Deng, J. Y.; Cui, Z. Q.; Wei, H. P.; Zhang, X. E., An auto-biotinylated bifunctional protein nanowire for ultra-sensitive molecular biosensing. *Biosens. Bioelectron.* **2010**, 26 (4), 1137-41. DOI: 10.1016/j.bios.2010.07.103.
201. Kay, B. K.; Thai, S.; Volgina, V. V., High-throughput biotinylation of proteins. *Methods in molecular biology* **2009**, 498, 185-96. DOI: 10.1007/978-1-59745-196-3_13.